

INTERNATIONAL SCHOOL FOR ADVANCED STUDIES (ISAS)

Trieste, Italy

Doctor of Philosophy Thesis

THE ROLE OF SPIN PHYSICS IN HADRONIC INTERACTIONS  
AT SHORT DISTANCES

Philip Ratcliffe

SUPERVISOR:  
Dr. N.S. Craigie

EXTERNAL EXAMINER:  
Prof. M. Ciafaloni



This thesis is dedicated to  
my Mother and Father



THE ROLE OF SPIN PHYSICS IN HADRONIC INTERACTIONS  
AT SHORT DISTANCES

Contents

- § 1 Introduction (notation, conventions and standard kinematics)
- § 2 Deep-inelastic scattering - an introduction to spin dependence
- § 3 Theoretical basis of spin asymmetries
- § 4 From theory to experiment
- § 5 Next-to-leading logarithmic corrections
- § 6 Asymmetries from higher-power mechanisms in QCD
- § 7 On the problem of transverse-spin asymmetries in QCD perturbation theory
- § 8 Helicity asymmetries as a test of supersymmetric QCD interactions
- § 9 Single-spin asymmetries in QCD

Appendices

- A1 Colour gauge group algebra
- A2 Dirac-spinor and spin-projector identities
- A3 Dimensional regularisation and D dimensional integrals
- A4 Parton distribution parameterisation and evolution

I should like to express my deep gratitude towards my supervisor Dr. N.S. Craigie for initially interesting me in this branch of particle physics and for all the subsequent help, encouragement and valuable tuition. I also thank the International School for Advanced Studies (ISAS) for the financial support afforded me in order to follow the Ph.D. course in Trieste. And finally I wish to thank Lidia and Alex for their patient typing of the manuscript.

A large part of the material contained in this thesis can also be found in N.S. Craigie, K. Hidaka, M. Jacob and F.M. Renard: "Spin physics at short distances" (to appear in Physics Rep.), where many aspects of spin physics not discussed here are reviewed and complimentary discussions may be found.

## 1.1 Opening remarks

In recent years an increasing number of physicists have been turning their attention to aspects of high-energy physics involving spin or polarisation phenomena. The motivation being the belief that this property, fundamental to the present picture of particle interactions, can open up new windows into many different features of the underlying theory.

While nobody to-day would seriously support the view that spin is merely an "inessential complication", its importance is still to some extent ignored. This thesis then is intended to go some way to providing a solid footing (within the context of high-energy hadronic physics) for the theory and phenomenology of spin. This is to be achieved by presenting a broad discussion of some of the interesting theoretical points, together with a description of the present experimental situation, and in so doing to demonstrate the following two statements:

- (i) Spin phenomenology is intimately dependent on the underlying (field) theoretical description of particle physics and thus can provide a great deal of information as to the validity of the present formulation of the latter.
- (ii) Much of spin physics is infact experimentally feasible and accessible to present day (or very near future) technology, and in many cases to virtually the same degree as the corresponding situation for unpolarised physics.

Clearly both the above two points are essential to the relevance of polarisation phenomena in high-energy physics: the theoretical dependence

## Chapter 1

## Introduction

- 1.1 Opening remarks
- 1.2 A brief survey of the rôle of spin in physics
- 1.3 Outline of contents
- 1.4 Notation and conventions



on spin should be non-trivial (i.e. unambiguous) and at the same time the predictions should be experimentally verifiable.

The important point is that if one considers for example the scattering of an electron (or other lepton) in a particular helicity state off a proton in a given helicity state then the theory leads to very precise predictions of the cross-section dependence on the relative polarisations of the two interacting particles, in particular that this dependence is strong. Through the parton picture and factorisation theorem the same statements are seen to hold true also for hadron-hadron interactions. With recent developments in experimental techniques highly polarised beams and targets will soon be available thus allowing access to these large spin effects.

## 1.2 A brief survey of the rôle of spin in physics

One of the many notable contributions of Dirac was to demonstrate that the spin degree of freedom emerges in a completely natural way from the field-theoretical description of particle physics [1]. It is this intimate and natural connection of spin to the present-day view of physics that candidates it as a useful tool with which to ascertain the validity of the theory.

It is indeed true that the downfall of Regge theory was due essentially to its failure to describe adequately the spin properties of hadrons [2]. While the phenomenological description of amplitudes in terms of Regge-pole contributions was quite successful with some differential cross-section data ( $\pi$ -nucleon charge exchange for example), corresponding polarisation data was not explained by this model. First and foremost the lesson to be learnt here is the necessity of a true theory and that phenomenological models, however sophisticated, can only ever be successful up to a point, sooner or later finding themselves unremediably in conflict with the data.

Equally true is the fact that any unexpected results could lead, at the very least, to modifications of the present theory and thus in any case to a deeper understanding. Such unexpected results do in fact already exist: the mechanisms responsible for generating single-spin asymmetries still lack a complete understanding and the large polarisation of hyperons produced at even very large  $p_T$  in unpolarised pp collisions [3] still requires a satisfactory explanation. Moreover the description of transverse spin, being intimately related to the bound-state and non-perturbative effects in QCD, is far from complete [4].

Coming more to the forefront of the present day research: if the hope that supersymmetry [5] can resolve the gauge-hierarchy or fine-tuning

problem of grand unification theories is realised then, since the basis of supersymmetry is the "unification" of Bosonic and Fermionic degrees of freedom, one could reasonably expect that spin-physics should play a significant rôle in determining the precise form of the supersymmetric theory at work in particle physics.

A rather remarkable phenomenon recently proposed by Rubakov [6] and Callan [7] is the possibility that a fermion scattering off a GUT monopole could change its identity. The point being that in addition to the contribution of the fermion helicity to the total orbital angular momentum of the fermion-monopole system there is also a part  $eg\hbar \vec{r}/r$  coming from the monopole field. Thus, in the s-wave, in order to satisfy both the Dirac condition  $eg = \frac{1}{2}$  and angular momentum conservation as the fermion passes the core and  $\vec{r} \rightarrow -\vec{r}$  one of two things happens: either the fermion helicity flips or its charge changes sign. In principle both can happen as a GUT monopole is an indefinite state of fermion number. One profound consequence of this is that monopoles could catalyse proton decay with a strong interaction rate. This effect would be observable if the monopole flux were sufficiently high and is due to the belief that in this situation helicity conservation is as fundamental as charge or baryon number conservation.

Since electro-weak interaction phenomenology will not be dealt with here it is perhaps worth taking this opportunity to make a few comments. Given the distinct ~~parity-violating~~ nature of electro-weak theory, spin is the obvious candidate as a mirror in which to reflect unambiguously this property. In the the Drell-Yan process one would expect the onset of a large single-spin (proton) asymmetry in the lepton-pair production cross-section at the  $Z^0$  threshold, indeed in proton-antiproton colliders strikingly large (and opposite sign) single-spin asymmetries should be registered for  $W^+$  and  $W^-$  production [8]. Moreover, the presence of a second heavier  $Z^0$  predicted by some theories [9], while not readily detectable from normal cross-section measurements at present energies would induce a very marked departure from the expected behaviour of the spin

asymmetry. Alternatively polarisation of the proton and antiproton beams provides a practical way of removing the QCD hadronic background.

One also expects parity violating single-spin asymmetries in nucleon-nucleon interactions. Estimates based on an effective parity-violating Lagrangian arising from light-boson exchanges put such asymmetries at around  $-10^{-7}$  in agreement with low energy experiment [10]. However at Argonne for  $p_{lab} = 6 \text{ GeV}/c$  large positive asymmetries of the order  $+3 \times 10^{-6}$  have been observed [11]. Although various mechanisms have been suggested, the most successful based on  $Z^0$  and  $W^\pm$  interactions between the valence quarks [12], this data is still lacking a completely satisfactory explanation.

Another topic not touched upon by this thesis is polarised  $e^+e^-$  experiments [13,14]. Although  $e^+e^-$  colliders have the major drawback of a much lower event rate than in proton-(anti)proton colliders, the great advantage they do have is that both the electrons and positrons are automatically highly polarised (down and up respectively) for free due to synchrotron radiation, according to the formula:

$$\mathcal{P}_{e^+} = \mathcal{P}_{e^-} = 0.924 / (1 + T_{pol}/T_{depol}) ,$$

where  $T_{pol}$  and  $T_{depol}$  are characteristic times for polarisation and depolarisation, depending on machine properties. Unfortunately so far it has not been possible to rapidly reverse the polarisation in  $e^+e^-$  rings, however it is possible experimentally to determine all the transverse-spin cross-sections. By inducing a depolarisation resonance (possible at any energy) one can obtain, besides the one available polarisation for each electron or positron, zero polarisation for either. This would also involve a certain loss of accuracy although in a year's running at PETRA (with approximately 20,000 events) one would expect a statistical error in the asymmetry measurement for hadron production of about 4% [14]. The systematic errors being much smaller, and in fact also much reduced with respect to normal unpolarised operation.

One use of such experiments might be to measure the ratio  $R$  of the  $e^+e^-$  cross-section for hadron production divided by that for muon-pair production. This would be a test of the one-photon exchange model in which  $R$

should be independent of the spin configuration of the annihilating leptons. Spin asymmetries would also provide a useful method to search for the  $Z^0$  at present PETRA energies [15]. Even for  $s = 30$  or  $40$  GeV there will be sizeable deviations of 5 or 10% from the standard 100% spin asymmetry in the one photon exchange model.

### 1.3 Outline of contents

The following and final section of chapter 1 consists of a list of the essential notation and conventions common to most of the other chapters, and in addition it contains a few useful expressions and basic kinematics.

By way of an introduction to spin dependence in hadronic interactions chapter 2 discusses deep-inelastic scattering, both in terms of the Wilson operator expansion and from the more physically intuitive approach of Altarelli and Parisi. The latter also giving a physical feeling for the spin properties of partons and their  $Q^2$ -evolution.

In chapter 3 the theory of spin within the framework of perturbative QCD is discussed. Starting with an examination of the QCD Lagrangian in the high energy limit, which reveals how helicity can be viewed as a conserved quantum number in hard (partonic) scattering processes, the hard scattering partonic cross-sections are calculated and their strong helicity dependence explicitly displayed. It is then shown how the factorisation theorem can be extended to include initial and final partons and hadrons in given helicity states. Finally via this theorem, which stated simply permits hadronic cross-sections to be expressed as convolutions of partonic cross-sections and partonic distributions, using models for the latter the helicity asymmetries for various processes are estimated and shown to be large for suitable kinematic configurations.

Chapter 4 contains a review of the present experimental situation with respect to spin measurements. The presently available data is discussed together with some of the more important technical problems involved in performing polarisation experiments at high energies.

Perturbative QCD as applied to hadronic interactions has several difficulties which limit its predictive power: the large radiative corrections associated with the Drell-Yan process for example, which lead to the well-known

K-factor, are discussed in Chapter 5 where it is shown that the large corrections to  $q\bar{q} \rightarrow \gamma^*$  (coming from real and virtual gluon contributions) cancel in the ratio one considers when forming the helicity asymmetry. Another important effect one would like to have control over is the importance of higher power  $p_T$  mechanisms which could provide large contributions at intermediate values of  $p_T$ . In chapter 6 a particular such mechanism is examined and the helicity dependence is found to be completely different from that of the leading mechanism thus supporting the idea that helicity asymmetry measurements could give important clues as to the higher power processes at work when  $p_T$  is not particularly large.

A problem which is not yet fully understood and which is intimately related to non-perturbative effects is the description of the transverse spin properties of hadrons. Chapter 7 contains a discussion of apparent discrepancies between various approaches and a model is used to perform explicit calculations in an attempt to indicate the source of the difficulties.

Chapter 8 examines the rôle helicity measurements could play in the search for evidence of a supersymmetric version of QCD. The essential point is that the new particles introduced in such a theory (scalar quarks, gauge fermions etc.) having different spin properties to those of the usual particles while still strongly interacting, can have profound effects on helicity dependence as one passes the production threshold (which may well lie within reach of present-day accelerators).

Normally unaccessible phases show up in the spin dependence of particle interactions; chapter 9 reviews recent progress in evaluating order  $\alpha_s^2$  interference effects in proton-proton scattering. Interestingly it turns out in this case that the effects, which in principle could be quite large, are suppressed by a coincidental partial cancellation between the colour factors of unrelated contributions.

The first of the four appendices contains details of the  $SU(N)$  gauge algebra including a list of common Casimirs (or group invariants) occurring in calculations and explains how the commutation relations and Bianchi identities may be exploited in diagrammatic form to simplify the final expression for interaction amplitudes.

Appendix A2 derives and lists various identities for external spin projectors which are useful in evaluating interaction amplitudes and thus avoiding the large number of terms encountered when using the trick of Feynman of squaring up to give full cross-sections. There is also a description of a new technique for simplifying computations involving several long strings of gamma matrices, such as those involved in calculations for exclusive processes.

The third appendix contains a discussion of the dimensional regularisation scheme with some useful formulae including the derivation of a general formula for symmetric integration for any number of loop momentum vectors occurring in the numerator. In particular the problem of defining  $\gamma_5$  and  $\epsilon^{\mu\nu\rho\kappa}$  in a non-integer number of dimensions is examined.

The fourth and final appendix lists the parametrisations usually used for the parton distribution functions and examines the effects of including charm, possible spin-dependent sea quark distributions and of evolving them with  $Q^2$  according to the Altarelli-Parisi equations.

The references for the chapters are to be found at the end each chapter while the references for all the four appendices are grouped together after appendix A4.



## 1.4 Notation and conventions

In this, the final section of chapter one, the general notation and a few basic conventions adopted in this thesis are given.

Apart from the chapter on supersymmetry the QCD Lagrangian will be taken to be:

$$\mathcal{L}(F_{\mu\nu}^a, \Psi_i) = -\frac{1}{4} F_{\mu\nu}^a F^{a\mu\nu} + \bar{\Psi}_i \mathcal{D}_{ij} \Psi_j - m \bar{\Psi}_i \Psi_i, \quad (1.4.1)$$

where the flavour content of the theory has been suppressed. The gluonic field strength is given by

$$F_{\mu\nu}^a = \partial_\mu A_\nu^a - \partial_\nu A_\mu^a + g f^{abc} A_\mu^b A_\nu^c, \quad (1.4.2)$$

and the covariant derivative by

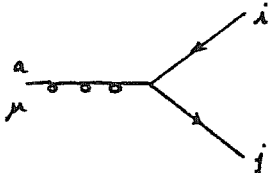
$$\mathcal{D}_{ij}^\mu = i \delta_{ij} \partial^\mu + g \tau_{ij}^a A^{a\mu}. \quad (1.4.3)$$

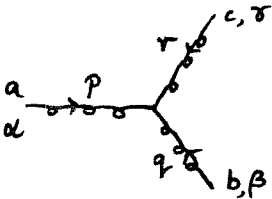
The  $f^{abc}$  are the structure constants of the colour gauge group and  $\tau_{ij}^a$  are the matrices of the group generators in the fermion representation obeying the commutation relations  $[\tau^a, \tau^b] = i f^{abc} \tau^c$ . Various useful relations and Casimirs of the SU(N) groups are listed in appendix A1.

For completeness, and also to avoid confusion over the different conventions on minus signs, the Feynman rules obtained from the above Lagrangian are listed here below.

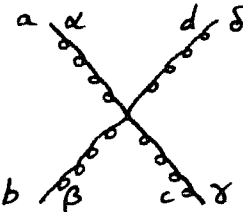
Gluon propagator  =  $-i \delta^{ab} g^{\mu\nu} / (k^2 + i\epsilon)$ ,

Quark propagator  =  $i \delta_{ij} (\not{p} + m) / (p^2 - m^2 + i\epsilon)$ ,

$A \bar{\psi} \psi$  vertex  =  $-ig \gamma^\mu \tau_{ij}^a$ ,

AAA vertex 

$$= -gf^{abc} [g_{\alpha\beta}(p-q)_\gamma + g_{\beta\gamma}(q-r)_\alpha + g_{\gamma\alpha}(r-p)_\beta],$$

AAAA vertex 

$$= -ig^2 [f^{abe} f^{cde} (g_{\alpha\gamma} g_{\beta\delta} - g_{\alpha\delta} g_{\beta\gamma}) + f^{ace} f^{bde} (g_{\alpha\beta} g_{\gamma\delta} - g_{\alpha\delta} g_{\beta\gamma}) + f^{ade} f^{cbe} (g_{\alpha\gamma} g_{\beta\delta} - g_{\alpha\beta} g_{\gamma\delta})].$$

(1.4.4)

Use will be made of two types of gauge: covariant gauges, in which a gauge fixing term  $-(\partial^\mu A_\mu^a)(\partial^\nu A_\nu^a)/\xi$  is added to the Lagrangian, and axial gauges [16] for which the gauge condition is  $\eta \cdot A = 0$  with  $\eta^\nu$  some arbitrary vector, the gauge fixing term is then  $-\eta \cdot \bar{A}(\partial^2 \eta \cdot \bar{A})/\xi \eta^2$ . For these two cases the gluon propagator is given by replacing  $g^{\mu\nu}$  in the above expression by the following:

Covariant gauge:  $g^{\mu\nu} - (1-\xi)k^\mu k^\nu/k^2,$   
 Axial gauge:  $g^{\mu\nu} - (k^\mu \eta^\nu + k^\nu \eta^\mu)/k \cdot \eta + (1-\xi)k^\mu k^\nu \eta^2/(k \cdot \eta)^2$ . (1.4.5)

Owing to the factor  $(k \cdot \eta)^{-2}$  the last term of the axial gauge propagator is very singular and thus rather undesirable, it may be removed by choosing the gauge parameter  $\xi = 1$ , this will be assumed throughout this thesis.

QCD being a non-abelian gauge theory also requires the inclusion of ghost terms to cancel the contribution of unphysical polarisations of the gluon. This can however be avoided by the use of physical gauges such as the axial gauge indicated above. Thus whenever necessary to avoid ghost contributions, in particular for external gauge particles, a physical gauge will be adopted.

For the Dirac-matrix and spinor algebra the conventions adopted will be those of Bjorken and Drell [17] with the exception that spinors will be normalised to  $2m$ . Thus for the spinors  $u$  and  $v$ , describing states of four-momentum  $p^\nu$  and covariant-spin  $s^\nu$ , satisfying the Dirac equation for fermion and antifermion respectively:

$$\begin{aligned} (\not{p} - m) u(p, s) &= 0, \\ (\not{p} + m) v(p, s) &= 0. \end{aligned} \quad (1.4.6)$$

the spin projectors are:

$$\begin{aligned} u(p, s) \bar{u}(p, s) &= (\not{p} + m)(1 + \gamma_5 \not{s})/2, \\ v(p, s) \bar{v}(p, s) &= (\not{p} - m)(1 + \gamma_5 \not{s})/2. \end{aligned} \quad (1.4.7)$$

This is more convenient for taking directly the limit of zero mass fermions, when the projectors go over to

$$\begin{aligned} u(p, h) \bar{u}(p, h) &= (1 + h \gamma_5) \not{p}, \\ v(p, h) \bar{v}(p, h) &= (1 - h \gamma_5) \not{p}, \end{aligned} \quad (1.4.8)$$

where  $u$  and  $v$  are now eigenstates of helicity,  $h = \pm 1$ . The left- and right-handed helicity projectors being the usual  $\frac{1}{2}(1 \pm \gamma_5)$ . This normalisation has the added advantage of giving partonic scattering cross-sections in the most convenient form for the factorised version of hadronic cross-section (see chapter 3).

For external gauge fields the usual convention is that, in the frame where the momentum is  $q^\nu = (Q, 0, 0, Q)$ , the polarisation vector is given by  $\xi^\nu(q, \lambda) = \sqrt{\frac{1}{2}}(0, -\lambda, i, 0)$ ,  $\lambda = \pm 1$ . This corresponds to taking the gauge projection operator,  $d^{\mu\nu}(q, \lambda) = \xi^\mu(\lambda) \xi^{\nu*}(\lambda)$ , in a covariant form as:

$$d^{\mu\nu}(q, \lambda) = \frac{1}{2} \left[ -q^\mu q^\nu + (q^\mu \eta^\nu + q^\nu \eta^\mu) / q \cdot \eta + i \lambda \epsilon^{\mu\nu\rho\sigma} q_\rho \eta_\sigma / q \cdot \eta \right], \quad (1.4.9)$$

where, in the aforementioned frame,  $\eta^\mu \propto (1, 0, 0, -1)$ . This is clearly equivalent to an axial gauge choice and therefore completely avoids the inclusion of ghost fields. In practical calculation one takes  $\eta'$  to be one of the other (light-like) vectors in the problem.

Of particular convenience in calculating matrix elements is the following expression for  $\xi^\mu$ :

$$\xi^\mu(q, \lambda; \eta, \eta') = \frac{1}{2}(\eta \cdot \eta' q^\mu + q \cdot \eta' \eta^\mu - q \cdot \eta \eta'^\mu + i\lambda \epsilon^{\mu\rho\sigma\kappa} q_\rho \eta_\sigma \eta'_\kappa) / \sqrt{q \cdot \eta \eta' \eta \cdot \eta'} \quad (1.4.10)$$

where  $\eta$  corresponds to that of (1.4.9) and  $\eta'$  is some other arbitrary (light-like) vector, usually also conveniently chosen as one of the other vectors in the problem. This also provides us with an interesting and very useful identity for the fermionic current,  $J^\mu$ , in the limit of massless particles:

$$\bar{u}(p', h') \gamma^\mu u(p, h) = 4 \sqrt{p \cdot p'} \xi^\mu(p, h; p', h') \delta_{hh'} \quad (1.4.11)$$

where  $\delta_{hh'} = \frac{1}{2}(1 + hh')$ . These expressions are particularly suited for use in algebraic manipulation programmes such as Schoonship [18] and, with a judicious choice of the gauge-fixing vector (which may be chosen independently for different external gauge particles), can even simplify hand calculations quite considerably.

In appendix A2 extensions of (1.4.10) and (1.4.11) are given and also many other formulae which the author has found useful in the manipulation of expressions involving Dirac matrices.

The by now most popular (and most generally applicable) method of regulating the divergences encountered in evaluating loop-momentum integrals in quantum field theories is the dimensional regularisation scheme of 't Hooft and Veltman [19] in which the number of spatial dimensions is continued to a non-integer value so that the overall number of space-time dimensions becomes  $D = 4 - 2\epsilon$ . The advantages this scheme has over others, apart from manifestly maintaining gauge and Lorentz invariances, lie in its simplicity of application and in the fact that it regulates not only the ultra-violet divergences but also the various infra-red divergences associated with massless field theories.

The divergences show up as  $1/\epsilon$  poles of varying order which are easily identified and subtracted out, this corresponds to the usual minimal subtraction

(MS) scheme [20]. Together with these poles one typically finds a finite term  $\ln 4\pi - \gamma_E$ , where  $\gamma_E = 0.5772\dots$  is the Euler gamma coming from the extension of  $D!$  to non-integer  $D$  and the extension of the angular integrals leads to the  $\ln 4\pi$ . These extra terms may be removed by including them in the subtraction, e.g. by defining the subtraction term as  $\frac{1}{\epsilon} = \frac{1}{\epsilon} + \ln 4\pi - \gamma_E$  this is the widely adopted modified minimal subtraction ( $\overline{\text{MS}}$ ) scheme [21]. It is perhaps rather more convenient to eliminate these undesirable terms from the start by redefining the continuation of the measure  $d^D k / (2\pi)^D$  by

$$[dk] = d^D k / (2\pi)^D \rightarrow \pi^{-\epsilon/2} [\Gamma(1-2\epsilon)]^{-1} d^D k / (2\pi)^4, \quad (1.4.12)$$

where  $\Gamma(n)$  is the usual continuation of  $(n-1)!$  to non-integer  $n$ . Note that in the limit  $D \rightarrow 4$  the two above forms are identical. Appendix A3 contains some useful formulae for Feynman integrals in  $D$  dimensions plus the extension of the Dirac matrix algebra including a discussion of the treatment of  $\gamma_5$  in a non-integer number of dimensions.

In hadronic physics various kinematic variables are used to parametrise interactions, in order to avoid confusion an attempt has been made to consistently use the same symbol for each individual variable. What follows is a list of some of the most important and frequently used symbols and their definition.

The four-momentum of particles will generally be indicated as follows  $p^\mu$  for external fermions,  $q^\mu$  for external gauge bosons and  $k^\mu$  for internal or loop momentum. The covariant spin-vector for fermions will be denoted by  $s^\mu$  (usually readily distinguishable from the Mandelstam invariant  $s$ ) while the helicity of fermions will be indicated by  $h$  and of gauge bosons by  $\lambda$ . Hadronic variables will usually be indicated by capitals and those of partons by lower case symbols, while the partonic Mandelstam variables and cross-sections will be differentiated from their hadronic correspondents by use of the circumflex (thus  $\hat{s}, d\hat{\sigma}$  etc. are the partonic invariants).

The Bjorken scaling variable,  $x_B = -q^2/p \cdot q$  for the deep-inelastic scattering of a virtual photon (space-like four-momentum  $q$ ) off a proton (four-mo-

momentum  $p$ ) will generally be denoted without the suffix B, unless necessary to avoid confusion. However the longitudinal and transverse momentum-fraction scaling variables for final state trigger particles, jets etc. will be written as  $x_F = 2p_{||} / \sqrt{s}$  and  $x_T = 2p_T / \sqrt{s}$  where  $p_{||}$  ( $p_T$ ) is the longitudinal (transverse) component of the trigger momentum with respect to the beam axis. Another experimentally useful parametrisation is in the rapidity variable  $y_R = \frac{1}{2} \ln [(E+p_{||})/(E-p_{||})]$ , where  $E$  is the energy of the trigger. In terms of  $x_F$  and  $x_T$  one has  $y_R = \frac{1}{2} \ln \left[ \frac{(\sqrt{x_F^2 + x_T^2} + x_F)}{(\sqrt{x_F^2 + x_T^2} - x_F)} \right]$ .

## References to Chapter 1

- [1] P.A.M. Dirac, Proc. Roy. Soc. (London), Ser. A., 117; 610 (1928).
- [2] See for example C. Bourrely, E. Leader and J. Soffer, Phys. Rep. 59, 95 (1980).
- [3] See ref. [4] chapter 4:
- [4] See chapter 7.
- [5] See chapter 8 and refs. therein.
- [6] V.A. Rubakov, Academy of Sciences, Moscow, preprint (1981).
- [7] C. Callan, Proc. of the Int. Conf. on Particle Physics, Paris (1982) and refs. therein.
- [8] J. Soffer, Marseille preprint CPT-83/P.1484 (1983) to appear in the Proc. of the SPS Fixed Target Workshop, CERN, Dec. 1982.
- [9] See for example E.H. de Groot and D. Schildknecht, Z. Phys. C10, 55 and 139 (1981).
- [10] D. Nagle et al., AIP Conf., Argonne, 1978 (ed. G. Thomas), Proc. No. 51, 224 (1979).  
M. Simonius in High Energy Physics with Polarised Beams and Targets, ed. by C. Joseph and J. Soffer (Birkhäuser Verlag, 1981), p 355.
- [11] R.E. Mische in High Energy Physics with Polarised Beams and Targets, (ed. C. Joseph and J. Soffer) Birkhäuser Verlag, 1981) p. 361.
- [12] J. Soffer in High Energy Physics with Polarised Beams and Targets, ed. by C. Joseph and J. Soffer (Birkhäuser Verlag, 1981), p 370.
- [13] J.D. Bjorken in Proc. of the 5th Int. Symp. on High Energy Spin Physics, Brookhaven Nat. Lab. (Sept. 1982), p. 268.
- [14] A.D. Krisch, Michigan preprint UM HE 82-5 (1982).

- [15] L.E.P. Summer Study, CERN preprint 79-01 (1979).
- [16] For an early application of axial gauges to QCD see L.N. Lipatov, Sov. J. Nucl. Phys. 20, 94 (1975).
- [17] J.D. Bjorken and S.D. Drell, Relativistic Quantum Mechanics; Relativistic Quantum Fields (McGraw-Hill, New York, 1965), appendix A.
- [18] See for example H. Strubbe, Comp. Phys. Comm. 8, 1 (1974).
- [19] G. 't Hooft and M. Veltman, Nucl. Phys. B44, 189 (1972).
- [20] G. 't Hooft, Nucl. Phys. B61, 433 (1973).
- [21] W.A. Bardeen, A.J. Buras, D.W. Duke and T. Muta, Phys. Rev. D18, 3998 (1978).



## 2.1 Operator-product expansion approach

The deep-inelastic scattering of leptons and nucleons in definite spin states can be described by the Fourier transform of the commutator of electromagnetic currents  $J^\mu(z)$  sandwiched between polarised nucleon states with four-momentum  $p$  and covariant-spin  $s$ :

$$W^{\mu\nu}(p, q, s) = \frac{1}{2\pi} \int d^4z e^{iq \cdot z} \langle p, s | [J^\mu(z/2), J^\nu(-z/2)] | p, s \rangle, \quad (2.1.1)$$

where  $q$  is the space-like momentum of the virtual photon. The leptonic part of the process being relatively trivial will not be discussed here.

We may decompose the tensor  $W^{\mu\nu}$  into its symmetric and antisymmetric parts:  $W_{\mu\nu} \equiv W_{(\mu\nu)}^S + i W_{[\mu\nu]}^A$ . The symmetric tensor  $W_{\mu\nu}^S$  is described in terms of the structure functions  $W_1$ ,  $W_2$  (and  $W_L$  etc.) which contribute to the spin-averaged process:

$$W_{\mu\nu}^S = \left( -g_{\mu\nu} + \frac{q_\mu q_\nu}{q^2} \right) W_1(x, Q^2) + \left( p_\mu - \frac{M\nu}{q^2} q_\mu \right) \left( p_\nu - \frac{M\nu}{q^2} q_\nu \right) \frac{W_2(x, Q^2)}{M^2}, \quad (2.1.2)$$

where  $M\nu = p \cdot q$ ,  $Q^2 = -q^2 > 0$ ,  $2M\nu x = Q^2$  and  $M$  is the nucleon mass,  $x$  is then the usual Bjorken scaling variable. Only parity non-violating processes will be considered here.

The spin-dependent contribution comes from the antisymmetric tensor  $W_{\mu\nu}^A$  which is composed of the structure functions  $V_1$  and  $V_2$ :

$$W_{\mu\nu}^A = -\epsilon_{\mu\nu\rho\sigma} q^\rho \left[ s^\sigma V_1(x, Q^2) + (M\nu s^\sigma - q \cdot s p^\sigma) \frac{V_2(x, Q^2)}{M^2} \right]. \quad (2.1.3)$$

In the scaling limit and neglecting logarithms of  $Q^2$  standard arguments show that [1]

$$\begin{aligned} \mathcal{F}_1 &\equiv 2M W_1, & \mathcal{F}_2 &\equiv \frac{\nu}{x} W_2, \\ \mathcal{G}_1 &\equiv 2\nu V_1, & \mathcal{G}_2 &\equiv \frac{2\nu^2}{M} V_2 - \mathcal{G}_1, \end{aligned} \quad (2.1.4)$$

## Chapter 2

## Deep-inelastic scattering - an introduction to spin dependence

2.1 Operator-product expansion approach

2.2 Intuitive approach

depend only on  $x$ , scale-breaking effects being limited to terms of order  $\ln Q^2$ . The script structure functions are slightly modified with respect to those usually defined, this will allow a more direct relation with the distributions functions of partons inside the nucleon. The relationship with the usual structure functions is:

$$\begin{aligned} \mathcal{F}_1 &= 2F_1 \quad , \quad \mathcal{F}_2 = F_2/x \quad , \\ \mathcal{G}_1 &= -2g_1 \quad , \quad \mathcal{G}_2 = -2(g_1 + g_2) \quad . \end{aligned} \quad (2.1.5)$$

The structure function  $\mathcal{G}_2$ , governing the process for transversely polarised beam and target, has as yet no interpretation within the parton model framework. Moreover evaluation of its  $Q^2$  dependence is not as straightforward as many authors believe. A detailed analysis of this problem is given in Chapter 7 while in this and other chapters the discussion will be restricted to the case of beam and target longitudinally polarised, i.e. in states of definite helicity. One may then neglect the nucleon mass (this has no bearing on usual target mass effects which may as is well-known be accounted for by  $\xi$ -scaling [2]) and then  $s_\mu \rightarrow h p_\mu / M$  ( $h$  is the nucleon helicity) and (2.1.3) reduces to

$$W_{\mu\nu}^A = -h \epsilon_{\mu\nu\rho\sigma} \frac{q^\rho p^\sigma}{p \cdot q} \mathcal{G}_1 \quad . \quad (2.1.6)$$

In the now standard approach one uses the Wilson operator-product expansion [3] for the product of two electromagnetic currents near the light-cone to write (schematically):

$$J_\mu(z/2) J_\nu(-z/2) = \sum_{i,n} C_n^i(z^2, q) \mathcal{O}_{\mu\nu\mu_1 \dots \mu_n}^i z^{\mu_1} \dots z^{\mu_n} \quad , \quad (2.1.7)$$

where  $n$  labels the spin of the operator and  $i$  the type of operator, for the sake of simplicity all kinematical details have been suppressed. Near the light-cone this expansion is dominated by the terms most singular in the limit  $z \rightarrow 0$ , these come from the operators of lowest twist,  $\tau = \text{dimension-spin}$  (spin here refers to the number of derivatives or equivalently free indices contained in the operator).

As in the spin-averaged case the leading operator governing the  $Q^2$  behaviour of  $\mathcal{G}_1$  is of twist two. It is infact simply the axial counterpart to the usual operator:

$$\begin{aligned} \mathcal{O}_F^{S,n} &= i^{n-1} \bar{\Psi} \gamma^{\mu_1} \mathcal{D}^{\mu_2} \dots \mathcal{D}^{\mu_n} \Psi, \\ \mathcal{O}_F^{A,n} &= i^{n-1} \bar{\Psi} \gamma_5 \gamma^{\mu_1} \mathcal{D}^{\mu_2} \dots \mathcal{D}^{\mu_n} \Psi, \end{aligned} \quad (2.1.8)$$

where symmetrisation over  $\mu_1 \dots \mu_n$  and removal of traces is understood the indices S and A indicate the operators governing the symmetric and antisymmetric parts of  $W_{\mu\nu}$  respectively while the suffix F indicates the fermion sector. Including the singlet sector one also has the following twist-two gluonic operators.

$$\begin{aligned} \mathcal{O}_G^{S,n} &= i^{n-1} F^{\mu_1 \alpha} \mathcal{D}^{\mu_2} \dots \mathcal{D}^{\mu_{n-1}} F^{\mu_n \alpha}, \\ \mathcal{O}_G^{A,n} &= i^{n-1} \epsilon^{\mu_1 \alpha \beta \gamma} F_{\beta \gamma} \mathcal{D}^{\mu_2} \dots \mathcal{D}^{\mu_{n-1}} F^{\mu_n \alpha}. \end{aligned} \quad (2.1.9)$$

For clarity explicit details will be given for the non-singlet sector the extension to the singlet operators being fairly straightforward and well documented in the literature.

First one introduces the electromagnetic current correlation function

$$T_{\mu\nu}(p, q, s) = i \int d^4z e^{iq \cdot z} \langle p, s | T(J_\mu(z/2) J_\nu(-z/2)) | p, s \rangle, \quad (2.1.10)$$

related to  $W_{\mu\nu}$  by

$$W_{\mu\nu} = \frac{1}{\pi} \text{Im} T_{\mu\nu} \quad (2.1.11)$$

then on substituting (2.1.7) into (2.1.10) one obtains

$$\begin{aligned} T_{\mu\nu} &= \left[ \text{terms symmetric under } \mu \leftrightarrow \nu \right] \\ &+ i h \epsilon_{\mu\nu\rho\sigma} \frac{q^\rho p^\sigma}{p \cdot q} \sum_{n, \text{ odd}} \left(\frac{1}{2x}\right)^n \tilde{C}_n^{A,i}(Q^2, g) a_n^{A,i} \end{aligned} \quad (2.1.12)$$

where the  $\tilde{C}_n^{A,i}(Q^2, g)$  are related to the Fourier transforms of the coefficients in the expansion (2.1.7) and the  $a_n^{A,i}$  are unknown constants defined by

$$\langle p,s | \mathcal{O}_i^{A,n} | p,s \rangle = a_n^{A,i} h p^{\mu_1} \dots p^{\mu_n} (s^\mu = h p^\mu / M), \quad (2.1.13)$$

for  $i = F$  or  $G$ .

Equation (2.1.12) is then converted into moment sum-rules for the structure function  $\mathcal{G}_1$ :

$$\mathcal{G}_1^{(n)}(Q^2) \equiv \int_0^1 dx x^{n-1} \mathcal{G}_2(x, Q^2) = \sum_i a_n^{A,i} \tilde{C}_n^{A,i}(Q^2, g) \quad (n \text{ odd}) . \quad (2.1.14)$$

As is well known the coefficient functions  $C_n^{iA}$  obey the renormalisation group equation [4]

$$\left( \mu \frac{\partial}{\partial \mu} + \beta(g) \frac{\partial}{\partial g} \right) \tilde{C}_n^{A,i}(Q^2, g) = \sum_j \gamma_{ij}^{(n)} \tilde{C}_n^{A,j}(Q^2, g), \quad (2.1.15)$$

where  $\mu$  is the mass scale introduced by the renormalisation procedure. The anomalous dimensions  $\gamma_{ij}^{(n)}$  are obtained from the renormalisation matrix for the operators in question, in dimensional regularisation they are just the coefficients of the  $1/\epsilon$  poles. To compute the  $\gamma^{(n)}$  matrix to lowest order in  $g$  it is necessary to evaluate the graphs of fig. 2.1.1 and extract the logarithmically divergent pieces. The calculations are somewhat tedious, particularly in the gluon sector, the rules for the vertex insertions may be found in ref. [5], where in fact full calculations were performed.

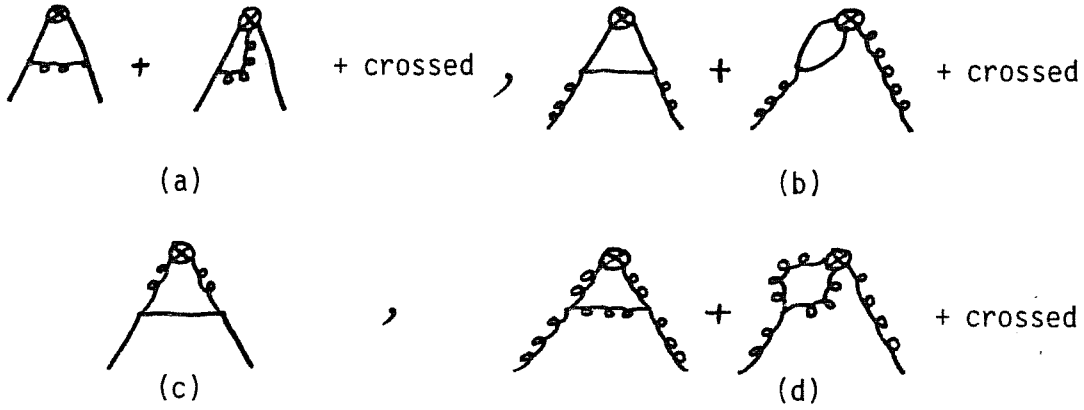


Fig. 2.1.1 - The diagrams to evaluate (a)  $\gamma_{FF}^{(n)}$ , (b)  $\gamma_{FG}^{(n)}$ , (c)  $\gamma_{GF}^{(n)}$ , (d)  $\gamma_{GG}^{(n)}$ .

N.B. For the diagonal elements one must also include the terms corresponding to the wave-function renormalisation of the legs.

Defining the perturbative expansion of the anomalous dimensions by

$$\gamma(g) = \gamma^{(n)} \frac{g^2}{16\pi^2} + O(g^4), \quad (2.1.16)$$

one then obtains for the operator  $\mathcal{O}^A$  [5]:

$$\gamma_{FF}^{(n)} = 2C_2(R) \left\{ 1 - \frac{2}{n(n+1)} + \sum_{j=2}^n \frac{4}{j} \right\}, \quad (2.1.17a)$$

$$\gamma_{FG}^{(n)} = -2T(R) \frac{4(n-1)}{n(n+1)}, \quad (2.1.17b)$$

$$\gamma_{GF}^{(n)} = -2C_2(R) \frac{2(n+2)}{n(n+1)}, \quad (2.1.17c)$$

$$\gamma_{GG}^{(n)} = 2 \left\{ C_2(A) \left[ \frac{1}{3} - \frac{8}{n(n+1)} + \sum_{j=2}^n \frac{4}{j} \right] + \frac{4}{3} T(R) \right\}. \quad (2.1.17d)$$

Since only the diagonalised form of  $\gamma_{ij}$  has any physical meaning  $\gamma_{FG}$  and  $\gamma_{GF}$  are not individually uniquely defined, however their product is, and it is only this quantity which should be compared between different calculations.

The solution of the renormalisation group equation [4] (2.1.15) then gives the leading high-energy behaviour for the moments of the non-singlet structure function as

$$\mathcal{G}_1^{(n)}(Q^2) = \mathcal{G}_1^{(n)}(Q_0^2) \left[ \frac{\alpha_s(Q^2)}{\alpha_s(Q_0^2)} \right]^{-\gamma_{FF}^{(n)}/2\beta_0}, \quad (2.1.18)$$

with the usual well-known extension to the flavour singlet case, where operator mixing occurs and diagonalisation of the mixing matrix is necessary.

Of particular significance is the identical high-energy behaviour of the non-singlet structure functions  $\mathcal{F}_2$  and  $\mathcal{G}_1$ . In the Wilson expansion approach this is seen to arise owing to the similarity of the two operators, see eqn. (2.1.8), and the fact that the  $\gamma_5$  plays no part in the calculation of the anomalous dimensions. In the next section, dealing with the intuitive approach of Alarelli and Parisi [6], we shall see how this is explained more physically in terms of helicity conservation.

## 2.2 Intuitive approach

The intuitive approach of Altarelli and Parisi [6] based on the parton model description of deep-inelastic scattering quite naturally includes spin. Indeed in addition to the more physically appealing picture it provides of high energy collisions the significance of the results of the previous section is made clear.

In this approach one considers directly the distribution of partons in the infinite-momentum frame thus  $q_+^i(x)$  and  $q_-^i(x)$  denote the number density of quarks of flavour  $i$  carrying a fraction  $x$  of the parent hadron momentum and having respectively positive and negative helicities as compared with the parent. Forming the sum and difference we then have the usual spin-averaged density:

$$q^i(x) = q_+^i(x) + q_-^i(x) , \quad (2.2.1)$$

and the helicity correlated density:

$$\Delta q^i(x) = q_+^i(x) - q_-^i(x) , \quad (2.2.2)$$

we have in the naïve parton model the following relationship to the structure functions [7]

$$\begin{aligned} \mathcal{F}_1(x) &= \mathcal{F}_2(x) = \sum_i e_i^2 q^i(x) , \\ \mathcal{G}_1(x) &= \sum_i e_i^2 \Delta q^i(x) , \end{aligned} \quad (2.2.3)$$

where the sum over  $i$  runs through quark and antiquark flavours,  $e_i$  is the charge of the  $i$ th quark in units of the proton charge.

Differentiating the equivalent of (2.1.18) for  $\mathcal{F}_2$  with respect to  $t = \ln(Q^2/Q_0^2)$  and inverting the moments one arrives at the following integro-differential equations for the non-singlet density:

$$\frac{dq^{NS}(x,t)}{dt} = \frac{\alpha(t)}{2\pi} \int_x^1 \frac{dy}{y} q^{NS}(y,t) P_{NS}(x/y) , \quad (2.2.4)$$



where  $P_{NS}(z)$  is defined by

$$\int_0^1 dz z^{n-1} P_{NS}(z) = -\frac{1}{4} \gamma_{NS}^n, \quad (2.2.5)$$

and is interpreted as the variation per unit  $t$  of the probability of finding a quark inside another with fraction  $z$  of the parent momentum. This can be calculated as the branching kernel represented diagrammatically in Fig. 2.2.1.

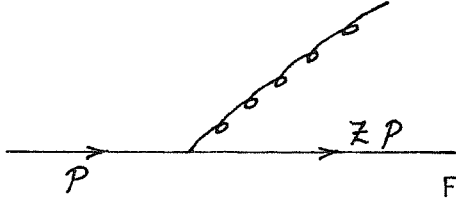


Fig. 2.2.1 Branching kernel.

The extension to spinning flavour-singlet densities using kernels representing the probability of finding quarks and gluons inside quarks and gluons and carrying fraction  $z$  of the parent momentum and having the same or opposite helicity leads to the series of integro-differential equations:

$$\begin{aligned} \frac{d}{dt} q_+^i(x, t) = \frac{\alpha(t)}{2\pi} \int_x^1 \frac{dy}{y} \left[ q_+^i(y, t) P_{qq}^{++}\left(\frac{x}{y}\right) + q_-^i(y, t) P_{qq}^{+-}\left(\frac{x}{y}\right) \right. \\ \left. + g_+(y, t) P_{qg}^{++}\left(\frac{x}{y}\right) + g_-(y, t) P_{qg}^{+-}\left(\frac{x}{y}\right) \right], \quad (2.2.6) \end{aligned}$$

etc.,

where  $g(y, t)$  are the gluon densities and  $P_{ab}^{ij}$  is the probability of finding parton  $a$  with helicity  $i$  inside parton  $b$  with helicity  $j$ .

Parity conservation in QCD implies the relations:

$$P_{ab}^{+\pm}(z) = P_{ab}^{-\mp}(z), \quad (2.2.7)$$

thus, forming the sums and differences:

$$\begin{aligned} P_{ab} &= P_{ab}^{++} + P_{ab}^{+-}, \\ \Delta P_{ab} &= P_{ab}^{++} - P_{ab}^{+-}, \end{aligned} \quad (2.2.8)$$

the sums and differences of eqns.(2.2.6) lead to the master equations for the  $Q^2$  - evolution of the various parton densities:

$$\frac{d}{dt} \Delta q^i(x,t) = \frac{\alpha(t)}{2\pi} \int_x^1 \frac{dy}{y} \left[ \Delta q^i(y,t) \Delta P_{qq}(\frac{x}{y}) + \Delta g(y,t) \Delta P_{qg}(\frac{x}{y}) \right], \quad (2.2.9)$$

$$\frac{d}{dt} \Delta g(x,t) = \frac{\alpha(t)}{2\pi} \int_x^1 \frac{dy}{y} \left[ \Delta g(y,t) \Delta P_{gg}(\frac{x}{y}) + \sum_{i=1}^{2f} \Delta q^i(y,t) \Delta P_{gq}(\frac{x}{y}) \right],$$

with the corresponding equations for the spin-averaged case being obtained by removal of the  $\Delta$  symbol.

These equations afford the simplest numerical approach to the  $Q^2$  -evolution of parton densities. Data at a given value of  $Q^2 = Q_0^2$  (large enough to be in the region of validity of perturbative QCD) provides the densities as boundary conditions or input for the numerical integration of the above equations from which the densities at any other (large) value of  $Q$  may be obtained. For more practical details see appendix 4.

The various branching kernels  $P_{ab}^{ij}$  have all been calculated by Altarelli and Parisi, these are now listed, beginning with the non-singlet sector. For quarks fragmenting into quarks one has:

$$P_{qq}^{-+}(z) = 0, \\ P_{qq}^{++}(z) = P_{qq}(z) = \Delta P_{qq}(z) = C_2(R) \left( \frac{1+z^2}{1-z} \right)_+. \quad (2.2.10)$$

The + regularisation of infra-red singularities is defined as usual by

$$\int_0^1 dz f(z) (k(z))_+ = \int_0^1 dz (f(z) - f(1)) k(z), \quad (2.2.11)$$

where  $f(z)$  is any test function sufficiently regular at the end points.

The reason for the identical  $Q^2$  -evolution of the spin-averaged and spin-correlated density in the quark sector is now clear; the vertex of Fig.2.2.1, in the limit of zero-mass quarks (or in the limit  $m^2/Q^2 \rightarrow 0$ ), is helicity conserving and thus  $P_{qq}^{-+}$  vanishes. This point is discussed in section 3.1.

The remaining kernels are, for quarks fragmenting into gluons:

$$P_{gq}^{++} = C_2(R) \frac{1}{z} \quad , \quad P_{gq}^{-+} = C_2(R) \frac{(1-z)^2}{z} \quad ,$$

thus

$$P_{gq} = C_2(R) \frac{1+(1-z)^2}{z} \quad , \quad \Delta P_{gq} = C_2(R) (2-z) \quad . \quad (2.2.12)$$

For gluons fragmenting into quarks:

$$P_{qg}^{++} = \frac{1}{2} z^2 \quad , \quad P_{qg}^{-+} = \frac{1}{2} (1-z)^2$$

thus

$$P_{qg} = \frac{1}{2} [z^2 + (1-z)^2] \quad , \quad \Delta P_{qg} = \frac{1}{2} (2z-1) \quad . \quad (2.2.13)$$

And finally the purely gluonic sector:

$$P_{gg}^{++} = C_2(A) (1+z^4) \left[ \frac{1}{z} + \frac{1}{(1-z)_+} \right] + \left[ \frac{11}{6} C_2(A) - \frac{2}{3} T(R) \right] \delta(1-z) \quad ,$$

$$P_{gg}^{-+} = C_2(A) \frac{(1-z)^3}{z} \quad ,$$

thus

$$P_{gg} = 2 C_2(A) \left[ \frac{z}{(1-z)_+} + \frac{1-z}{z} + z(1-z) \right] + \left[ \frac{11}{6} C_2(A) - \frac{2}{3} T(R) \right] \delta(1-z) \quad ,$$

$$\Delta P_{gg} = 2 C_2(A) \left[ \frac{z}{(1-z)_+} + 2(1-z) \right] + \left[ \frac{11}{6} C_2(A) - \frac{2}{3} T(R) \right] \delta(1-z) \quad . \quad (2.2.14)$$

Taking moments with respect to  $z$  of these kernels one readily obtains the anomalous dimensions given in the previous section.

Although intuitive and not totally rigorous this approach finds its justification in the more complete diagrammatic methods based on ladder diagram summation [8] or factorisation of mass singularities [9] in planar or light-like axial gauge. Here the branching kernel is given by two-particle-irreducible ladder rungs as in Fig. 2.2.2.

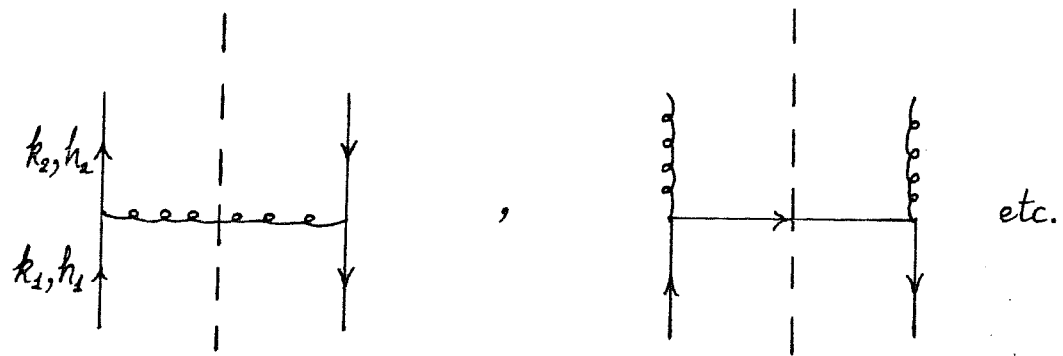


Fig. 2.2.2 Examples of two-particle irreducible kernels.

Dressing the vertices and propagators makes the coupling constant in the evolution equations run [8,9]

## References to Chapter 2

- [1] J.D. Bjorken, Phys. Rev. 179, 1547 (1969).
- [2] O. Nachtmann, Nucl. Phys. B63, 237 (1973).
- [3] K. Wilson, Phys. Rev. 179, 1499 (1969).  
N. Christ, B. Hasslacher and A.H. Mueller, Phys. Rev. D6, 3543 (1972).  
A.H. Mueller, Phys. Rev. D9, 963 (1974).
- [4] M. Gell-Mann and F. Low, Phys. Rev. 95, 1300 (1954).  
E.C.G. Stueckelberg and A. Peterman, Helv. Phys. Acta 26, 499 (1953).  
D.J. Gross in Methods in Field Theory, Les Houches 1975, (ed. R. Balian and J. Zinn-Justin, North Holland, Amsterdam), chap. 4.  
H.D. Politzer, Phys. Rep. 14, 129 (1974).
- [5] M. Ahmed and G.G. Ross, Nucl. Phys. B111, 441 (1976).
- [6] G. Altarelli and G. Parisi, Nucl. Phys. B126, 298 (1977).
- [7] R.P. Feynman, Photon-hadron interactions (Benjamin, New York, 1972).  
J. Kogut and L. Susskind, Phys. Rev. 8, 76 (1973).  
A.J.G. Hey and J.E. Mandula, Phys. Rev. D5, 2610 (1972).  
R.L. Heimann, ref [9] to chap. 4.
- [8] Yu. L. Dokshitser, D.I. D'Yakonov and S.I. Troyan, Phys. Rep. 58, 269 (1980).  
N.S. Craigie and H.F. Jones, Nucl. Phys. B172, 59 (1980).  
D. Amati, R. Petronzio and G. Veneziano, Nucl. Phys. B140, 54 (1978);  
B146, 29 (1978).
- [9] R.K. Ellis, H. Georgi, M. Machacek, H.D. Politzer and G.G. Ross, Nucl. Phys. B152, 285 (1979).  
G. Curci, W. Furmanski and R. Petronzio, Nucl. Phys. B175, 27 (1980).

## Chapter 3      The theoretical basis of spin asymmetries

- 3.1    Helicity as a conserved quantum number
- 3.2    Basic partonic scattering processes
- 3.3    Factorisation in QCD
- 3.4    Helicity-dependent parton densities
- 3.5    Asymmetry prediction for semi-inclusive processes

### 3.1 Helicity as a conserved quantum number

The Lagrangian of QCD, equation (3.1.1), contains all the essential qualities of the theory. Let us begin therefore this review of the theoretical basis of the spin properties of hadronic physics by examining the status of spin within the fermionic sector of the QCD Lagrangian:

$$\mathcal{L}_{\text{ferm}} = \bar{\Psi} \not{D} \Psi - m \bar{\Psi} \Psi . \quad (3.1.1)$$

In the high energy limit, where the parton model finds its vindication through perturbative QCD, the above Lagrangian permits of a particularly simple description of the helicity properties of quarks. Transverse-spin dependence is however a rather more complex matter which, in any case, since it is essentially a mass effect, will always be suppressed at high energies ( $E \gg m$ ) with respect to helicity dependence by a factor  $\sim m/E$  where  $m$  is a quark (current) mass and  $E$  a typical energy or momentum transfer. A detailed discussion of transverse spin within the framework of perturbative QCD is given in chapter 7.

Thus neglecting the mass term of (3.1.1) and applying the helicity projectors  $\frac{1}{2}(1 \pm \gamma_5)$  to decompose the quark fields into their left- and right-handed components one obtains a natural separation into the left- and right-handed quark sectors:

$$\lim_{E \gg m} \mathcal{L}_{\text{ferm}} \longrightarrow \bar{\Psi}_L \not{D} \Psi_L + \bar{\Psi}_R \not{D} \Psi_R . \quad (3.1.2)$$

The significance of this is that the two helicity sectors are entirely decoupled at high energies and thus the following two statements become true to all orders of perturbation theory:

i) helicity is conserved along quark lines and

ii) quark-antiquark annihilation occurs solely from opposite helicity states.

In other words the status of helicity is elevated to that of a conserved quantum number such as charge, flavour, lepton number, etc. The fact that these statements

are true to all orders of perturbation theory, which is self-evident from the Lagrangian(3.1.1), means that, provided one can follow a quark line through a hard scattering process, the final helicity will be that of the initial quark independently of how many gluons (hard or soft) are emitted during the process. Of course for intermediate states when the quark may be highly virtual this has no significance.

Non-perturbative effects such as chiral symmetry breaking, confinement etc. will have a bearing on the above statements. However the importance of all such effects will always be suppressed by a factor  $\sim M/E$  where  $M$  is some hadronic mass-scale (e.g. the constituent quark mass or some transverse momentum cut-off).

In terms of helicity asymmetries at the level of partonic hard-scattering cross-sections the implications are simple: one expects spin-spin correlations of the order of 100%. For processes involving initial or final gluons in definite helicity states there is no clear statement, although in the next section we will see from explicit evaluation that the correlations are still very large and often with a strong kinematical dependence.



### 3.2 Basic partonic scattering processes

The driving helicity dependence of hadronic processes in general will come from that of the hard-scattering subprocesses. In this section a complete list of asymmetries is given for QCD partonic cross-sections at large momentum transfers.

In what follows details of individual hard-scattering subprocesses will be given, together with helicity dependent amplitudes - the cross-sections and asymmetries being reported in table 3-I.

#### (a) Quark-quark scattering

For unidentical quark-quark scattering (or equally antiquark-antiquark) the only contribution is from t-channel exchange diagram of Fig. 3.2.1

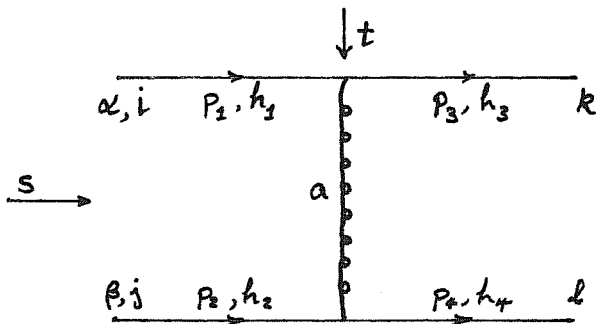


Fig. 3.2.1. The only contribution to unidentical quark scattering.  $\alpha, \beta$  are flavour indices. The colour indices  $i, j, k$ , run from 1 to 3 while  $a$  runs over 1 to 8.

$$M_{\pm}(q_{\alpha} q_{\beta} \rightarrow q_{\alpha} q_{\beta}) = 2ig^2 \delta_{h_1 h_3} \delta_{h_2 h_4} \left[ \delta_{h_1 h_2} \frac{s}{t} + \delta_{h_1 \bar{h}_2} \frac{u}{t} \right] \tau_{ki}^a \tau_{lj}^a. \quad (3.2.1)$$

For identical quarks there is the additional u-channel diagram of Fig. 3.2.2

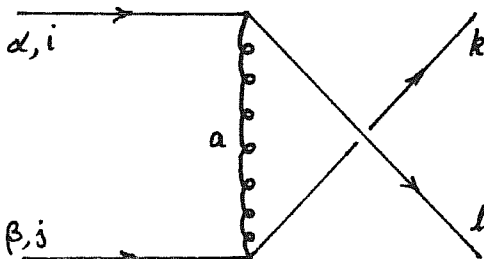


Fig. 3.2.2. Contribution to quark-quark scattering from identical quarks.

$$M_u(q_{\alpha} q_{\alpha} \rightarrow q_{\alpha} q_{\alpha}) = 2ig^2 \delta_{h_1 h_4} \delta_{h_2 h_3} \left[ \delta_{h_1 h_2} \frac{s}{u} + \delta_{h_1 \bar{h}_2} \frac{t}{u} \right] \tau_{li}^a \tau_{kj}^a. \quad (3.2.2)$$

(b) Quark-antiquark scattering

For quark and antiquark of different flavour the only diagram is again a t-channel exchange, see Fig. 3.2.3.

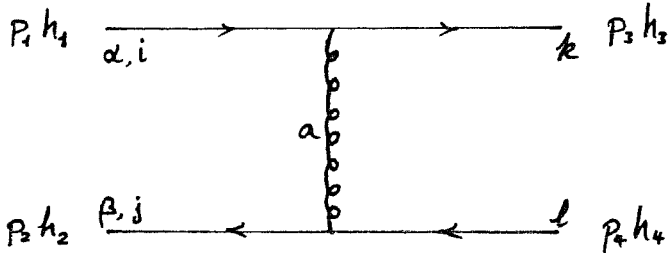


Fig. 3.2.3. Sole contribution to quark antiquark scattering for different flavours.

$$\mathcal{M}_t(q_{\alpha} \bar{q}_{\beta} \rightarrow q_{\alpha} \bar{q}_{\beta}) = 2ig^2 \delta_{h_1 h_3} \delta_{h_2 h_4} \left[ \delta_{h_1 h_2} \frac{s}{t} + \delta_{h_1 \bar{h}_2} \frac{u}{t} \right] \tau_{ki}^a \tau_{jl}^a. \quad (3.2.3)$$

For quark and antiquark of the same flavour there is also the s-channel diagram of Fig. 3.2.4

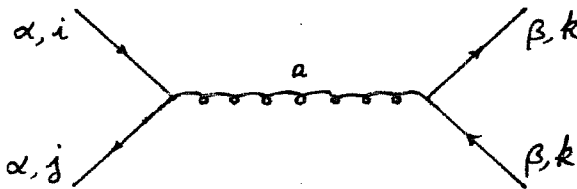


Fig. 3.2.4. Contribution to quark antiquark scattering for identical flavours.

$$\mathcal{M}_s(q_{\alpha} \bar{q}_{\alpha} \rightarrow q_{\beta} \bar{q}_{\beta}) = 2ig^2 \delta_{h_1 \bar{h}_2} \delta_{h_3 \bar{h}_4} \left[ \delta_{h_1 h_3} \frac{u}{s} - \delta_{h_1 \bar{h}_3} \frac{t}{s} \right] \tau_{ji}^a \tau_{kl}^a. \quad (3.2.4)$$

All the above four amplitudes are completely equivalent through crossing. Notice that the vanishing of (for example) the amplitude  $\mathcal{M}_s$  for  $h_1 = h_3$  at  $u = 0$  is consistent with helicity conservation along quark lines and conservation of total angular momentum, however such arguments are not necessarily always reliable as will be seen in the case of quark-gluon scattering.

(c) QCD Compton scattering

For this process all three channels are available and the diagrams are given in Fig. 3.2.5.

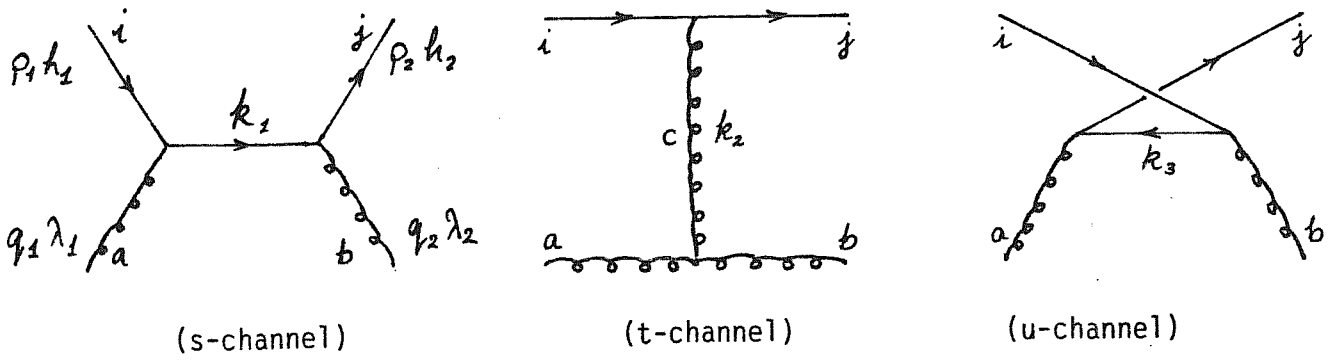


Fig. 3.2.5. Diagrams contributing to quark-gluon (QCD Compton) scattering.

With gauge particles as external states the above amplitudes are separately gauge dependent: however in the full amplitude all gauge dependence disappears.

$$\begin{aligned}
 \mathcal{M}(qg \rightarrow qg) &= \mathcal{M}(\bar{q}g \rightarrow \bar{q}g) \\
 &= -2ig^2 \delta_{h_1 h_2} \delta_{\lambda_1 \lambda_2} \frac{\sqrt{s(-u)}}{(-t)} \left\{ \left[ \delta_{h_1 \lambda_1} + \delta_{h_1 \bar{\lambda}_1} \frac{(-u)}{s} \right] \tau_{jk}^b \tau_{ki}^a \right. \\
 &\quad \left. - \left[ \delta_{h_1 \lambda_1} \frac{s}{(-u)} + \delta_{h_1 \bar{\lambda}_1} \right] \tau_{jk}^a \tau_{ki}^b \right\} \quad (3.2.5)
 \end{aligned}$$

Use has been made, in writing the above expression, of the colour gauge-group algebra (see Appendix A1) in order to write the colour factor of the t-channel diagram in terms of the other two.

Although the amplitude disappears in the backward direction for  $h_1 = -h_2$ , one still requires p-wave scattering in order to conserve total angular momentum for  $h_1 = h_2$ . Thus care must be taken in applying naïve angular-momentum conservation arguments to these scattering processes.

(d) Quark-antiquark annihilation into gluons

This process is related to quark-gluon scattering via crossing and the diagrams, essentially the same, are given in Fig. 3.2.6.

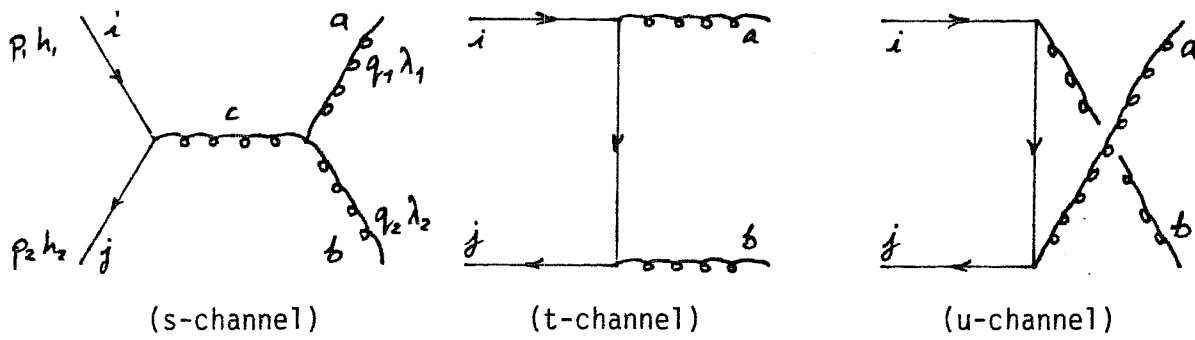


Fig. 3.2.6. Diagram for the process of gluon production via quark-antiquark annihilation.

$$\begin{aligned}
 M_i(q\bar{q} \rightarrow gg) = & 2ig^2 \delta_{h_1\bar{h}_2} \delta_{\lambda_1\bar{\lambda}_2} \left\{ \left[ \delta_{h_1\lambda_1} \frac{u}{t} + \delta_{h_1\bar{\lambda}_1} \right] \tau_{jk}^b \tau_{ki}^a \right. \\
 & \left. - \left[ \delta_{h_1\lambda_1} + \delta_{h_1\bar{\lambda}_1} \frac{t}{u} \right] \tau_{jk}^a \tau_{ki}^b \right\} \frac{\sqrt{tu}}{s} \quad (3.2.6)
 \end{aligned}$$

(e) Gluon fusion into quark-antiquark pair

This, the third of the crossing partners, has the same diagrams as for  $q\bar{q}$ -annihilation and thus the amplitude is identical.

(f) Four-gluon scattering

In this case apart from the usual three channels one also has a contact term coming from the four-point gluon vertex.

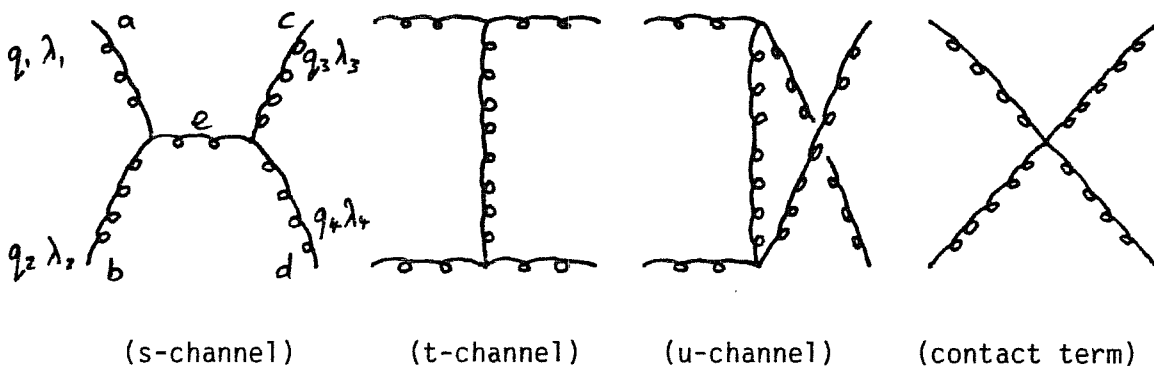


Fig. 3.2.7. Diagrams contributing to the four-gluon interaction process.

$$M(gg \rightarrow gg) = -2ig^2 \left\{ \left[ \delta_{\lambda_1 \lambda_2} \delta_{\lambda_3 \lambda_4} \delta_{\lambda_1 \lambda_4} \left( \frac{s}{-t} \right) + \delta_{\lambda_1 \lambda_2} \left( \delta_{\lambda_1 \lambda_3} \delta_{\lambda_2 \lambda_4} \left( \frac{u}{t} + \frac{u}{s} \right) + \delta_{\lambda_1 \lambda_3} \delta_{\lambda_2 \lambda_4} \left( \frac{-t}{s} \right) \right) \right] \right. \\ \left. \times \begin{matrix} ace & dbe \\ f & f \end{matrix} + \left[ \delta_{\lambda_1 \lambda_2} \delta_{\lambda_3 \lambda_4} \delta_{\lambda_1 \lambda_4} \left( \frac{s}{-u} \right) + \delta_{\lambda_1 \lambda_2} \left( \delta_{\lambda_1 \lambda_3} \delta_{\lambda_2 \lambda_4} \left( \frac{-u}{s} \right) + \delta_{\lambda_1 \lambda_3} \delta_{\lambda_2 \lambda_4} \left( \frac{t}{u} + \frac{t}{s} \right) \right) \right] \begin{matrix} ade & cbe \\ f & f \end{matrix} \right\}. \quad (3.2.7)$$

Here use has been made of the colour group algebra of the adjoint representation to write the colour factor of the contact graph in terms of the other three and then that of the s-channel in terms of the t- and u-channels (see Appendix A1)

Squaring up these amplitudes and considering particular helicity configurations one obtains the various helicity-correlated cross-sections. Table 3-I lists the basic subprocesses, their spin-averaged cross-sections and helicity asymmetries (both reflected [1] and transmitted). The differential cross-section with respect to t is related to the amplitude by

$$\frac{d\sigma}{dt} = \frac{|M|^2}{16\pi s^2}. \quad (3.2.8)$$

TABLE 3 - I

Table of QCD hard-scattering cross-sections and asymmetries. All cross-sections have a common factor of  $\pi \alpha_s / S^2$ .

Process $\vec{a} \vec{b} \rightarrow \vec{c} \vec{d}$	Reflected asymmetry $a^{ii}$	Transmitted asymmetry $a^{if}$
$qq' \rightarrow qq'$	$\frac{d\sigma}{dt} = \frac{4}{9} \left[ \frac{s^2 + u^2}{t^2} \right]$	
	$\frac{s^2 - u^2}{s^2 + u^2}$	1
$qq \rightarrow qq$	$\frac{d\sigma}{dt} = \frac{4}{9} \left[ \frac{s^2 + u^2}{t^2} + \frac{s^2 + t^2}{u^2} - \frac{2}{3} \frac{s^2}{tu} \right]$	
	$\frac{(2 \frac{s^2}{tu} - 3)}{(3 \frac{s^2}{tu} - 1)(\frac{s^2}{tu} - 3)}$	$\frac{[3 \frac{s^4}{tu^2} - 10 \frac{s^2}{tu} + 3 - 3 \frac{t^2}{u^2}]}{(3 \frac{s^2}{tu} - 1)(\frac{s^2}{tu} - 3)}$

Process $\vec{a}\vec{b} \rightarrow \vec{c}\vec{d}$	Reflected asymmetry $a^{ii}$	Transmitted asymmetry $a^{if}$
$q\bar{q}' \rightarrow q\bar{q}'$	$\frac{d\sigma}{dt} = \frac{4}{9} \left[ \frac{s^2+u^2}{t^2} \right]$	
	$\frac{\left(\frac{s^2-u^2}{t^2}\right) - \left(\frac{t^2+u^2}{s^2}\right)}{\left(\frac{s^2+u^2}{t^2}\right) + \left(\frac{t^2+u^2}{s^2}\right)}$	1
$q\bar{q} \rightarrow q'\bar{q}'$	$\frac{d\sigma}{dt} = \frac{4}{9} \left[ \frac{t^2+u^2}{s^2} \right]$	
	-1	$\frac{u^2-t^2}{u^2+t^2}$
$q\bar{q} \rightarrow q\bar{q}$	$\frac{d\sigma}{dt} = \frac{4}{9} \left[ \frac{s^2+u^2}{t^2} + \frac{t^2+u^2}{s^2} - \frac{2}{3} \frac{u^2}{st} \right]$	
	$\frac{\left[\frac{s^2-u^2}{t^2} - \frac{u^2+t^2}{s^2} + \frac{2}{3} \frac{u^2}{st}\right]}{\left[\frac{s^2+u^2}{t^2} + \frac{u^2+t^2}{s^2} - \frac{2}{3} \frac{u^2}{st}\right]}$	$\frac{\left[\frac{s^2+u^2}{t^2} + \frac{u^2-t^2}{s^2} - \frac{2}{3} \frac{u^2}{st}\right]}{\left[\frac{s^2+u^2}{t^2} + \frac{u^2+t^2}{s^2} - \frac{2}{3} \frac{u^2}{st}\right]}$
$qq \rightarrow qq$ $\bar{q}\bar{q} \rightarrow \bar{q}\bar{q}$	$\frac{d\sigma}{dt} = \frac{s^2+u^2}{t^2} \left[ 1 + \frac{4}{9} \frac{t^2}{(-su)} \right]$	
	$\frac{s^2-u^2}{s^2+u^2}$	1
$q\bar{q} \rightarrow gg$	$\frac{d\sigma}{dt} = \frac{32}{27} \left[ \frac{t}{u} + \frac{u}{t} \right] \left[ 1 - \frac{9}{4} \frac{tu}{s^2} \right]$	
	-1	$\frac{u^2-t^2}{u^2+t^2}$
$gg \rightarrow q\bar{q}$	$\frac{d\sigma}{dt} = \frac{1}{6} \left[ \frac{t}{u} + \frac{u}{t} \right] \left[ 1 - \frac{9}{4} \frac{tu}{s^2} \right]$	
	-1	$\frac{u^2-t^2}{u^2+t^2}$
$gg \rightarrow gg$	$\frac{d\sigma}{dt} = \frac{9}{4} \left( \frac{s^2}{tu} \right)^2 \left( 1 - \frac{tu}{s^2} \right)^3$	
	$\frac{(2s^2-tu)tu}{(s^2-tu)}$	$\frac{s^3(us-t^2)(us-2t^2)}{t(s^2-tu)^3}$

A further set of subprocesses with a similar, simple yet striking, helicity dependence is obtained by substituting one (or even two) of the gluons of the previous processes with a photon (or photons). For completeness listed here are the processes of photoproduction and prompt-photon production.

(a) Photon-quark scattering

This process is similar to the QCD Compton scattering already discussed, although now no t-channel is available. The diagrams are given in Fig. 3.2.8.

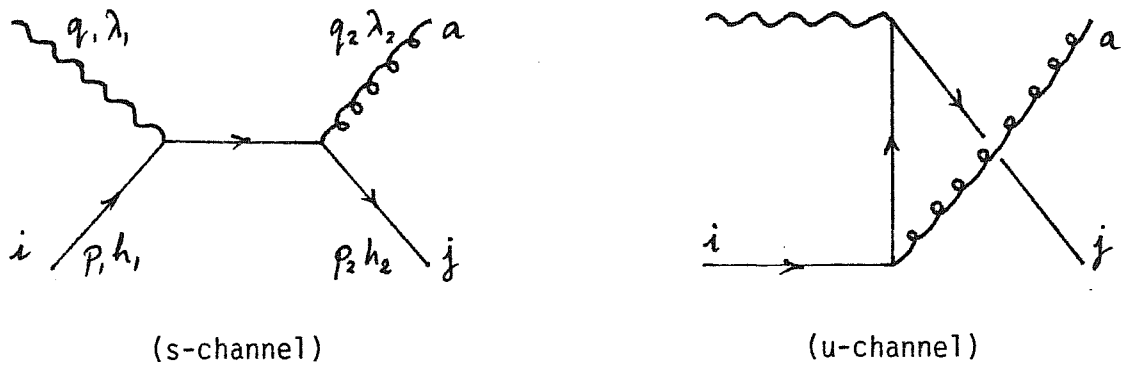


Fig. 3.2.8

$$\mathcal{M}(\gamma q \rightarrow g q) = -2i e_q e g \delta_{h_1 h_2} \delta_{\lambda_1 \lambda_2} \left[ \delta_{h_1 \lambda_1} \sqrt{\frac{s}{-u}} + \delta_{h_1 \lambda_1} \sqrt{\frac{-u}{s}} \right] \tau_{ji}^a, \quad (3.2.9)$$

where  $e_q$  is the charge in units of the proton charge of the quark concerned. The effect of having a photon in the final state in place of the gluon is to replace  $g \tau_{ij}^a$  by  $e_q$ .

(b) Photon-gluon scattering

To the same order one also has photon-gluon interactions via production of a  $q\bar{q}$  pair, this is related to the above scattering through crossing and the relevant diagrams are given in Fig. 3.2.10.

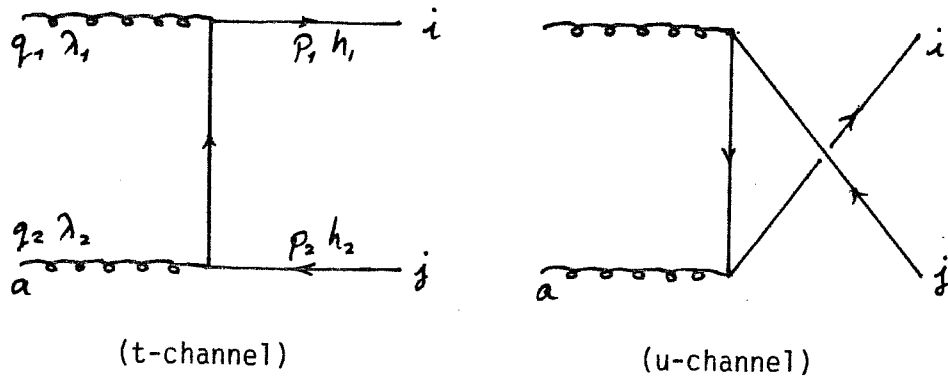


Fig. 3.2.9.

$$M(\gamma q \rightarrow q \bar{q}) = 2ie_2 e q \delta_{h_1 \bar{h}_2} \delta_{\lambda_1 \bar{\lambda}_2} [\delta_{h_1 \lambda_1} \sqrt{\frac{u}{t}} + \delta_{h_1 \bar{\lambda}_1} \sqrt{\frac{t}{u}}] \tau_{ij}^a. \quad (3.2.10)$$

Again the amplitude for the corresponding photon-photon process is obtained by replacing  $gt_{ij}^a$  with  $e_q$ .

The amplitudes for the corresponding processes with the photon in the final state are of course identical to those given. The full set of cross-sections and asymmetries are reported in Table 3-II below.

Note that since there is always a channel with an asymmetry of  $\pm 1$  the asymmetries not given here ( $\vec{q}g \rightarrow \vec{\gamma}q$  for example) can be obtained from those given. For example,  $a^{if}(\vec{q}g \rightarrow \vec{\gamma}q) = a^{ii}(\vec{q}g \rightarrow q\gamma)$ .



TABLE 3-II

Table of hard-scattering cross-section and asymmetries for processes involving photons. Single-photon processes have a common factor of  $\pi e_q^2 \alpha_s / s^2$  and the two-photon processes  $3/8 \pi e_q^4 \alpha_s^2 / s^2$  [2].

Process $\vec{a}\vec{b} \rightarrow \vec{c}\vec{d}$	Reflected asymmetry $a^{ii}$	Transmitted asymmetry $a^{if}$
$\gamma q \rightarrow gq$	$\frac{d\sigma}{dt} = \frac{16}{9} \left[ \frac{s}{(-u)} + \frac{(-u)}{s} \right]$	
	$\frac{s^2 - u^2}{s^2 + u^2}$	1
$\gamma g \rightarrow q\bar{q}$	$\frac{d\sigma}{dt} = \frac{2}{3} \left[ \frac{t}{u} + \frac{u}{t} \right]$	
	-1	$\frac{u^2 - t^2}{u^2 + t^2}$
$gq \rightarrow \gamma q$	$\frac{d\sigma}{dt} = \frac{2}{9} \left[ \frac{s}{(-u)} + \frac{(-u)}{s} \right]$	
	$\frac{s^2 - u^2}{s^2 + u^2}$	1
$q\bar{q} \rightarrow \gamma g$	$\frac{d\sigma}{dt} = \frac{16}{27} \left[ \frac{t}{u} + \frac{u}{t} \right]$	
	-1	$\frac{u^2 - t^2}{u^2 + t^2}$

### 3.3 Factorisation in QCD

The kinematical details (including helicity dependence) of the subprocesses discussed in the previous section are transmitted to the level of the hadronic process via the factorisation theorem (or more correctly conjecture) of perturbative QCD [3]. In the lowest order this simply corresponds to the parton model picture in which any inclusive hard hadronic process can be described as in Fig. 3.3.1.

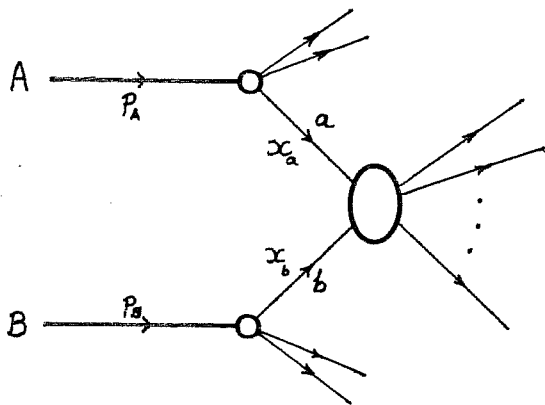


Fig. 3.3.1. Schematic representation of factorisation. The small blobs represent the fragmentation of hadrons A and B into quarks a and b respectively, the large blob represents the hard scattering process.

This amplitude squared corresponds schematically to the factorised cross-section

$$\sigma^{AB} = \int dx_a dx_b D_A^a(x_a) D_B^b(x_b) \hat{\sigma}^{ab}, \quad (3.3.1)$$

where  $D_A^a(x_a)$  is the usual probability of finding a parton of type a inside hadron A with fraction  $x_a$  of its momentum and  $\hat{\sigma}^{ab}$  is the relevant subprocess cross-section. A sum over parton types a,b is understood. The extension to semi-inclusive processes (where one triggers on one or more final state particles) is achieved by the inclusion of fragmentation functions,  $\bar{D}_C^c(x_c)$ , describing the fragmentation of a final parton of type c into a hadron C with fraction  $x_c$  of the parton momentum.

Within the framework of perturbative QCD, factorisation remains only a conjecture since a complete proof would require a knowledge of the details of the hadronic bound state (the quark distributions are non-perturbative in origin). Some of the difficulties (spectator interactions, non-cancellation of infra-red

singularities etc.) are discussed in chapter 5, here however these problems will be ignored.

In analogy to the treatment of deep-inelastic scattering discussed in chapter 2, one assumes that the effects of renormalisation can be accounted for in term of anomalous dimensions governing the  $Q^2$  behaviour (which should be common to all processes) and a coefficient function which is process dependent). The  $Q^2$  dependence is factored off into the various partonic channels leading to  $Q^2$ -dependent (and hopefully process independent) distribution and fragmentation functions, while the coefficient function must be calculated for each process separately. To leading-logarithmic order the effect of this is simply to replace  $a_s$  by  $a_s(Q^2)$  the running coupling constant and  $D_A^a(x_a)$  by  $D_A^a(x_a, Q^2)$  the scale-breaking distribution functions.

At next-to-leading-logarithmic order one must also introduce a process dependent coefficient function which is known to provide large corrections ( $\sim 100\%$ )

[4] to the Drell-Yan process for example. Such corrections could, in principle, have a drastic effect on spin asymmetries, however (as shown in chapter 5) for some processes these large effects actually cancel in an asymmetry and may thus be neglected. Thus in general the leading-logarithmic approximation will be adopted in this and other chapters.

To include a spin-dependent description of any process is a straightforward matter [1] considering particular helicity channels one may write schematically:

$$d\sigma^{++} = \int [dx] \left[ D_{A_+}^{a_+} D_{B_+}^{b_+} d\hat{\sigma}^{++} + D_{A_+}^{a_-} D_{B_+}^{b_+} d\hat{\sigma}^{-+} \right. \\ \left. + D_{A_+}^{a_+} D_{B_+}^{b_-} d\hat{\sigma}^{-+} + D_{A_+}^{a_-} D_{B_+}^{b_-} d\hat{\sigma}^{--} \right], \quad (3.3.2)$$

and similarly for  $d\sigma^{+-}$  etc. Taking the relevant sums and differences, in terms of the helicity transfer densities of chapter 2 and the helicity correlated cross-section defined above, including also the  $Q^2$  dependence one obtains the following expressions for the helicity-dependent cross-sections (the corresponding spin-averaged expression being obtained by removal of the  $\Delta$  symbol)

for the semi-inclusive process  $AB \rightarrow CX$ , i.e. triggering on a final particle C:

$$E_C \frac{d\Delta\sigma}{d^3\vec{p}_C}(\vec{AB} \rightarrow CX) = \sum_{ab \rightarrow cd} \int_0^1 dx_a dx_b \frac{dx_c}{x_c^2} \frac{\hat{s}}{\pi} \delta(\hat{s} + \hat{t} + \hat{u}) \Delta D_A^a(x_a, Q^2) \Delta D_B^b(x_b, Q^2) \bar{D}_C^c(x_c, Q^2) \frac{d\Delta\hat{\sigma}}{d\hat{t}}(\vec{ab} \rightarrow cd), \quad (3.3.3)$$

for the reflected (initial-initial) helicity correlated cross-section and (in a similar fashion):

$$E_C \frac{d\Delta\sigma}{d^3\vec{p}_C}(\vec{AB} \rightarrow \vec{CX}) = \sum_{ab \rightarrow cd} \int_0^1 dx_a dx_b \frac{dx_c}{x_c^2} \frac{\hat{s}}{\pi} \delta(\hat{s} + \hat{t} + \hat{u}) \Delta D_A^a(x_a, Q^2) D_B^b(x_b, Q^2) \Delta \bar{D}_C^c(x_c, Q^2) \frac{d\Delta\hat{\sigma}}{d\hat{t}}(\vec{ab} \rightarrow \vec{cd}), \quad (3.3.4)$$

for the transmitted (initial-final) helicity correlated cross-section. The subprocess Mandelstam variables  $\hat{s}, \hat{t}, \hat{u}$  are related to those for the hadronic process by

$$\hat{s} = x_a x_b s, \quad \hat{t} = \frac{x_a}{x_c} t, \quad \hat{u} = \frac{x_b}{x_c} u. \quad (3.3.5)$$

The scale,  $Q^2$ , at which the distributions and running coupling constant should be taken is not determined at this order, its precise value being fixed by higher order corrections. Among various possible choices are  $(\hat{s} \hat{t} \hat{u})^{1/3}$  and  $2\hat{s}\hat{t}\hat{u}/(\hat{s}^2 + \hat{t}^2 + \hat{u}^2)$  although many others are possible [5,6].

If one now defines a quantity  $\lambda(x)$  by

$$\lambda(x) = \Delta D(x) / D(x), \quad (3.3.6)$$

(simply the fractional polarisation of the parton beam with respect to the hadron beam) one can obtain an approximate expression for the hadronic asymmetry given by expression (3.3.3) or (3.3.4) divided by the corresponding spin-averaged cross-section:

$$\mathcal{A} = \frac{d\Delta\sigma^{AB}}{d\sigma^{AB}} \sim \langle \lambda_A^a(x) \rangle \langle \lambda_B^b(x) \rangle \langle a^{ab}(\hat{s}, \hat{t}, \hat{u}) \rangle, \quad (3.3.7)$$

where  $\langle \rangle$  indicates the average value of the quantity with respect to the parton distributions, and  $a^{ab}$  is the relevant reflected or transmitted partonic asymmetry. This of course gives only a very rough guide to the asymmetry one might expect, especially in view of the fact that the  $x$  dependence of  $a^{ab}$  usually implies domination of the hadronic cross-sections by the small  $x$  region.

One sees then that the quantities  $\lambda(x)$  have a depleting effect on the overall asymmetry. It is to these, or more precisely the helicity dependent densities, that, in the next section, we turn our attention, to show in particular that fortunately  $\Delta D \sim D$  and thus  $\lambda \sim 1$ .

### 3.4 Helicity dependent parton densities

The parton model provides us with a picture of hadronic interactions consisting essentially of two elements: a hard scattering cross-section calculable in QCD perturbation theory (listed in sect. 3.2) and non-perturbative partonic densities whose  $Q^2$ -evolution is calculable and which can therefore be extracted from one set of data (i.e. for one process at a given energy) and used as input to make predictions for other processes and energies.

At the present, experimental data on helicity dependent distributions is very limited (the little in existence is discussed in sect. 4.1) and thus in order to evaluate the importance of spin effects one needs a reliable model with which to estimate the partonic spin content of hadrons.

There are numerous models [7,8,9] available for constructing the various partonic distributions, most of which are able to explain only poorly the existing data. In this section the discussion will be restricted to the first three of the above references these being the most popular.

One of the basic ingredients of any model is the Bjorken sum rule [10] which in parton language is expressed in the form

$$\int_0^1 dx [\Delta u(x) - \Delta d(x) + \Delta \bar{u}(x) - \Delta \bar{d}(x)] = |g_A/g_V| \left[ 1 - \frac{\alpha_s}{\pi} + \dots \right], \quad (3.4.1)$$

where  $|g_A/g_V|$  is the ratio of the axial-vector to the vector coupling in neutron  $\beta$ -decay. Since the axial current has no anomalous dimensions ( $n = 1$  moment for  $\mathcal{S}_1$  in eqns. 2.1.16a and 2.1.17) this sum-rule must scale to leading-logarithmic order. This sum rule is derived from very general theoretical arguments. Experimentally the ratio has the value [11]

$$|g_A/g_V| = 1.2546 \pm 0.0063 \quad . \quad (3.4.2)$$

This is a first indication that the magnitude, at least of  $\Delta D_{val}(x)$ , is comparable with that of  $D_{val}(x)$ .

A further constraint is provided by the projection of the z-component

of the total angular momentum:

$$\langle J_z \rangle = \frac{1}{2} = \frac{1}{2} \int_0^1 dx [\Delta V(x) + \Delta \Sigma(x)] + \int_0^1 dx \Delta g(x) + \langle L_z \rangle, \quad (3.4.3)$$

where  $V$  and  $\Sigma$  refer to the sum over valence and sea quarks respectively and  $\langle L_z \rangle$  is the expectation value of the z-component of orbital angular momentum summed over all constituents. Generally one assumes that the proton has  $L = 0$ .

(a) Conservative SU(6) distributions

In the SU(6) model of the proton [1] all of its spin is carried by the valence quarks and thus in the SU(6) limit one has

$$\begin{aligned} \int_0^1 dx \Delta u_v(x) &= \frac{4}{3}, \\ \int_0^1 dx \Delta d_v(x) &= -\frac{1}{3}, \\ \int_0^1 dx \Delta q_{\text{sea}}(x) &= 0. \end{aligned} \quad (3.4.4)$$

This however is in direct conflict with the Bjorken sum rule (3.4.1) since it predicts

$$|g_A/g_V| = \frac{5}{3} \quad (3.4.5)$$

which disagrees with the experimental value.

To resolve this discrepancy the simplest modification is to permit the sea to carry some of the proton spin. By examining the perturbation theory diagrams which lead to generation of the sea (examples in Fig. 3.4.1.) the authors of ref. [1] developed an ansatz for the estimation of the sea polarisation

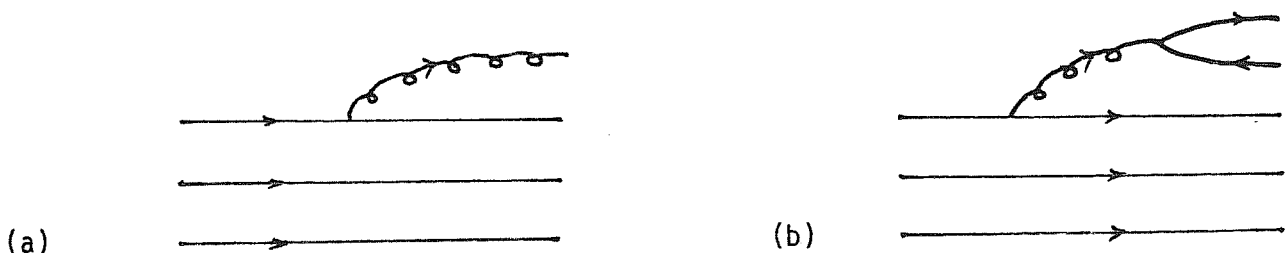


Fig. 3.4.1. (a) Diagram contributing to the gluon content of the sea. (b) Contribution to quark-antiquark sea.

The gluon content of the proton comes from bremsstrahlung off valence quarks, i.e. by diagrams such as Fig. 3.4.1 (a). The helicity of the emitted gluon is then fixed by angular momentum conservation and will therefore be, in particular, a function of the momentum fraction it carries off. In turn, a quark antiquark pair produced by this gluon, through the diagram of Fig. 3.4.1 (b) for example, will also retain a memory of the helicity of the original valence quark. Thus for the parametrisation of the sea one adopts the following

$$\begin{aligned} \lim_{x \rightarrow 1} \bar{q}_{++}(x) &= c (1-x)^n [2 + (1-x)^2], \\ \lim_{x \rightarrow 1} \bar{q}_{+-}(x) &= c (1-x)^n [1 + 2(1-x)^2]. \end{aligned} \quad (3.4.6)$$

Matching the normalisation to the antiquark distributions deduced from massive lepton pair data at  $x = 0.3$  [12] :

$$\bar{q}(x) \approx \frac{0.6}{x} (1-x)^{10}, \quad (3.4.7)$$

one therefore obtains the following simple parametrisations

$$\begin{aligned} \bar{q}_{++}(x) &= \frac{0.13}{x} (1-x)^{10} [2 + (1-x)^2], \\ \bar{q}_{+-}(x) &= \frac{0.13}{x} (1-x)^{10} [1 + 2(1-x)^2], \end{aligned} \quad (3.4.8)$$

and thus the helicity correlated distribution:

$$\Delta \bar{q}(x) = 0.13 (1-x)^{10} (2-x). \quad (3.4.9)$$

The amount of helicity carried by sea quarks and antiquarks is then

$$2 \langle S_z \rangle_q = 2 \times 3 \times \frac{1}{2} \int_0^1 dx \Delta \bar{q}(x) = 0.068. \quad (3.4.10)$$

Using a similar ansatz for the gluon distributions one can use the parameterisation



$$g_{++}(x) = \frac{c'}{x} (1-x)^{n'} [2 + (1-x)^2] ,$$

$$g_{+-}(x) = \frac{c'}{x} (1-x)^{n'} [1 + 2(1-x)^2] . \quad (3.4.11)$$

The normalisation of these distributions is now fixed by the momentum sum rule

$$\int_0^1 dx x g(x) \simeq \frac{1}{2} . \quad (3.4.12)$$

This gives  $c' = 1/6(n'+1)(n'+3)/(2n'+4)$ . In their calculation the authors of ref. [1] took  $n' = 6$  and thus for the gluon densities one obtains

$$g(x) = \frac{1.97}{x} (1-x)^6 [1 + (1-x)^2] , \quad (3.4.13)$$

$$\Delta g(x) = 0.66 (1-x)^6 [2 - x] .$$

Inserting these expressions into the constraint equations (3.4.1) and (3.4.3), assuming  $\Delta u_v(x) \sim u_v(x)$  and  $\Delta d_v(x) \sim d_v(x)$  one obtains:

$$\Delta u_v(x) \simeq 0.44 u_v(x) , \quad (3.4.14)$$

$$\Delta d_v(x) \simeq -0.35 d_v(x) .$$

Of course there will also be other more complicated non-perturbative mechanisms for generating the sea, however the dominance of such effects (excitations of the bag for example) should be restricted to the small  $x$  region so that the gluon bremsstrahlung model outlined above should give a qualitatively correct description for large  $x$ .

Looking at Fig. 3.4.2 we see that while there is rough agreement with experiment there is a tendency to underestimate the data at large  $x$ .

#### (b) Diquark distributions

Another picture, advocated in ref. [9], is given by assuming that, in certain limits, the proton may be treated as a quark-diquark system. Thus at large momentum the isospin and helicity of the proton are carried by the fastest (or leading) quark. Partial experimental support for this idea comes from the

result [ 13 ] .

$$\lim_{x \rightarrow 1} \frac{\nu W_2^{en}}{\nu W_2^{ep}(x)} \approx \frac{1}{4} \quad , \quad (3.4.15)$$

however this hypothesis has still to be tested with respect to spin.

Thus, in the limiting case of this picture, applying the Bjorken and  $\langle J_z \rangle$  sum rule constraints we have

$$\begin{aligned} \Delta u_v(x) &= 0.61 u_v(x) \quad , \\ \Delta d_v(x) &= \Delta q_s(x) = \Delta g(x) = 0 \end{aligned} \quad (3.4.16)$$

The predictions for this model (see Fig. 3.4.2) are in slightly better agreement with the data than the previous model however one really needs more accurate large  $x$  data to discuss seriously the relevance of either model.

#### (c) Carlitz-Kaur distributions

The third and most popular of the models to be discussed here is that developed in refs. [9] . Here the idea is to incorporate the valence quark's "loss of memory" of the parent polarization at small  $x$ , this being due to interactions with the sea.

Let  $\sin^2\theta$  be the probability that a valence quark's helicity will change in interactions with the sea. Then if  $N(x)$  is the relative density of the sea one has

$$\sin^2\theta = \frac{1}{2} H(x) N(x) / [1 + H(x) N(x)] \quad . \quad (3.4.17)$$

Assuming the sea quarks and antiquarks to be unpolarised and that the gluons have a  $(1-x)^2$  fall off, the result is not very sensitive to the power of  $(1-x)$ , one arrives at the following expression

$$H(x) N(x) = H_0 (1-x)^2 / \sqrt{x} \quad , \quad (3.4.18)$$

with  $H_0 = 0.052$  being fixed by the Bjorken sum rule.

The  $\langle J_z \rangle$  sum rule indicates that 11.6% of the proton's helicity is carried by gluons. Thus using the same parametrisation for the gluon distributions as before (see eq. 3.4.9) one obtains the following for the Carlitz-Kaur distributions.

$$\begin{aligned} \Delta u_v(x) &= \left[ u_v(x) - \frac{2}{3} d_v(x) \right] \cos(2\theta) \quad , \\ \Delta d_v(x) &= -\frac{1}{3} \cos(2\theta) d_v(x) \quad , \\ \Delta q_s(x) &= 0 \quad , \\ \Delta g(x) &= 0.43 (1-x)^6 (2-x) \quad . \end{aligned} \tag{3.4.19}$$

where the spin-dilution factor is

$$\cos(2\theta) = \left[ 1 + 0.052 (1-x)^2 / dx \right]^{-1} \quad . \tag{3.4.20}$$

Again the predictions of the model are compared with the ep scattering data [14] in Fig. 3.4.1.

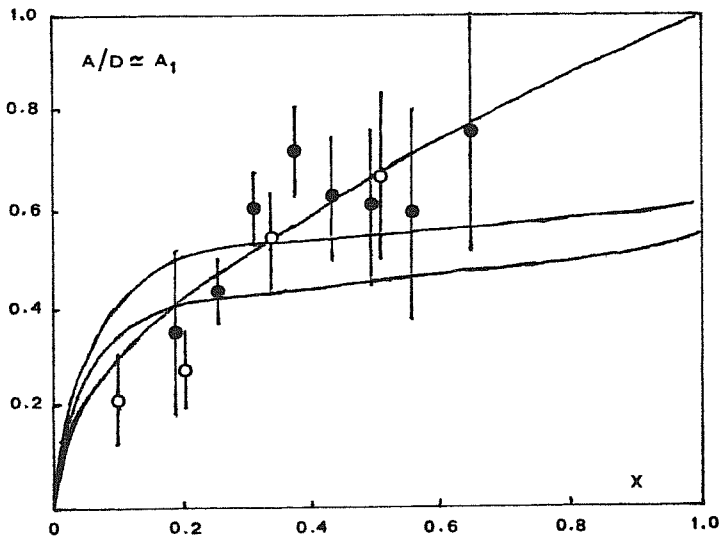


Fig. 3.4.2. Comparison of the SLAC data on polarised ep experiments with the models: (a) SU(6), (b) diquark and (c) Carlitz-Kaur.

### 3.5 Asymmetry predictions for semi-inclusive processes

In this, the final section of chapter three, the basic ingredients as outlined in the previous sections are put together to provide predictions of asymmetries for various semi-inclusive hadronic processes.

The model generally adopted for the helicity correlated densities is that of Carlitz and Kaur, the other models giving similarly shaped asymmetries of rather smaller magnitude. The fragmentation functions used are those of Field and Feynman [8]. The  $Q^2$  evolution of these distributions is discussed in appendix A4.

Let us begin with a comparison of the various models for estimating the spin-dependent parton distributions. A convenient process to choose is  $pp(\bar{p}) \rightarrow \text{jet} + X$ , thus eliminating the inclusion of the final particle fragmentation function (this being simply replaced by a delta-function). In Fig. 3.5.1 the asymmetry  $\alpha_{LL}^{ii}$  for the above reactions is shown plotted against  $x_T$  at  $\vartheta_{CM} = 90^\circ$ .

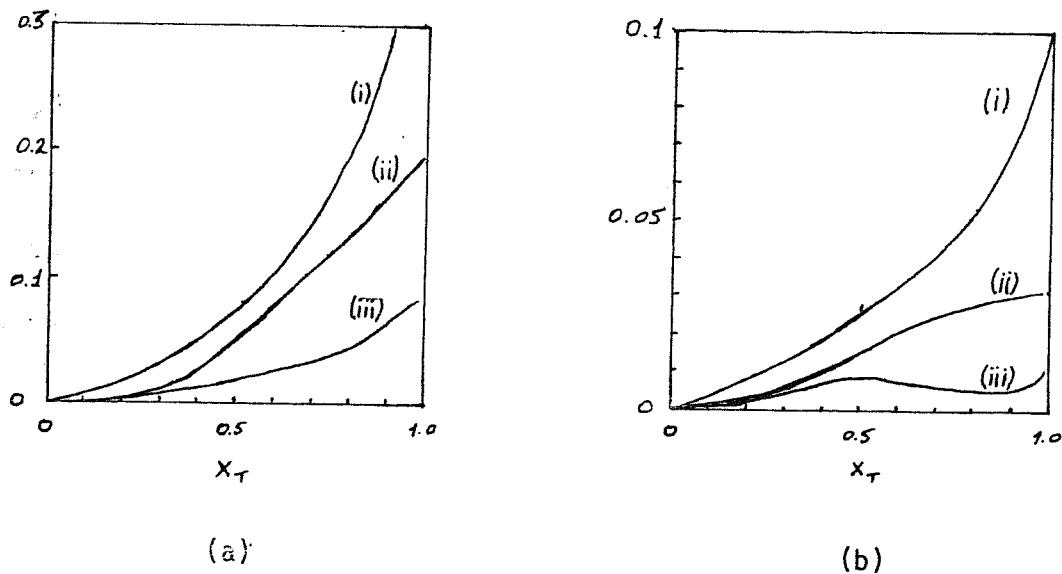


Fig. 3.5.1. Asymmetry  $\alpha_{LL}^{ii}$  for (a)  $pp \rightarrow \text{jet} + X$  and (b)  $pp \rightarrow \text{jet} + X$  as a function of  $x_T$  for distribution models (i) Carlitz-Kaur, (ii) Diquark and (iii) Conservative (taken from [1]).

Thus one sees that the predictions of the Carlitz-Kaur model are generally three or four times larger than the other two models. It is also interesting to consider the relative contributions of the different partonic subprocesses to the total hadronic asymmetry. In all cases for pp scattering at large  $x_T$  the dominant process is  $qq \rightarrow qq$  while for  $p\bar{p}$ ,  $q\bar{q} \rightarrow q\bar{q}$  plays the dominant role and hence the much smaller asymmetry.

In the literature there are many examples of the asymmetry predictions for various high energy processes obtained via relatively straightforward calculations in leading order QCD. Possible corrections to those are discussed in some detail in chapters 5 and 6. Some of the most relevant asymmetries are now listed.

A simple modification of the predictions for jet production allows for the detection of a final state particle, for example a pion. In Fig. 3.5.1 (a) and (b) the asymmetry predictions for pp and  $p\bar{p} \rightarrow \pi^0 X$  respectively are plotted. The large difference in the curves for pion- and jet-production in  $p\bar{p}$  is due to the increased importance of the subprocess  $q\bar{q} \rightarrow qq$  which, while contributing normally to jet production is considerably suppressed by the gluon fragmentation function into pions. In Fig. 3.5.1.(c) the asymmetries for  $\pi^+$  and  $\pi^-$  production are compared. The relative magnitude of  $\mathcal{A}_{LL}^{ii}$  for  $\pi^-$  to that for  $\pi^+$  production reflects the degree to which spin information is carried by the d quark relative to the u quark in the polarised proton, the sign difference is due to the negativity of  $\Delta d(x)$  in the Carlitz-Kaur model for the distributions.

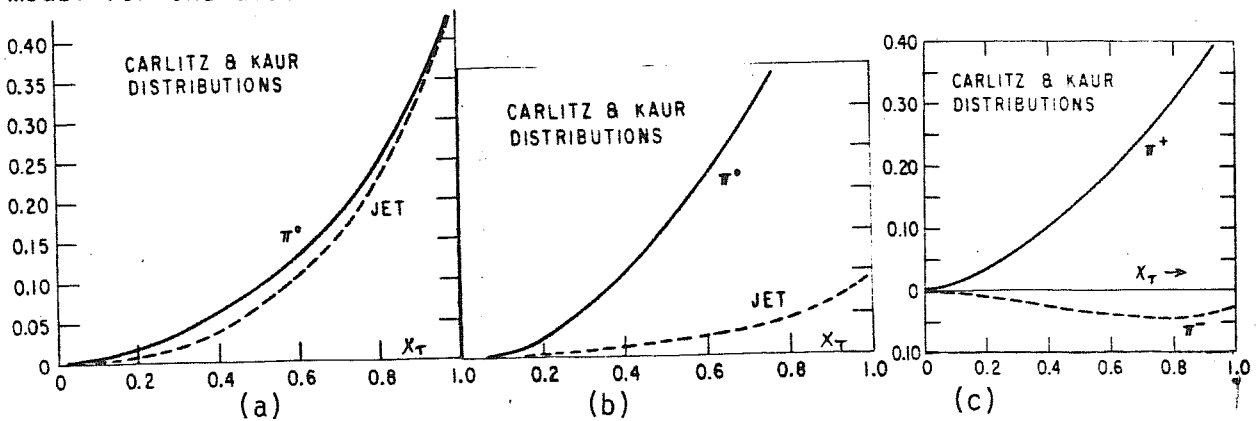


Fig. 3.5.2. The asymmetry  $\mathcal{A}_{LL}^{ii}$  for (a)  $pp \rightarrow \pi^0(\text{jet})+X$ , (b)  $p\bar{p} \rightarrow \pi^0(\text{jet})+X$  and (c)  $pp \rightarrow \pi^\pm X$  (taken from [1]).

The above asymmetries are essentially only sensitive to the polarisation information carried by the valence quarks of the proton. In order to have access to the gluon distributions one may consider hyperon production in proton-proton collisions [15]. The dominant contribution to this reaction comes from the subprocess indicated in Fig. 3.5.3.

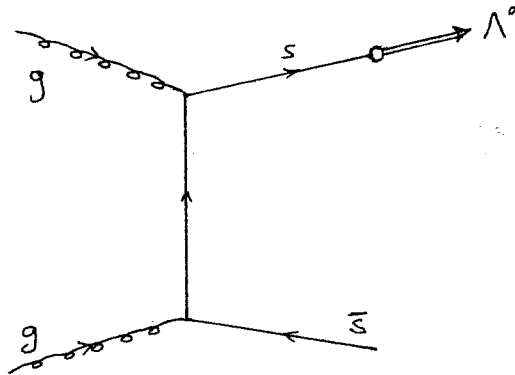


Fig. 3.5.3 The gluon fusion subprocess, dominant in  $\Lambda^0$  production in pp collisions.

The background coming from interactions involving constituent strange quarks could be eliminated by requiring an away-side anti-strange trigger.

Besides insight into the polarisation of the gluon content of the proton this process could also provide interesting information as to the transmission of polarisation in the fragmentation process. This is by virtue of the fact that the polarisation of the detected lambda can be measured with very high precision (to within about 1%). Thus the information obtainable and the simplicity of the production mechanism (which implies a general transparency of the results) makes this a very attractive process to study. In Fig. 3.5.4 the transmitted and reflected asymmetries are plotted for the process  $pp \rightarrow \Lambda^0 X$ . The fragmentation function was taken to be a delta function.

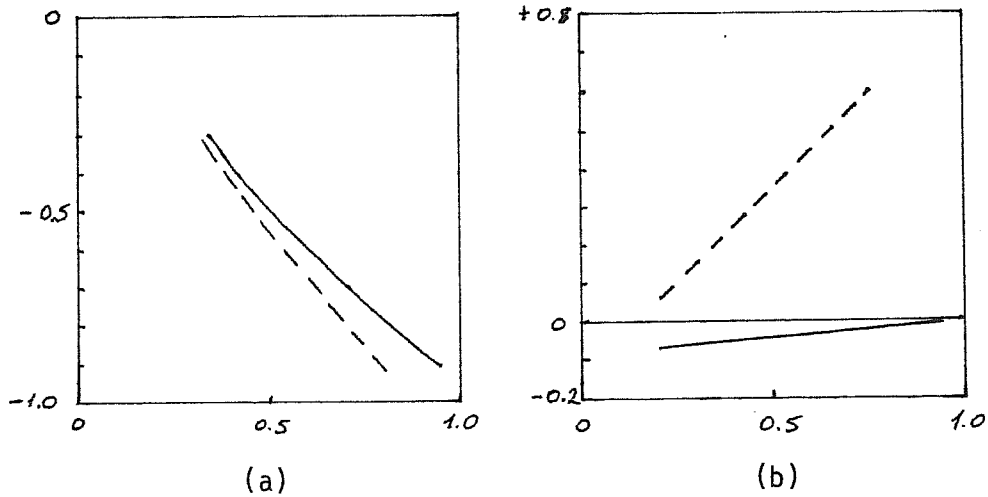


Fig.3.5.4. (a) The reflected asymmetry and (b) the transmitted asymmetry for lambda-production in pp collisions as a function of  $x_T$  for  $\theta_{CM} = 90^\circ$  (solid curves) and  $60^\circ$  (dashed curves) graphs taken from [15].

A further interesting process also sensitive to the gluon distributions is prompt photon production [2]. The partonic level contributions have already been discussed in section 1 of this chapter. In Fig. 3.5.5 the predictions of the transmitted asymmetry  $\mathcal{A}_{LL}^{if}(\vec{p}p \rightarrow \vec{\gamma}X)$  are plotted as a function of  $x_F$  for various  $x_T$ . While the behaviour near  $x_F = +1$  is determined by the valence distributions the behaviour for  $x_F \sim -1$  is a measure of  $\Delta g(x)/g(x)$ .

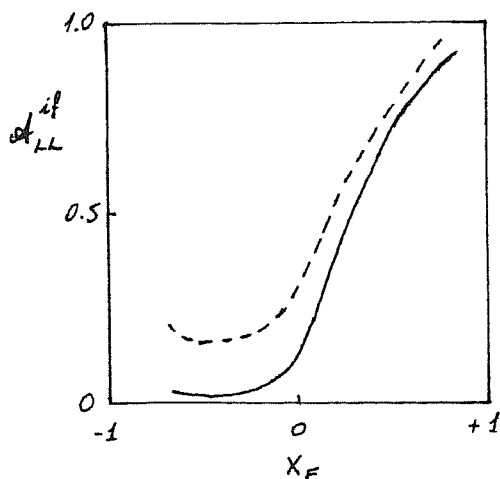


Fig. 3.5.5.  $\mathcal{A}_{LL}^{if}(\vec{p}p \rightarrow \vec{\gamma}X)$  as a function of  $x_F$  for  $x_T = 0.1$  (solid line) and 0.5 (dashed line) as given in [2].

Finally, let us consider asymmetries in the lepton-pair production or the Drell-Yan process [16]. The author of [16] considered the contributions from real gluon emission and quark-gluon interactions and calculated the asymmetry at fixed  $x_F$  and  $x_T$  (thus avoiding the problem of infra-red singularities

coming from very soft gluons to be discussed in chapter 5), these are reproduced below in Fig. 3.5.6. The increase in magnitude of  $\mathcal{A}$  with  $x_T$  and  $\tau = Q^2/S$  stems from the fast increase in the corresponding magnitude of the Compton subprocess asymmetry (dominant at large  $x_T$  or  $\tau$ ).

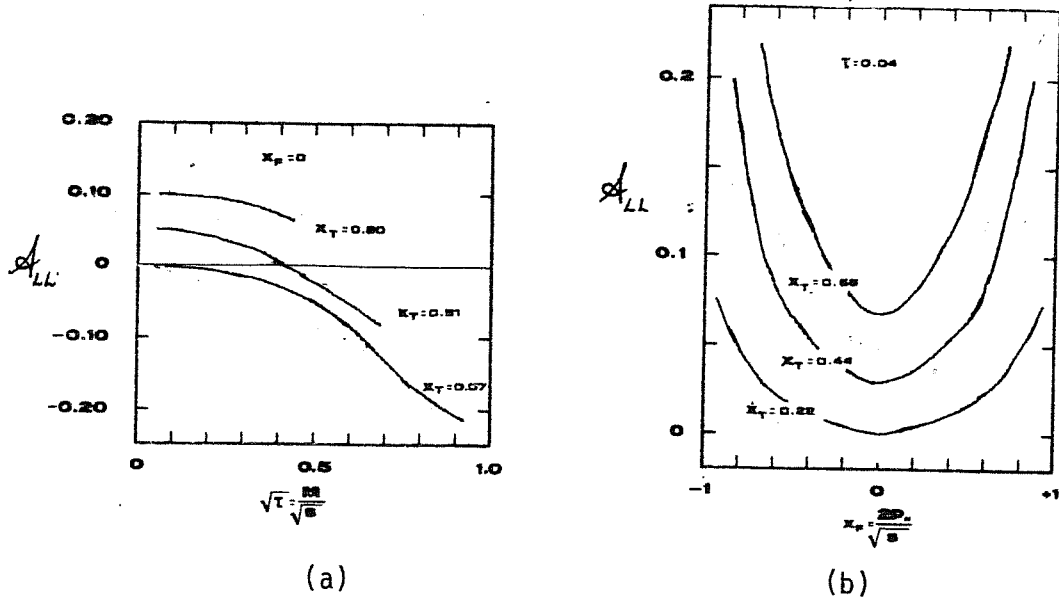


Fig. 3.5.6. Predictions for  $\mathcal{A}_{LL}^{ii}(pp \rightarrow \mu^+ \mu^- \chi)$  plotted against (a)  $\sqrt{\tau}$  and (b)  $x_F$  for various  $x_T$ , as given in [16].



References to chapter 3

- [1] These cross-sections and asymmetries (initial-initial only) have also been calculated by J. Babcock, E. Monsay and D. Sivers, Phys. Rev. D19, 1483 (1979). The table presented here agrees completely with their results.
- [2] The cross-sections and asymmetries (initial-final only) for the process  $gq \rightarrow \gamma q$  have also been calculated by N.S. Craigie, K. Hidaka, M. Jacob, A. Penzo and J. Soffer, Marseille preprint CDT-81/P.1339 (1981). The table presented here agrees completely with their results.
- [3] See refs. [8, 9] chapter 2.
- [4] See chapter 5 and refs. therein.
- [5] R.D. Field, Phys. Rev. Lett. 40, 997 (1976).  
J.F. Owens, E. Reya and M. Glück, Phys. Rev. D18, 1503 (1978).  
A.P. Contogouris, R. Gaskell and A. Nicolaidis, Phys. Rev. D17, 839 (1978);  
Prog. Theor. Phys. 58, 1238 (1977).
- [6] R.P. Feynman, R.D. Field and G.C. Fox, Phys. Rev. D18, 3320 (1978).
- [7] J. Kuti and V.W. Weisskopf, Phys. Rev. D4, 3418 (1971).  
G.W. Look and E. Fischbach, Phys. Rev. D16, 211 (1977).  
L.M. Sehgal, Phys. Rev. D10, 1663 (1974).  
R.L. Jaffe, Phys. Rev. D11, 1953 (1975).  
R.J. Hughes, Phys. Rev. D16, 662 (1977).  
J. Schwinger, Nucl. Phys. B123, 223 (1977).  
G. Preparata, see ref. [2] to chapter 4.
- [8] R.D. Field and R.P. Feynman, Phys. Rev. D15, 2590 (1977).
- [9] R. Carlitz and J. Kaur, Phys. Rev. Lett. 38, 673 (1977); 38, 1102 (E) (1977).  
J. Kaur, Nucl. Phys. B128, 219 (1977).

- [10] J.D. Bjorken, Phys. Rev. 148, 1467 (1966).
- [11] Particle Data Group Phys. Lett. 111B (1982).
- [12] D.M. Kaplan et al., Phys. Rev. Lett. 40, 435 (1978).
- [13] H.L. Anderson et al., Phys. Rev. Lett. 37, 4 (1976).
- [14] See sec. 4.3 and refs. therein.
- [15] N.S.Craigie, V. Roberto and D. Whould, Z.Phys. C12, 173 (1982).
- [16] K. Hidaka, Phys.Rev. D21, 1316 (1980).

Chapter 4      From theory to experiment

- 4.1    Double-spin asymmetries
- 4.2    Single-spin asymmetries
- 4.3    Present data on quark helicity distributions in the proton
- 4.4    Status and future possibilities for polarisation experiments

#### 4.1 Double-spin asymmetries

What exactly does one measure in a double-spin asymmetry experiment? Consider for the moment only initial state polarisations, i.e. beam and target polarised (or both beams in a collider). The polarisations may be either longitudinal or transverse (with respect to the beam direction). The basic idea is then to measure the cross-section with the polarisations parallel,  $d\sigma^{++}$  (longitudinal) or  $d\sigma^{\uparrow\uparrow}$  (transverse), and antiparallel,  $d\sigma^{+-}$  or  $d\sigma^{\uparrow\downarrow}$ . From these cross-sections one then forms the following asymmetries:

$$A_{LL} = \frac{d\sigma^{++} - d\sigma^{+-}}{d\sigma^{++} + d\sigma^{+-}} ,$$

$$A_{TT} = \frac{d\sigma^{\uparrow\uparrow} - d\sigma^{\uparrow\downarrow}}{d\sigma^{\uparrow\uparrow} + d\sigma^{\uparrow\downarrow}} . \quad (4.1.1)$$

Since these asymmetries are only relevant for strong interaction physics it is not necessary to consider all spin configurations, i.e.  $d\sigma^{--}$ ,  $d\sigma^{--}$  etc, since parity is conserved and the asymmetries expected here are much larger than those due to the parity violating effects of weak interactions in most cases.

The second question is then: how do the quantities defined above, as measured, relate to the corresponding quantities as calculated from the theory? First of all it is important to notice that since the asymmetry is a ratio of cross-sections the overall normalisation cancels out and is therefore not a problem. However one must take into consideration that the beam and target are never in the ideal spin eigenstates but can only be polarised to some fraction  $\mathcal{P}$ . Thus if one considers the simplified approximation of sect. 3.3:

$$A \sim \langle \lambda_1 \rangle \langle \lambda_2 \rangle \langle a \rangle , \quad (4.1.2)$$

where  $a$  is the hard-scattering asymmetry and  $\lambda_i$  the effective polarisations of the parton beam with respect to the parent hadron beam, then the following relation between experimental and theoretical asymmetries clearly takes into account the polarisation of the beam,  $\mathcal{P}_B$  and target  $\mathcal{P}_T$  :

$$A_{\text{expt.}} = \mathcal{P}_B \mathcal{P}_T A_{\text{theory}} \quad (4.1.3)$$

In the case where one considers the correlation between the spin of one of the initial particles and a final state trigger particle the obvious modification of equation (4.1.3) is to remove the polarisation,  $\mathcal{P}$ , corresponding to the unpolarised particle.

As already discussed in the previous chapter the predictions for  $\mathcal{A}_{LL}$  are very large, however transverse spin asymmetries are proportional to the hadron mass (or more generally some hadronic mass scale) and should therefore be suppressed by a factor  $M/\sqrt{s}$  relative to other effects. In the case of elastic proton-proton scattering large transverse spin asymmetries have been measured [1] (see Fig. 4.1.1). Such large effects are not predicted within the framework of purely perturbative QCD and a better understanding of non-perturbative approaches is required to accurately describe these asymmetries [2].

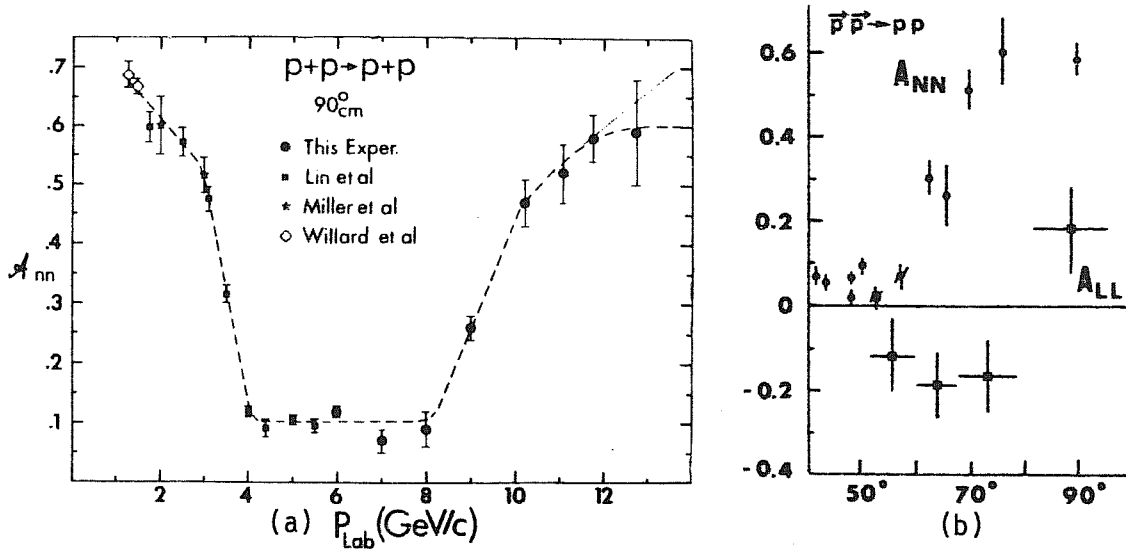


Fig. 4.1.1. (a)  $\mathcal{A}_{NN}$  at  $\theta_{CM} = 90^\circ$  and different energies,  
 (b)  $\mathcal{A}_{NN}$  and  $\mathcal{A}_{LL}$  at  $P_T = 11.75$  GeV/c.

## 4.2 Single-spin asymmetries

Pure single-spin asymmetries require parity violating processes and thus are zero for strong interactions (except for very small corrections due to weak interactions). However if one considers correlations between spin and kinematical configuration, then owing to interference effects, non-zero asymmetries can be generated.

For longitudinal polarisations one can define the following integrated asymmetry

$$A_L = \frac{\int_0^1 d\cos\theta \left[ \int_0^\pi d\varphi - \int_\pi^{2\pi} d\varphi \right] (d\sigma^+ - d\sigma^-)}{\int_0^1 d\cos\theta \left[ \int_0^\pi d\varphi + \int_\pi^{2\pi} d\varphi \right] (d\sigma^+ + d\sigma^-)} \quad (4.2.1)$$

Thus one considers the correlation between initial particle helicity and the hemisphere (forward or backward) of the final trigger particle, jet,  $\mu^+\mu^-$  pair etc.

In the case of a transversely polarised initial particle one defines the asymmetry with respect to the left and right hemispheres:

$$A_N = \frac{\int d\Omega \int d^3\vec{s} \vec{n} \cdot \vec{s} d\sigma}{\int d\Omega \int d^3\vec{s} d\sigma} \quad , \quad (4.2.2)$$

where  $\vec{s}$  is the polarisation unit-three-vector and  $\vec{n}$  defines the normal to the reaction plane, the latter defined by the initial and final particles. As in the previous section, the measured asymmetry corresponds to the above expressions evaluated from the theory and multiplied by the beam or target polarisation factor  $\mathcal{P}$ .

One can of course consider the polarisation of an inclusively produced final particle, the complementary quantity to the asymmetry of eq.(4.2.2). In this case one defines the following polarisation

$$\mathcal{P}_N = \frac{\int d\Omega \vec{n} \cdot \vec{s} d\sigma}{\int d\Omega d\sigma} \quad (4.2.3)$$

where now  $\vec{s}$  is the spin three-vector of the emitted particle.

As far as longitudinal single-spin asymmetries are concerned the theoretical

importance of these is discussed in some detail in chapter 9 . Recent perturbative calculations [3] have put the value of the asymmetry  $\mathcal{A}_L(pp \rightarrow \mu^+ \mu^- X)$  at around 1% (however as discussed later it is the smallness of this result which is of significance).

For the reasons already discussed one would naïvely expect single transverse spin asymmetries to be very small at large energies. The data however shows strikingly large single transverse spin dependences. The first process in which such large effects were first noticed was in the production of  $\Delta^0$  hyperons (and later other hyperons) in proton-proton collisions [4] see Fig. 4.2.1 (a). The polarisation is seen to be independent of energy (i.e. there is scaling) and persists up to large values of  $p_T$  , indeed it increases more or less linearly with  $p_T$  . Interestingly  $\Xi^0$  ,  $\Xi^-$  polarisations are very similar to that of the  $\Delta^0$  while  $\Sigma^+$  has opposite polarisation of almost equal magnitude and  $\bar{\Lambda}^0$  are unpolarised. Qualitatively these results can be understood very roughly in terms of the SU(6) picture of hadrons and a quark-antiquark pair-production model [5] . Equally surprising are the results of measurements of  $\mathcal{A}_N(pp \rightarrow \pi^0 X)$  for the scattering of protons off polarised Be and hydrogen targets [6] see Fig. 4.2.1 (b). The energy dependence of this effect has yet to be measured but again one notes the marked increase of the asymmetry with increasing  $p_T$  .

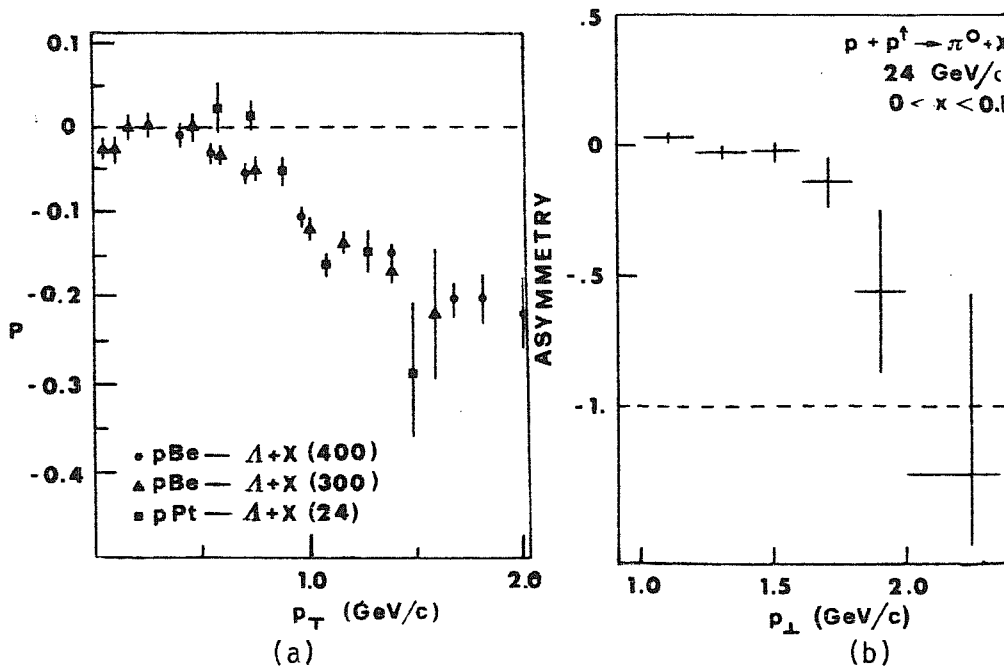


Fig. 4.2.1. (a)  $\mathcal{P}_N(pp \rightarrow \Delta^0 X)$  as a function of  $p_T$  at different energies, (b)  $\mathcal{A}_N(pp \rightarrow \pi^0 X)$  at 24 GeV/c.

Models based on final state interference effects go some way to explaining the  $\Delta^0$  data [2] however more work needs to be done before a complete explanation can be given.



#### 4.3 Present data on quark helicity distributions in the proton

The only systematic measurements of double spin asymmetries (i.e. aimed at extracting the spin-dependent quark distributions) performed to date are those of the SLAC group [7].

This experiment measured the spin-asymmetry in the deep-inelastic scattering of longitudinally polarised electrons off longitudinally polarised protons in the kinematic range  $0.1 < x < 0.7$  and  $1 < Q^2 < 9$  (GeV/c)<sup>2</sup>.

The basic quantity measured  $\mathcal{A}_{LL}(\vec{e}\vec{p} \rightarrow eX)$  is given by

$$\mathcal{A}_{LL} = A = D(A_1 + \eta A_2) \quad , \quad (4.3.1)$$

where  $D$  and  $\eta$  are simple known kinematic expressions,  $A_2$  is an interference term ( $A_2$  being small in the scaling limit) and  $A_1$  the real target of the measurement, is given by

$$A_1 = \frac{\sigma_{1/2} - \sigma_{3/2}}{\sigma_{1/2} + \sigma_{3/2}} \quad (4.3.2)$$

where  $\sigma_{1/2}$  ( $\sigma_{3/2}$ ) is the total absorption cross-section when the component of angular momentum of the virtual photon plus proton in the direction of the photon momentum is  $\frac{1}{2}$  ( $\frac{3}{2}$ ).

In the scaling limit  $A_1 \simeq -2xg_1/F_2$  (the sign depends on the particular definition of  $g_1$  adopted). Thus in terms of the quark distribution functions (see eqn. 2.2.3) one has

$$A_1(x) = \frac{\mathcal{G}_1(x)}{\mathcal{F}_2(x)} = \frac{\sum_i e_i^2 \Delta q_i(x)}{\sum_i e_i^2 q_i(x)} \quad . \quad (4.3.3)$$

This quantity then is essentially a measure of the fractional polarisation of up quarks in the proton ( $e_i^2 = 4/9$  vs.  $1/9$  for down quarks), see eqn. 3.3.6.

In Fig. 4.3.1. the data are plotted against  $Q^2$  for different ranges of

The values of  $\mathcal{A}_{LL}/D$  have been divided by  $\sqrt{x}$  (which describes well all the  $x$ -dependence of the data), one sees that within the errors scaling holds.

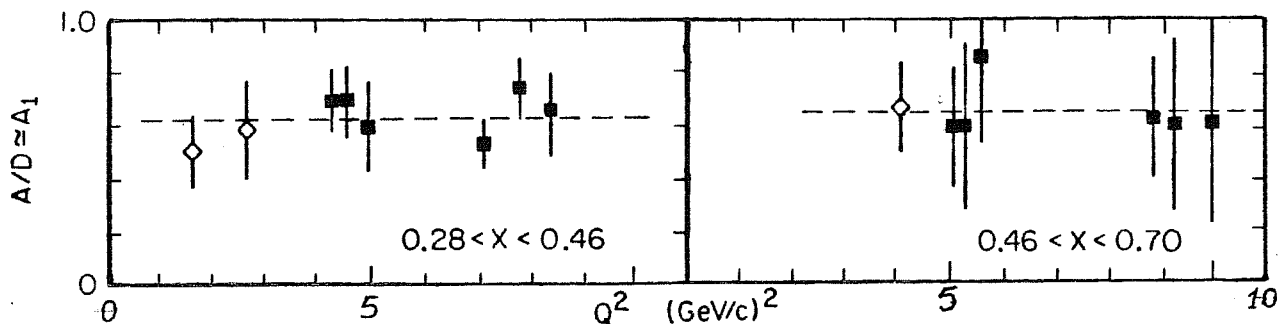


Fig. 4.3.1. Plot of  $(A/D)/\sqrt{x}$  for two different regions of  $x$ . The dotted line is a least-squares straight line fit.

The full set of data, best described by  $A/D = 0.94 \sqrt{x}$ , has already been displayed in Fig. 3.4.2. This shows the tendency at large  $x$  for the helicity of the proton to be carried, by the leading quark.

There are two sum rules that may be compared with this data: the Ellis-Jaffe sum rule [8] for the proton

$$\int_0^1 \mathcal{G}_1^p dx = \int_0^1 \frac{dx}{x} \frac{A_1^p F_2^p}{1+R^p} = \frac{0.89}{3} \left| \frac{g_A}{g_V} \right| \quad (4.3.4)$$

$$= 0.372 \pm 0.002,$$

where  $R$  is the ratio of longitudinal to transverse photon cross-sections for the proton. Using the Regge theory prediction of  $A_1 \propto x^{1.14}$  [9] for the small  $x$  region and the  $\sqrt{x}$  fit for large  $x$  gives

$$\int_0^1 \mathcal{G}_1^p dx = 0.33 \pm 0.10, \quad (4.3.5)$$

which is consistent with the predicted value.

One can also partially test the Bjorken sum rule which in terms of  $A_1^p$  and  $A_1^n$  for the proton and neutron respectively is:

$$\int_0^1 (\mathcal{G}_1^p - \mathcal{G}_1^n) dx = \int_0^1 \frac{dx}{x} \left\{ \frac{A_1^p F_2^p}{1+R^p} - \frac{A_1^n F_2^n}{1+R^n} \right\} = \frac{1}{3} \left| \frac{g_A}{g_V} \right|$$

$$= 0.4182 \pm 0.0021 \quad . \quad (4.3.6)$$

Under the assumption that  $A_1^n$  is small the results are also consistent with the Bjorken sum rule.

It would clearly be valuable to measure  $A_1$  for the neutron and also the other structure function  $A_2$  for both the proton and the neutron. Use of a polarised deuteron target as well as a polarised proton target allows for the determination of the neutron structure functions. To determine  $A_2$  the nucleon polarisation must be transverse to the momentum and spin directions of the incident electron and lie in the scattering plane. A proposal has been made for an experiment at SLAC which would be capable of determining  $A_1^p$ ,  $A_2^n$  and  $A_1^n$  with accuracies about the same as those for the measurement of  $A_1^p$ . This would provide a knowledge of the structure function  $\mathcal{G}_2$  on precisely the same experimental footing as  $\mathcal{G}_1$ .  $A_2$  and  $\mathcal{G}_2$  are related as follows:

$$A_2 = \frac{2\sigma_{TL}}{\sigma_{+1/2} + \sigma_{-1/2}} = 2x \frac{\sqrt{M^2}}{\sqrt{Q^2}} (1+R) \frac{\mathcal{G}_2(x)}{\mathcal{F}_2(x)} \quad . \quad (4.3.7)$$

#### 4.4 Status and future possibilities for polarisation experiments

In this, the final section on the experimental status of spin physics research the present facilities for polarisation experiments are discussed together with projects for future measurements. A more complete discussion can be found in ref. [10] where a comparative list is given of the parameters one might expect for typical densities, beam intensities etc.

One of the essential requisites for these experiments is a highly polarised beam and/or target. Let us begin by discussing the production of polarised beams.

##### (a) Polarised beams

Primary polarised proton beams from polarised source have been accelerated up to 12.75 GeV in the ZGS at Argonne [11] and recently at SATURNE II up to 2.5 GeV. Future plans include the conversion of the AGS at Brookhaven to polarised operation, similar plans exist at KEK and JINR at DUBNA has reported acceleration of polarised deuterons up to full energy in the Synchrotron.

The main problem is the avoidance of depolarising resonances which occur about every 520 MeV in the acceleration cycle. At the ZGS and SATURNE II these were handled quite successfully by techniques of resonance jumping, spin flip and orbit corrections. However for significantly higher energies the resonances become too numerous to handle individually. In large machines this difficulty can be circumvented by the use of one or two Siberian Snakes [12]. These devices consist of a combination of horizontal and vertical deflecting magnets inserted in a straight section of the ring. The effect is to cause a precession of the spin by 180 degrees around either the longitudinal or radial axis. This is feasible at high energies by virtue of the fact that the spin turning angle in traversing a given magnet and orbit angle is independent of the energy. The spin precession due to the bending field is also energy independent, thus a particle initially longitudinally polarised at a point  $180^\circ$  from the snake precesses through some angle  $\alpha$  in travelling around to the snake which then flips this angle to  $-\alpha$  and therefore on returning to its original position the particle also returns to

its initial longitudinal polarisation. This method is, of course, particularly well suited for high energy accelerators (with moderately high injection energies  $\geq 10$  GeV) since these large machines typically have enough free space for the many magnets (about 14 sets occupying about 22 metres) necessary for the snakes.

With present polarised  $H^+$  sources the AGS at Brookhaven will be able to accelerate  $10^{10}$  polarised protons per pulse and planned source improvements will raise this figure to well over  $10^{11}$ . It should be possible to reach about 22 GeV before hitting an impenetrable resonance at which point one can reasonably expect to have maintained 70-80% of the initial 100% polarisation. This would then be suitable for injection into ISABELLE (the projected 400 GeV proton collider) where use of a Siberian snake would allow acceleration of polarised protons at something like a third of the expected unpolarised luminosity i.e. stable atomic hydrogen could in principle provide a polarised beam at the same intensity as the unpolarised beam.

For some time now an alternative method for obtaining good quality beams of polarised protons and also antiprotons from the parity-violating decays of  $\Lambda^0$  and  $\bar{\Lambda}^0$  hyperons has been known [13]. It is now planned to construct such a polarised beam at Fermilab in connection with the TEVATRON II fixed target program.

The underlying principle of this technique is that parity violation in weak decays of unpolarised lambdas leads to protons which are polarised in a direction determined by the geometry of the decay, independently of the energy. When  $\Lambda^0$  particles are produced at sufficiently high energy by primary (unpolarised) protons striking a target, the resultant polarised protons are concentrated in a narrow cone around the incident beam direction. To select these polarised protons all prompt charged particles are swept away by a magnetic field. They are then collected in a beam channel which conserves polarisation and are focussed onto the target. The same method is used to obtain a polarised  $\bar{p}$  beam from  $\bar{\Lambda}^0$  decay. At Fermilab it is estimated that this technique will provide about  $3 \times 10^7$  polarised protons or  $10^6$  polarised antiprotons per spill with a polarisation of about 45% up to energies in an initial phase of 200 GeV (there exists a detailed project to increase this to 450 GeV).

(b) Polarised targets

Several new solid polarised target materials are at various stages of development. Of these irradiated  $\text{NH}_3$  is now replacing the usual alcohol targets and offering inherent resistance to radiation damage. One can expect to obtain polarisations between 70 and 90%.

Another promising new development uses gaseous stable atomic hydrogen, which becomes virtually 100% proton polarised at high density ( $\sim 10^{17} \text{ cm}^{-3}$ ), high field ( $\sim 10\text{T}$ ) and low temperature ( $\sim 300 \text{ mK}$ ). In this high density state the polarisation cannot easily be reversed, however at lower density one can spin select one or other of the two lowest hyperfine states by exciting one of the EPR lines in a suitable flat field area. This will allow dynamic proton polarisation with straightforward reversal by microwave frequency shift. The spin flipped atoms are rejected from the magnetic confinement area.

This technique for producing a polarised gas jet target is to be adopted by the now approved UA6 project for the CERN collider [14], where the expected luminosity for unpolarised operation with either the proton or antiproton beam will be about  $2 \times 10^{31} \text{ cm}^{-2} \text{ sec}^{-1}$  and with the target polarised about  $10^{30} - 10^{31}$  with a possibility for improvement. Two big advantages of this set up are the rapid spin reversal ( $\sim 10^3 \text{ Hz}$ ), which will eliminate systematic errors, and the possibility of having any polarisation desired. This experiment then will be able to perform the full range of single spin asymmetry measurements  $p(\bar{p}) + \vec{p} \rightarrow A + X$  where A is a lepton pair, prompt photon,  $\pi^0$ ,  $\Delta^0$  etc. And, with respect to this last, double-spin correlation measurements, the polarisation of the  $\Delta^0$  (or  $\bar{\Delta}^0$ ) being measurable to within 1% accuracy from its decay distribution.

By way of a summary table 4I reproduces part of the appendix of Ref. [10], listing some of the parameters and characteristics of polarised beams and targets as discussed in this chapter. An estimate of the statistical error involved in the measurement of an asymmetry  $\mathcal{A}$  may be obtained using the following formula:

$$\delta \mathcal{A} = \frac{1}{\mathcal{P}_B \mathcal{P}_T} \frac{1}{\sqrt{L \sigma T}} \quad , \quad (4.4.1)$$

where  $L$  is the luminosity,  $\sigma$  the spin-averaged cross-section per nucleon and  $T$  the running time.

TABLE 4I

(a) Typical luminosities ( $\text{cm}^{-2} \text{sec}^{-1}$ )

Beam	Liq.Hyd.T	Pol.Prot.T	Pol.Jet T	Coll. Beams
Unpol.primary	$10^{37}$	$2 \times 10^{34}$	$2 \times 10^{32}$	$10^{32}$
Pol.primary	$4 \times 10^{34}$	$10^{34}$	$10^{31}$	$10^{30}$
Pol.secondary	$4 \times 10^{30}$	$8 \times 10^{29}$	—	—

(b) Magnitudes of polarisation

Polarised Beam or Target	Polarisation
Primary proton beam	$\mathcal{P}_B \sim 0.7$ (0.6 to 0.8)
Secondary proton beam	$\mathcal{P}_B \sim 0.45$ (0.4 to 0.5)
$\text{NH}_3$ target	$\mathcal{P}_T \sim 0.8$ (0.7 to 0.9)
Hydrogen gas jet target	$\mathcal{P}_T \sim 1.0$

These figures give typical double spin accuracies for a beam intensity of  $10^{10} \text{sec}^{-1}$  on a 20 cm target running for one month with an interaction cross-section of  $10^{-33} \text{cm}^2$ :

$$\delta \mathcal{A} (\text{elastic } \vec{p}\vec{p}) \sim 3 \times 10^{-3} ,$$

$$\delta \mathcal{A} (\vec{p}\vec{p} \rightarrow hX) \sim 2 \times 10^{-2} . \quad (4.4.2)$$

The typical systematic errors for beam and target polarisation measurement are 3 to 5%.

References to Ch. 4

- [1] P.G. Crabb et al. Phys.Rev.Lett. 41, 1257 (1978).
- [2] G. Preparata in High Energy Physics with Polarised Beams and Targets, ed. by C. Joseph and J. Soffer (Birkhäuser Verlag, 1981), p. 121.
- [3] See chapter 9.
- [4] G. Bunce et al. Phys.Rev.Lett. 36, 1113 (1976).  
K. Heller et al. Phys.Lett. 68B, 480 (1977).  
G. Bunce in High Energy Physics with Polarised Beams and Targets, ed. by C. Joseph and J. Soffer (Birkhäuser Verlag, 1981), p. 141 and references therein.
- [5] K. Heller et al., Phys.Rev.Lett. 41, 607 (1978).
- [6] J. Antille et al., Phys.Lett. 94B, 523 (1980).
- [7] M.J. Alguard et al., Phys.Rev.Lett. 37, 1258 (1976); 37, 1261 (1976); 41, 70 (1978).  
R.F. Oppenheimer et al. SLAC-PUB-3026 (1982), final results.  
V.W. Hughes in High Energy Physics with Polarised Beams and Targets, ed. by C. Joseph and J. Soffer (Birkhäuser Verlag, 1981), p. 331.
- [8] J. Ellis and R. Jaffe, Phys.Rev. D9, 1444 (1974).
- [9] R.L. Heiman, Nucl.Phys. B64, 429 (1973).
- [10] N.S. Craigie, T. Niinikoski, A. Penzo, L. van Rossum, R.D. Ruth, D. Sivers and J. Soffer, Survey of Hadron Spin Physics for High Energy laboratories (report on a study meeting following the 1982 Symposium on High Energy Spin Physics held at Brookhaven), Saclay preprint DPhPE 83-01(1983).
- [11] I.R. O'Fallon et al., Phys.Rev.Lett. 39, 733 (1977).  
D.G. Crabb et al., Phys.Rev.Lett. 41, 1257 (1978).  
A. Lin et al., Phys.Lett. 74B, 273 (1978).



- [12] Ya. Derbenev et al., Particle Accel. 8, 115 (1978).  
E.D. Courant et al., AIP Conf.Proc. 42, 41 and 94 (1978).
- [13] O.E. Overseth, NAL 1969 Summer Study Report, SS-118, vol. I.
- [14] R. Cool in the Proc. of A Topical Seminar on New Perspectives and Methods for High Energy Spin Physics, Florence 1983 (to appear).

## Chapter 5      Next-to-leading logarithmic corrections

- 5.1      Factorisation and higher order  $\alpha_s$  corrections
- 5.2      Spectator interactions in the Drell-Yan process
- 5.3      Parton densities, deep-inelastic scattering and Drell-Yan beyond leading order
- 5.4      Calculation of the coefficient function to order  $\alpha_s$  in deep-inelastic scattering
- 5.5      Calculation results for helicity asymmetries in the Drell-Yan process
- 5.6      Numerical results for helicity asymmetries in the drell-Yan process.

## 5.1 Factorisation and higher order $\alpha_s$ corrections

As already mentioned in section 3.3 beyond the leading logarithmic order the factorisation conjecture remains unproven in general. In particular, processes with two hadrons in the initial state such as the Drell-Yan process for example receive contributions from interactions involving spectator partons (see Fig. 5.1.1) which spoil the factorisation proof [1,2,3] .

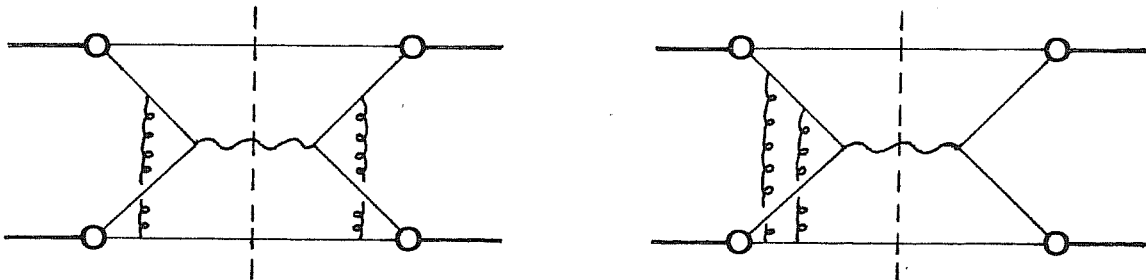


Fig. 5.1.1. Examples of interactions involving spectator quarks in the Drell-Yan process.

Another difficulty arising from the non-Abelian nature of QCD is in the cancellation of infra-red divergences [4]. It seems that this only occurs at the non-leading twist level (i.e. is suppressed by powers of  $Q^2$ ), although a proof of this to all orders does not exist, so it may not be a problem.

The problem of non-factorising spectator interactions has yet to receive a general consensus of opinion: while references [1,2] claim to have found factorisation violating initial state contributions at the two-loop level (although differing on what this contribution is), the authors of reference [3] present a method of demonstrating factorisation at measured dimuon  $Q_T$ , which they maintain is generalisable to higher orders. The essential claim of these last is that the authors of the first two references failed to take into account correctly the Glauber region, a part of the low-momentum gluon-region.

In the rest of this chapter the more optimistic attitude of reference [3] will be adopted and factorisation assumed to hold in its strong form, namely that the full hadronic cross-section for any process is imply the convolution of the relevant parton distributions, extracted from some chosen process

with a partonic hard-scattering cross-section (which may be considered as a coefficient function) whose higher order corrections are calculable in perturbative QCD.

There still remains the problem of evaluating the spectator contributions, this is the subject of the next section.

## 5.2 Spectator interactions in the Drell-Yan process

For some time now the discrepancy between experiment and leading order calculation of the Drell-Yan cross-section (the famous K-factor almost constant with energy and having a value  $\sim 2$ ) has been known and understood in terms of large but calculable radiative cross-section to the basic process.

These corrections, of order  $\alpha_s$  as opposed to the leading-logarithmic order  $\alpha_s \ln Q^2$ , come from the infra-red region and as such are sensitive to the method of regularising the singularities encountered in loop-momenta integrals in this region. It is then natural to ask whether the standard techniques, i.e. on mass-shell with dimensional regularisation, necessarily give the correct answer. Indeed one might expect the more physical method of off-mass-shell regularisation to be most probably correct and certainly these two schemes give differing answers, for example in the case of photon-quark vertex renormalisation [5,6] .

A more complete treatment, including the contributions of spectator diagrams [7] has shown that there is no ambiguity; the two methods give identical answer provided they are implemented correctly, i.e. spectator contributions correctly accounted for in the physical off-mass-shell case.

The technique adopted (also in references [2,3] ) is based on the simplifying use of a scalar model [8] for hadrons and quarks in which the hadronic wave function is replaced by the (effective) interactive term

$$\mathcal{L}_{int} = -\lambda (\varphi \chi^\dagger \chi + h.c.) , \quad (5.2.1)$$

where  $\varphi$  is a scalar meson and  $\chi$  a scalar quark.

An advantage of choosing a superrenormalisable coupling between the meson and quarks is that it induces a transverse momentum cut-off characteristic of the distribution functions of physical mesons, the authors of reference [3] show this coupling leads to a  $k_T^{-4}$  behaviour for the distributions instead of the  $k_T^{-2}$  behaviour

that would arise from a dimensionless (for example derivative) coupling.

The K-factor for Drell-Yan takes the form

$$K = 1 + \frac{\alpha_s}{2\pi} C_2(R) \left[ 1 + \frac{\pi^2}{3} + C \pi^2 \right], \quad (5.2.2)$$

where the value of C for purely active quark contributions varies according to the calculational procedure, although it is independent of the precise values chosen for the regulating parameters (off-shellness of external parton legs for example). The following three possibilities were considered:

- (a) both incoming parton line on mass-shell, in which case no spectator contributions are included,
- (b) both incoming parton lines off mass-shell, in which case the full set of spectator interactions are included,
- (c) one quark on and one off mass-shell, only spectator interactions in the off-mass-shell channel are considered.

Note of course that the coefficient function for the deep-inelastic scattering process (through which the parton distributions are defined beyond leading order) must also be calculated in the same manner as the corresponding channel in the Drell-Yan process.

The results of the calculations performed in reference [7] are summarised in Table 5-I. The conclusion one draws then is that any regularisation procedure will give the same, and presumably correct, answer provided one takes into account the fact that off-shell partons are necessarily bound in hadrons and therefore attention must be paid to include correctly the contributions of spectator interactions.

TABLE 5-1 . Contributions to the constant  $C$  in K-factor, equation (5.4.2). The labels A and S (active and spectator) refers to the type of interaction contributing. The labels on- and off-shell refer to the active quarks.

	AA	AS	SS	Total
on-on shell	1	-	-	1
off-off shell	2	-2	1	1
on-off-shell	3	-2	-	1

It must be remarked that these results, while very encouraging, do not constitute a complete understanding of the problem in that a priori there was no reason to assume the equivalence between the methods. indeed while in the case of active-quark/ active-quark interactions the  $\pi^2$  term is associated with a large logarithm, this is not so for interactions involving spectators where there is no large logarithm.

Thus in the rest of this chapter it will be assumed that on-mass-shell scheme is a legitimate form of regularisation for such one-loop calculations. On the contrary in chapter 7 it is shown that for transverse spin such calculations lead to different coefficients for even the large logarithm.

### 5.3 Parton densities, deep-inelastic scattering and Drell-Yan beyond leading order

The corrections considered here are non-leading in the sense that they are suppressed by one power of  $\ln Q^2$  relative to the leading terms and hence are negligible in the asymptotic region. At the subasymptotic energies of most present day experiments they play an important rôle, providing the K-factor already discussed. For the spin-averaged cross-section the first complete analysis was performed in ref. [9] and many others have also performed these calculations either in part or completely [5,10]. The helicity dependent cross-section has also recently been calculated to this order [11].

To leading order as already discussed in sect. 2.2 one unambiguously identifies the structure functions  $\mathcal{F}_2$  and  $\mathcal{G}_1$  with the spin-averaged and spin-dependent quark densities respectively. Beyond the leading order one has a certain freedom in the definitions, the distributions after all are not physical quantities in the sense that they are renormalisation scheme dependent. This dependence is cancelled however by a corresponding dependence in the coefficient functions to be evaluated later. It is convenient then to require that the form of eqs. (2.2.3) be preserved in higher orders thus one writes

$$\begin{aligned}\mathcal{F}_2(x, t) &= \sum_i e_i^2 q^i(x, t) , \\ \mathcal{G}_1(x, t) &= \sum_i e_i^2 \Delta q^i(x, t) ,\end{aligned}\tag{5.3.1}$$

where  $t$  is given by  $t = \ln Q^2/\mu^2$  with  $\mu$  an arbitrary mass scale. To this order it is no longer true that  $\mathcal{F}_1 = \mathcal{F}_2$ , the difference being proportional to the longitudinal cross-section. This is just the statement that while to leading logarithmic order longitudinally polarised photons give no contribution they do contribute to the radiative corrections.

Calculating the leptonproduction structure functions  $\mathcal{F}_k(x, t)$  and  $\mathcal{G}_l(x, t)$  in perturbation theory one has, in terms of the "bare" parton distributions  $q_0^i(x)$  and  $g_0(x)$ :



$$\begin{aligned}
\mathcal{F}_k(x,t) &= \int_x^1 \frac{dy}{y} \left\{ \sum_i e_i^2 \left[ \delta(1-\frac{x}{y}) + \frac{\alpha_s}{2\pi} t P_{qq}(\frac{x}{y}) + \frac{\alpha_s}{2\pi} f_{q,k}(\frac{x}{y}) \right] q_0^i(y) \right. \\
&\quad \left. + \left( \sum_i e_i^2 \right) \left[ \frac{\alpha_s}{2\pi} t P_{qq}(\frac{x}{y}) + \frac{\alpha_s}{2\pi} f_{g,k}(\frac{x}{y}) \right] g_0(y) \right\}, \\
\mathcal{G}_1(x,t) &= \int_x^1 \frac{dy}{y} \left\{ \sum_i e_i^2 \left[ \delta(1-\frac{x}{y}) + \frac{\alpha_s}{2\pi} t \Delta P_{qq}(\frac{x}{y}) + \frac{\alpha_s}{2\pi} \Delta f_q(\frac{x}{y}) \right] \Delta q_0^i(y) \right. \\
&\quad \left. + \left( \sum_i e_i^2 \right) \left[ \frac{\alpha_s}{2\pi} t \Delta P_{qg}(\frac{x}{y}) + \frac{\alpha_s}{2\pi} \Delta f_g(\frac{x}{y}) \right] \Delta g_0(y) \right\}, \quad (5.3.2)
\end{aligned}$$

where  $f_{q,k}$  and  $\Delta f_q$  etc. represent the order  $\alpha_s$  cross-sections to the coefficients function. Eqs. (5.3.1) imply that to first order in  $\alpha_s$  the relationship between bare and renormalised quark densities is given by:

$$\begin{aligned}
\Delta q^i(x,t) &= q_0^i(x,t) + \frac{\alpha_s}{2\pi} \int_x^1 \frac{dy}{y} \left\{ \left[ t \Delta P_{qq}(\frac{x}{y}) + \Delta f_q(\frac{x}{y}) \right] \Delta q_0^i(y) \right. \\
&\quad \left. \left[ t \Delta P_{qg}(\frac{x}{y}) + \Delta f_g(\frac{x}{y}) \right] \Delta g_0(y) \right\}, \quad (5.3.3)
\end{aligned}$$

with a similar expression for  $q^i(x,t)$ , obtained by removing the  $\Delta$ 's. Henceforth only expressions for the helicity correlated quantities will be given where the corresponding expressions for the spin-averaged quantities may be obtained by substituting  $\mathcal{F}_2$  for  $\mathcal{G}_1$ , and removal of the  $\Delta$ 's. The suffix 2 will be dropped from  $f_{q,2}$  etc., identification 5.3.1 being understood.

Note that the absorption of the  $f$ 's into the distribution functions only changes the derivative with respect to  $t$  in next order in  $\alpha_s(t)$  since

$$\frac{d}{dt} = \beta(\alpha_s(t)) \frac{d}{d\alpha_s(t)} \simeq -\frac{\beta_0}{4\pi} \alpha_s^2(t) \frac{d}{d\alpha_s(t)}. \quad (5.3.4)$$

The quark and gluon densities therefore continue to satisfy the standard evolution equations in order  $\alpha_s$  (see eqs. 2.2.9).

Turning now to Drell-Yan and defining

$$\begin{aligned}
d\sigma^{DY} &= \frac{1}{2} (d\sigma^{++} + d\sigma^{+-}), \\
d\Delta\sigma^{DY} &= \frac{1}{2} (d\sigma^{++} - d\sigma^{+-}), \quad (5.3.5)
\end{aligned}$$

where the  $\pm$  indices refer to the helicities of the incoming hadrons, one has to lowest order

$$Q^2 \frac{d\Delta\sigma^{DY}}{dQ^2} = - \frac{4\pi\alpha}{9S} \int_0^1 \frac{dx_1}{x_1} \frac{dx_2}{x_2} \sum_i e_i^2 \Delta q_o^{[1]}(x_1) \Delta \bar{q}_o^{[2]}(x_2) \delta\left(1 - \frac{\tau}{x_1 x_2}\right), \quad (5.3.6)$$

where  $Q^2$  is the invariant mass-squared of the lepton pair and  $S$  that of the initial hadronic system,  $\tau = Q^2/S$  and the sum runs over all quark and antiquark types. The minus sign with respect to the spin-averaged cross-section expresses the usual quark-helicity conservation rule.

To the basic  $q\bar{q}$  annihilation process the corrections come from  $q\bar{q} \rightarrow \gamma^* g$  and  $gq(\bar{q}) \rightarrow \gamma^* q(\bar{q})$  together with the virtual gluon corrections to the quark wave function and photon-quark vertex. Schematically one has

$$\begin{aligned} \frac{d\Delta\sigma^{DY}}{dQ^2} = & - \int [dx] \left\{ \Delta q_o^{[1]}(x_1) \Delta \bar{q}_o^{[2]}(x_2) \left[ \delta(1-z) + \Theta(1-z) \frac{\alpha_s}{2\pi} 2 \left( \pm \Delta P_{qg}^{DY}(z) + \Delta f_{q,DY}^{(z)} \right) \right] \right. \\ & \left. + \left[ \left( \Delta q_o^{[1]}(x_1) \Delta g_o^{[2]}(x_2) + (1 \leftrightarrow 2) \right) \Theta(1-z) \frac{\alpha_s}{2\pi} \left( \pm \Delta P_{qg}^{DY}(z) + \Delta f_{g,DY}^{(z)} \right) \right] \right\}, \quad (5.3.7) \end{aligned}$$

where  $z = \tau/x_1 x_2 = Q^2/\hat{s}$  with  $\hat{s} = x_1 x_2 s$  the invariant mass-squared of the partonic subprocesses. The factor of 2 in front of the kernel for the  $q\bar{q}$  annihilation part merely represents the fact that this process has a quark in both channels with which is associated a large logarithm.

The statement of the factorisation theorem is that the kernel of (5.3.7) and (5.3.3) are identical:

$$\Delta P_{ab}^{DY}(x) = \Delta P_{ab}(x) \quad ; \quad a, b = q, g \quad (5.3.8)$$

Thus reexpressing (5.3.7) in terms of the scale-dependent densities, restoring all factors and renormalisation group improving  $\alpha_s$  to  $\alpha_s(t)$  one has

$$\begin{aligned} Q^2 \frac{d\Delta\sigma^{DY}}{dQ^2} = & - \frac{4\pi\alpha}{9S} \int_0^1 \frac{dx_1}{x_1} \frac{dx_2}{x_2} \left\{ \sum_i e_i^2 \Delta q^{[1]}(x_1, t) \Delta \bar{q}^{[2]}(x_2, t) \left[ \delta(1-z) \right. \right. \\ & \left. \left. + \frac{\alpha_s(t)}{2\pi} \Theta(1-z) 2 \left( \Delta f_{q,DY}^{(z)} - \Delta f_q^{(z)} \right) \right] + \left[ \left( \Delta g^{[1]}(x_1, t) \Delta g^{[2]}(x_2, t) + (1 \leftrightarrow 2) \right) \right. \right. \\ & \left. \left. \times \frac{\alpha_s(t)}{2\pi} \Theta(1-z) \left( \Delta f_{g,DY}^{(z)} - \Delta f_g^{(z)} \right) \right] \right\} \quad (5.3.9) \end{aligned}$$

The next-to-leading logarithmic corrections are governed by the differences  $\Delta f_{q,DY}(z) - \Delta f_q(z)$  etc. An important point to note is that these quantities, being differences are scheme independent.

5.4 Calculation of the coefficient function to order  $\alpha_s$  in deep-inelastic scattering

Since one first extracts the parton densities from deep-inelastic scattering data it is natural to start here by evaluating the relevant coefficient functions to extract the  $\Delta f_q$  etc. as defined in the previous section.

To identify the three structure functions in  $W_{\mu\nu}$  (see sect. 2.1) it is convenient to employ the following projections for a target of helicity  $h$ , the relations are given for  $D$  dimensions anticipating the use of dimensional regularisation (see appendix A3).

$$\begin{aligned}
 -g^{\mu\nu} W_{\mu\nu} &= (1-\epsilon) \mathcal{F}_2(x, Q^2) - \left(\frac{3}{2}-\epsilon\right) (\mathcal{F}_2(x, Q^2) - \mathcal{F}_1(x, Q^2)) , \\
 p^\mu p^\nu W_{\mu\nu} &= \frac{Q^2}{8x^2} (\mathcal{F}_2(x, Q^2) - \mathcal{F}_1(x, Q^2)) , \\
 ih \epsilon^{\mu\nu\lambda\kappa} \frac{q_\lambda p_\kappa}{p \cdot q} W_{\mu\nu} &= \tilde{\Gamma}(3-2\epsilon) \mathcal{G}_1(x, Q^2) ,
 \end{aligned}
 \tag{5.4.1}$$

where  $\tilde{\Gamma}(N-2\epsilon)$  is defined by (see appendix A3)

$$\tilde{\Gamma}(N-2\epsilon) = \Gamma(N) (1 + a_N \epsilon) .
 \tag{5.4.2}$$

The ambiguity,  $a_N$ , as will be demonstrated also appears in the Drell-Yan coefficient function and in fact cancels in the difference  $(\Delta f_{q,DY} - \Delta f_q)$ .

Let us consider first the quark sector, the lowest order graph, Fig.5.4.1 (a), gives  $\mathcal{F}_2 = \mathcal{G}_1 = \delta(1-x)$ , with this defining the normalisation of the partonic cross-section. To the next order one must also calculate the real-gluon emission graphs, Fig. 5.4.2 and the interference from Fig. 5.4.1 (b,c,d) with the lowest order diagram.

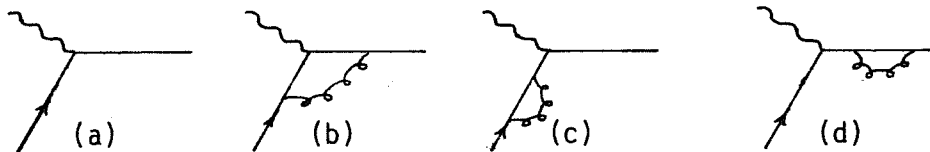


Fig. 5.4.1. (a) Lowest order diagram for the process  $\gamma^* q \rightarrow q$ ,  
 (b) vertex correction,  
 (c) and (d) wave-function corrections.

The real gluon emission graphs describe the reaction

$$\gamma^*(q) + q(p) \rightarrow q(p') + g(k), \quad (5.4.3)$$

where the symbols in brackets are the momenta carried by the fields.

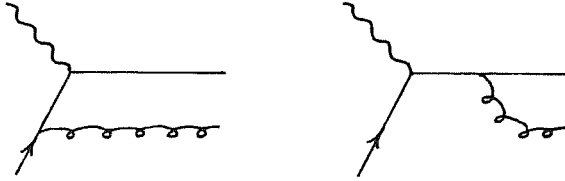


Fig. 5.4.2. Real-gluon emission corrections to the basic process.

In D dimensions the invariant matrix elements for this reaction:

$$\begin{aligned} |m_{\gamma^* q \rightarrow qg}|^2 &= \frac{1}{2} \{ |m_{\gamma^* q^+ \rightarrow qg}| + |m_{\gamma^* q^- \rightarrow qg}| \}, \\ \Delta |m_{\gamma^* q \rightarrow qg}|^2 &= \frac{1}{2} \{ |m_{\gamma^* q^+ \rightarrow qg}| - |m_{\gamma^* q^- \rightarrow qg}| \}, \end{aligned} \quad (5.4.4)$$

are given by

$$\begin{aligned} |m_{\gamma^* q \rightarrow qg}|^2 &= 4\alpha_s C_2(R) (1-\epsilon) (\mu^2)^\epsilon \left\{ (1-\epsilon) \left( \frac{s}{-t} + \frac{-t}{s} + \frac{2uQ^2}{st} + 2\epsilon \right) \right. \\ \Delta |m_{\gamma^* q \rightarrow qg}|^2 &= 4\alpha_s C_2(R) \tilde{\Gamma}(3-2\epsilon) (\mu^2)^\epsilon \left\{ (1-\epsilon) \left( \frac{s}{-t} - \frac{-t}{s} + \frac{2uQ^2}{st} \right) \right. \\ &\quad \left. \left. + 2(1-\epsilon) \left( \frac{Q^2+t}{Q^2+s} + \frac{-t}{s} \right) \right\} \end{aligned} \quad (5.4.5)$$

where the subprocess Mandelstam variables (here without circumflex) are given by

$$s = (p+q)^2, \quad t = (p-k)^2, \quad u = (p-p')^2. \quad (5.4.6)$$

The two-particle phase space (PS) in D dimensions for the production of two on-shell massless objects may be written

$$PS = \frac{1}{8\pi} s^{-\epsilon} \int_0^1 dy [y(1-y)]^{-\epsilon}, \quad (5.4.7)$$

where the  $\overline{MS}$  scheme has been anticipated and the necessary alterations made

(see eq.1.4.12),  $y = \frac{1}{2}(1+\cos\vartheta)$  with  $\vartheta$  the partonic subprocess centre-of-mass angle between incoming quark and outgoing gluon and all integrations over unspecified angles have been performed. The variables  $s, t$  and  $u$  are given in terms of  $x$  and  $y$  as

$$s = \frac{Q^2(1-x)}{x}, \quad t = \frac{-Q^2(1-y)}{x}, \quad u = \frac{-Q^2 y}{x}. \quad (5.4.8)$$

So we obtain the contributions to  $\mathcal{F}_{2|\text{real}}$  and  $\mathcal{G}_{1|\text{real}}$  as

$$\begin{aligned} \mathcal{F}_{2|\text{real}} &= \frac{\alpha_s}{2\pi} \frac{4}{3} \left(\frac{\mu^2}{Q^2}\right)^\epsilon \left\{ 3x + x^\epsilon(1-x)^{-\epsilon} \int_0^1 dy [y(1-y)]^{-\epsilon} \right. \\ &\quad \left. \times \left[ \left( \frac{1-x}{1-y} + \frac{1-y}{1-x} \right) (1-\epsilon) + \frac{2xy}{(1-x)(1-y)} \right] \right\}, \\ \mathcal{G}_{1|\text{real}} &= \frac{\alpha_s}{2\pi} \frac{4}{3} \left(\frac{\mu^2}{Q^2}\right)^\epsilon \left(\frac{x}{1-x}\right)^\epsilon \int_0^1 dy [y(1-y)]^{-\epsilon} \\ &\quad \times \left[ (1-\epsilon) \left( \frac{1-x}{1-y} - \frac{1-y}{1-x} \right) + \frac{2xy}{(1-x)(1-y)} + 2(1-\epsilon) \left( 1 + \frac{1-y}{1-x} \right) \right], \quad (5.4.9) \end{aligned}$$

where the contribution from the longitudinal cross-section has been included in the expression for  $\mathcal{F}_2$  (see ref. [9]). Performing the integral over  $y$  one obtains

$$\begin{aligned} \mathcal{F}_{2|\text{real}} &= \frac{\alpha_s}{2\pi} \frac{4}{3} \left(\frac{\mu^2}{Q^2}\right)^\epsilon \frac{\Gamma^2(1-\epsilon)}{\Gamma(1-2\epsilon)} \left\{ \frac{2}{\epsilon^2} \delta(1-x) - \frac{1}{\epsilon} \frac{1+x^2}{(1-x)_+} + \frac{3}{2\epsilon} \delta(1-x) \right. \\ &\quad \left. + \left[ (1+x^2) \left( \frac{\ln(1-x)}{1-x} \right)_+ - \frac{3}{2} \frac{1}{(1-x)_+} - \frac{1+x^2}{1-x} \ln x + 3 + 2x + \frac{7}{2} \delta(1-x) \right] \right\}, \\ \mathcal{G}_{1|\text{real}} &= \frac{\alpha_s}{2\pi} \frac{4}{3} \left(\frac{\mu^2}{Q^2}\right)^\epsilon \frac{\Gamma^2(1-\epsilon)}{\Gamma(1-2\epsilon)} \left\{ \frac{2}{\epsilon^2} \delta(1-x) - \frac{1}{\epsilon} \frac{1+x^2}{(1-x)_+} + \frac{3}{2\epsilon} \delta(1-x) \right. \\ &\quad \left. + \left[ (1+x^2) \left( \frac{\ln(1-x)}{1-x} \right)_+ - \frac{3}{2} \frac{1}{(1-x)_+} - \frac{1+x^2}{1-x} \ln x + 2 + x + \frac{7}{2} \delta(1-x) \right] \right\}, \quad (5.4.10) \end{aligned}$$

where use has been made of the following identities to express all divergent quantities in terms of  $1/\epsilon$  singularities

$$x^\epsilon (1-x)^{-1-\epsilon} = -\frac{1}{\epsilon} \delta(1-x) + \frac{1}{(1-x)_+} - \epsilon \left( \frac{\ln(1-x)}{1-x} \right)_+ + \epsilon \frac{\ln x}{1-x} + O(\epsilon^2),$$

$$x^\epsilon (1-x)^{-\epsilon} = 1 + \epsilon \ln \frac{x}{1-x} + O(\epsilon^2), \quad (5.4.11)$$

with the usual definition of the + regularisation (see eq. 2.2.11).

We must now include the contribution of the interference terms of Fig. 5.4.1 (b,c,d). By adopting the Landau gauge this part of the calculation is reduced to that of the vertex correction, Fig. 5.4.1(b). This is given by

$$\Gamma(q^2) = \gamma^\mu \left\{ 1 + \frac{\alpha_s}{2\pi} C_2(R) \left( \frac{\mu^2}{Q^2} \right)^\epsilon \frac{\Gamma(1+\epsilon)\Gamma(1-\epsilon)}{\Gamma(1-2\epsilon)} \left[ -\frac{2}{\epsilon^2} - \frac{3}{\epsilon} - 8 \right] \right\}. \quad (5.4.12)$$

after use of the expansion,

$$\Gamma(1+\epsilon)\Gamma(1-\epsilon) = 1 + \epsilon^2 \frac{1}{6} \pi^2 + O(\epsilon^4), \quad (5.4.13)$$

the virtual gluon contribution to  $\mathcal{F}_2$  and  $\mathcal{G}_1$  may be written as

$$\mathcal{F}_{2|\text{virtual}} = \mathcal{G}_{1|\text{virtual}} = \delta(1-x) \left\{ 1 + \frac{\alpha_s}{2\pi} \frac{4}{3} \left( \frac{\mu^2}{Q^2} \right)^\epsilon \frac{\Gamma(1-\epsilon)}{\Gamma(1-2\epsilon)} \left[ -\frac{2}{\epsilon^2} - \frac{3}{\epsilon} - 8 - \frac{\pi^2}{3} \right] \right\}, \quad (5.4.14)$$

Finally adding the real and virtual contributions we obtain

$$\begin{aligned} \mathcal{F}_2(x, Q^2) &= \delta(1-x) - \frac{1}{\epsilon} \frac{\alpha_s}{2\pi} P_{qq}(x) \left( \frac{\mu^2}{Q^2} \right)^\epsilon \frac{\Gamma(1-\epsilon)}{\Gamma(1-2\epsilon)} \\ &+ \frac{\alpha_s}{2\pi} \frac{4}{3} \left[ (1+x^2) \left( \frac{\ln(1-x)}{1-x} \right)_+ - \frac{3}{2} \frac{1}{(1-x)_+} - \frac{1+x^2}{1-x} \ln x \right. \\ &\left. + 3 + 2x - \left( \frac{9}{2} + \frac{\pi^2}{3} \right) \delta(1-x) \right], \\ \mathcal{G}_1(x, Q^2) &= \mathcal{F}_2(x, Q^2) - \frac{\alpha_s}{2\pi} \frac{4}{3} (1+x). \end{aligned} \quad (5.4.15)$$

Thus extracting the required functions  $f_q$  and  $\Delta f_q$  we have

$$f_q(x) = \frac{4}{3} \left\{ (1+x^2) \left( \frac{\ln(1-x)}{(1-x)_+} \right) - \frac{3}{2} \frac{1}{(1-x)_+} - \frac{1+x^2}{1-x} \ln x \right. \\ \left. + 3 + 2x - \left( \frac{q}{2} + \frac{\pi^2}{3} \right) \delta(1-x) \right\}, \quad (5.4.16)$$

$$\Delta f_q(x) = f_q(x) - \frac{4}{3} (1+x),$$

where the  $1/\varepsilon$  pole has been subtracted out.

The moments of  $f_q$  and  $\Delta f_q$  defined by

$$f_q^{(n)} = \int_0^1 dx x^{n-1} f_q(x), \quad (5.4.17)$$

are easily derived:

$$f_q^{(n)} = \frac{4}{3} \left[ 2 \sum_{k=1}^n \frac{1}{k} \sum_{j=1}^k \frac{1}{j} - 2 \sum_{j=1}^n \frac{1}{j^2} - \frac{1}{n(n+1)} \sum_{j=1}^n \frac{1}{j} + \frac{1}{n^2} \right. \\ \left. + \frac{3}{2} \sum_{j=1}^n \frac{1}{j} + \frac{3}{2n} + \frac{2}{(n+1)} - \frac{q}{2} \right],$$

$$\Delta f_q^{(n)} = f_q^{(n)} - \frac{4}{3} \left( \frac{1}{n} + \frac{1}{n+1} \right). \quad (5.4.18)$$

Notice that while the first moment of  $f_q$  vanishes, the same is not true of  $\Delta f_q$ . This corresponds to the fact that the Adler sum rule [12] (related to the conservation of valence quark number) is true beyond leading order while the Bjorken sum rule receives order  $\alpha_s$  corrections.

The result (5.4.18) has also been derived in ref. [13] using dimensional regularisation, the results quoted here are in complete agreement. The same authors repeated the calculation using the Pauli-Villars cut-off technique [14], and owing to the scheme dependence obtained a different answer.

Finally at this order there is also a contribution from the gluon content of the hadron via the diagrams of Fig. 5.4.3, from which  $f_g$  and  $\Delta f_g$  will now be



extracted.

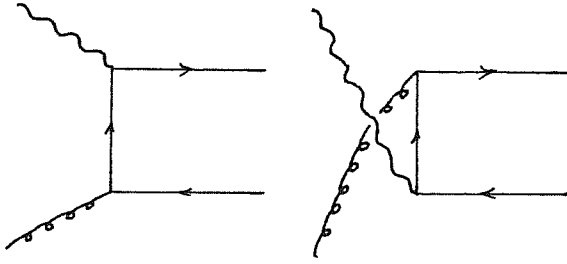


Fig. 5.4.3. Gluon sector contribution to deep-inelastic scattering at order  $\alpha_s$ .

While the spin-averaged cross-section for this process can be obtained from the previous from eq.(5.4.5) by crossing, the spin-dependent part cannot as the gluon polarisation is now being considered.

The matrix elements are

$$|M_{g^*g \rightarrow q\bar{q}}|^2 = 4\alpha_s T(R) (\mu^2)^\epsilon (1-\epsilon) \left[ (1-\epsilon) \left( \frac{u}{t} + \frac{t}{u} \right) - \frac{2Q^2 s}{ut} - 2\epsilon \right],$$

$$\Delta |M_{g^*g \rightarrow q\bar{q}}|^2 = 4\alpha_s T(R) (\mu^2)^\epsilon \tilde{\Gamma}^2(3-2\epsilon) \frac{1}{2!} \left[ \frac{u}{t} + \frac{t}{u} - \frac{2Q^2 s}{ut} - \frac{4s}{t+u} - \frac{2s^2}{ut} \right]. \quad (5.4.19)$$

The phase space is as before, thus integrating over the angular variable  $y$  one obtains the gluonic contributions:

$$\begin{aligned} \frac{1}{2} \mathcal{F}_2(x, Q^2) &= -\frac{1}{\epsilon} \frac{\alpha_s}{2\pi} P_{qg}(x) \left( \frac{\mu^2}{Q^2} \right)^\epsilon \\ &+ \frac{\alpha_s}{2\pi} \frac{1}{2} \left[ (x^2 + (1-x)^2) \ln \frac{1-x}{x} + 6x(1-x) \right], \\ \frac{1}{2} \mathcal{G}_1(x, Q^2) &= -\frac{1}{\epsilon} \frac{\alpha_s}{2\pi} \Delta P_{qg}(x) \left( \frac{\mu^2}{Q^2} \right)^\epsilon \\ &+ \frac{\alpha_s}{2\pi} \frac{1}{2} \left[ (2x-1) \ln \frac{1-x}{x} - a(2x-1) \right] \end{aligned} \quad (5.4.20)$$

where  $P_{qg} = \frac{1}{2} x^2 + (1-x)^2$  and  $P_{qg} = \frac{1}{2}(2x-1)$ . The term  $a(2x-1)$  represents the ambiguity in the definition of  $\epsilon^{\mu\nu\rho\sigma}$  in  $D$  dimensions. The factor of  $\frac{1}{2}$  multiplying the structure functions arises because  $f_g$  and  $\Delta f_g$  give the gluon correction for either a quark or antiquark whereas the gluon splits into both a quark and an antiquark. The quantities  $f_g$  and  $\Delta f_g$  may now be

extracted from eqs. (5.4.20)

$$f_g(x) = \frac{1}{2} \left[ (x^2 + (1-x)^2) \ln \frac{1-x}{x} + 6x(1-x) \right],$$

$$\Delta f_g(x) = \frac{1}{2} \left[ (2x-1) \ln \frac{1-x}{x} - a(2x-1) \right]. \quad (5.4.21)$$

In moment form one has

$$f_g^{(n)} = \frac{1}{2} \left[ \frac{4}{(n+1)(n+2)} + \frac{1}{n^2} - \frac{n^2+n+2}{n(n+1)(n+2)} \sum_{j=1}^n \frac{1}{j} \right],$$

$$\Delta f_g^{(n)} = \frac{1}{2} \left[ \frac{3-n}{n^2(n+1)} - \frac{(n-1)}{n(n+1)} \sum_{j=1}^n \frac{1}{j} \right]. \quad (5.4.22)$$

This completes the calculation of the coefficient functions for deep-inelastic scattering.

Before moving on to the Drell-Yan coefficient functions let us make a remark on the similarity of the behaviour between the non-singlet structure functions  $\mathcal{F}_2^{NS}$  and  $\mathcal{G}_1^{NS}$ . The fact that they have the same anomalous dimensions suggests an interesting method for isolating the order  $\alpha_s$  corrections [15].

In moment form one can express  $\mathcal{F}_2$  and  $\mathcal{G}_1$  to order  $\alpha_s$  as [16]:

$$\mathcal{F}_2^{(n)}(Q^2) = A_n \left[ 1 + \frac{\alpha_s(Q^2)}{2\pi} \left( f_g^{(n)} + \frac{\gamma_1^{(n)}}{4\beta_0} - \frac{\beta_1 \gamma_0^{(n)}}{4\beta_0^2} \right) \right] \left( \frac{\alpha_s(Q^2)}{\alpha_s(Q_0^2)} \right)^{\gamma_0^{(n)}/2\beta_0}, \quad (5.4.22)$$

with a similar expression for  $\mathcal{G}_1^{(n)}$ , where  $\gamma_0^{(n)}$ ,  $\gamma_1^{(n)}$ ,  $\beta_0$  and  $\beta_1$  are defined by

$$\gamma^{(n)}(g) = \gamma_0^{(n)} \frac{g^2}{16\pi^2} + \gamma_1^{(n)} \left( \frac{g^2}{16\pi^2} \right)^2 + \dots,$$

$$\beta(g) = \beta_0 \frac{g^3}{16\pi^2} + \beta_1 \frac{g^5}{(16\pi^2)^2} + \dots \quad (5.4.23)$$

The unknown constants  $A_n$  are related to the matrix of the relevant operator evaluated between nucleon states.

Recall that although  $f_q^{(n)}$  is scheme dependent, so too is  $\gamma_1^{(n)}$  and in fact the combination  $f_q^{(n)} + \gamma_1^{(n)}/4\beta$  is renormalisation scheme independent [17]. Thus for the ratio  $\mathcal{G}_1^{(n)}/\mathcal{F}_2^{(n)}$  (again scheme independent) one has

$$\mathcal{G}_1^{(n)}/\mathcal{F}_2^{(n)} = C_n \left[ 1 + \frac{\alpha_s(Q^2)}{2\pi} (\Delta f_q^{(n)} - f_q^{(n)}) \right] \quad (5.4.24)$$

Taking the logarithm one obtains:

$$R^{(n)} = \ln \left[ \mathcal{G}_1^{(n)}/\mathcal{F}_2^{(n)} \right] = a_n - \frac{\alpha_s}{2\pi} \frac{4}{3} \left( \frac{1}{n} + \frac{1}{n+1} \right) + b_n \alpha_s^2 + \frac{c_n}{Q^2} + \dots \quad (5.4.25)$$

The constant  $a_n$  can be removed by subtracting for a particular value of  $Q^2$  the terms  $b_n \alpha_s^2$  and  $c_n/Q^2$  represent higher order and higher power corrections respectively. Initially one assumes these terms to be small, for  $Q^2 > 10 \text{ GeV}^2$  say.

One then compares (5.4.25) with the data to extract a value of  $\Lambda$ .

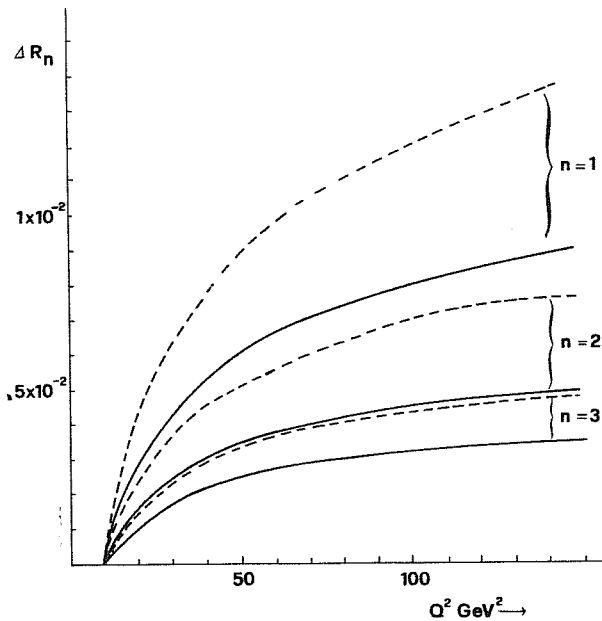


Fig. 5.4.4. Plot of  $\Delta R^{(n)} = R^{(n)}(Q^2) - R^{(n)}(Q_0^2)$  with  $Q_0^2 = 10 \text{ GeV}^2$ . The solid curves correspond to  $\Lambda = 100 \text{ MeV}$  and the dashed curves to  $\Lambda = 200 \text{ MeV}$ .

5.5. Calculation of the coefficient function to order  $\alpha_s$  in the Drell-Yan process

The corresponding calculations must now be performed for the production of a time-like photon. The lowest order diagram, Fig. 5.5.1 (a), for  $q\bar{q}$  annihilation has the matrix element:

$$|M_{q\bar{q} \rightarrow \gamma^*}^{hh'}|^2 = \frac{(1-\epsilon)}{2N} \frac{s}{2\pi} 2\delta_{hh'} \quad , \quad (5.5.1)$$

where  $h, h'$  are the helicities of the quark and antiquark respectively and the phase space is now

$$P.S. = \frac{2\pi}{s} \delta(1-z) \quad , \quad (5.5.2)$$

with  $z$  for the subprocess defined as  $Q^2/s$ . Thus the subprocess cross-sections are, to lowest order

$$\frac{d\sigma}{dQ^2}(z, Q^2) = - \frac{d\Delta\sigma}{dQ^2}(z, Q^2) = \delta(1-z) \quad , \quad (5.5.3.)$$

where the factor  $(1-\epsilon)/2N$  has been divided out as will be done for all the following.

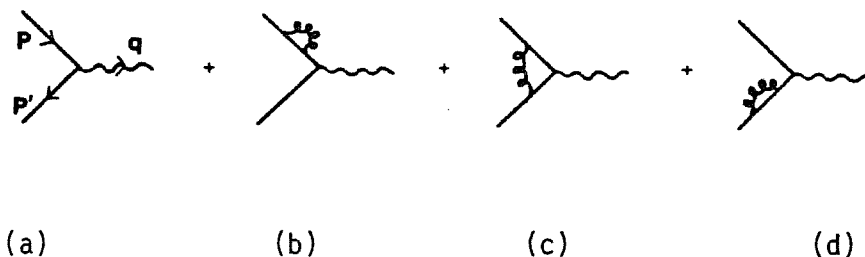


Fig. 5.5.1. (a) Lowest order diagram for  $q\bar{q} \rightarrow \gamma^*$ ,  
 (b) vertex renormalisation correction,  
 (c) and (d) wave function renormalisation corrections to the basic process.

The diagrams of Fig. 5.5.2 describe the emission of a real gluon:

$$q(p, h) + \bar{q}(p', h') \rightarrow g(k) + \gamma^*(q) . \quad (5.5.4)$$

The matrix element for this process is

$$|M_{\bar{q}q \rightarrow \gamma^*g}^{hh'}|^2 = \delta_{hh'} 4\alpha_s C_2(R) \frac{1-\epsilon}{2N} (\mu^2)^\epsilon \left\{ (1-\epsilon) \left( \frac{u}{t} + \frac{t}{u} + \frac{2Q^2 s}{ut} - 2\epsilon \right) \right\} . \quad (5.5.5)$$

The phase-space, in  $4-2\epsilon$  dimensions for the production of a massive photon is (in  $\overline{\text{MS}}$ )

$$\text{P.S.} = \frac{1}{8\pi} \left( \frac{1}{Q^2} \right)^\epsilon z^\epsilon (1-z)^{1-2\epsilon} \int_0^1 dy [y(1-y)]^{-\epsilon} , \quad (5.5.6)$$

with  $y$  as in sec. 5.4, but now the subprocess invariants are

$$s = \frac{Q^2}{z} , \quad t = -Q^2 \frac{(1-z)}{z} (1-y) , \quad u = -Q^2 \frac{(1-z)}{z} y . \quad (5.5.7)$$

Integrating as usual over  $y$  we obtain

$$\begin{aligned} \left. \frac{d\sigma_{q\bar{q}}}{dQ^2} \right|_{\text{real}} &= - \left. \frac{d\Delta\sigma_{q\bar{q}}}{dQ^2} \right|_{\text{real}} = \frac{\alpha_s}{2\pi} \frac{4}{3} \left( \frac{\mu^2}{Q^2} \right)^\epsilon \frac{\Gamma^2(1-\epsilon)}{\Gamma(2-\epsilon)} \left\{ \frac{2}{\epsilon^2} \delta(1-z) \right. \\ &\quad \left. - \frac{2}{\epsilon} \frac{1+z^2}{(1-z)_+} + 4(1+z^2) \left( \frac{\ln(1-z)}{1-z} \right)_+ - 2 \left( \frac{1+z^2}{1-z} \right) \ln z \right\} . \end{aligned} \quad (5.5.8)$$

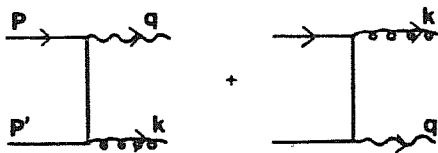


Fig. 5.5.2.. Real gluon emission corrections to the basic process

The virtual gluon contributions (corresponding to Fig. 5.5.1(b) in the Landau gauge) can be obtained from eq.(5.4.12) by substituting  $Q^2 \rightarrow -Q^2$  and expanding the extra factor of  $(-1)^\epsilon$  up to order  $\epsilon^2$ , this gives:

$$\left. \frac{d\sigma}{dQ^2} \right|_{\text{virtual}} = - \left. \frac{d\Delta\sigma}{dQ^2} \right|_{\text{virtual}} = \delta(1-z) \left\{ 1 + \frac{\alpha_s}{2\pi} \frac{4}{3} \left( \frac{\mu^2}{Q^2} \right)^\epsilon \frac{\Gamma^2(1-\epsilon)}{\Gamma(1-2\epsilon)} \left[ -\frac{2}{\epsilon^2} - \frac{3}{\epsilon} - 8 + \frac{2\pi^2}{3} \right] \right\}. \quad (5.5.9)$$

Adding the real and virtual contributions gives

$$\begin{aligned} \frac{d\sigma}{dQ^2} \Big|_{\text{total}} = - \frac{d\Delta\sigma}{dQ^2} \Big|_{\text{total}} = & \delta(1-z) - \frac{2}{\epsilon} \frac{\alpha_s}{2\pi} P_{qq}(z) \left( \frac{\mu^2}{Q^2} \right)^\epsilon \\ & + \frac{\alpha_s}{2\pi} \frac{4}{3} \left[ 4(1+z^2) \left( \frac{\ln(1-z)}{1-z} \right)_+ - 2 \left( \frac{1+z^2}{1-z} \right) \ln z + \left( \frac{2\pi^2}{3} - 8 \right) \delta(1-z) \right]. \end{aligned} \quad (5.5.10)$$

And thus we can extract the required quantities  $f_{q,DY}$  and  $\Delta f_{q,DY}$ :

$$f_{q,DY} = \Delta f_{q,DY} = \frac{4}{3} \left[ 2(1+z^2) \left( \frac{\ln(1-z)}{1-z} \right)_+ - \left( \frac{1+z^2}{1-z} \right) \ln z + \left( \frac{2\pi^2}{3} - 4 \right) \delta(1-z) \right]. \quad (5.5.11)$$

Lastly one must calculate the quark-gluon (QCD Compton) scattering of Fig. 5.5.3.

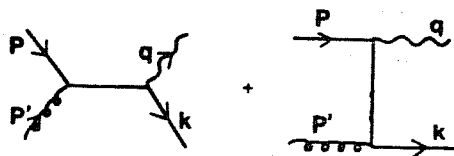


Fig. 5.5.3. Quark-gluon scattering contribution to the Drell-Yan process at order  $\alpha_s$ .

One obtains the following

$$\begin{aligned}
 |M_{q\bar{q} \rightarrow \gamma^* q}|^2 &= 4 \alpha_s \frac{1}{2} \frac{1-\epsilon}{2N} \left\{ (1-\epsilon) \left( \frac{s}{-t} + \frac{-t}{s} \right) - \frac{2Q^2 u}{s\epsilon} + 2\epsilon \right\}, \\
 \Delta |M_{q\bar{q} \rightarrow \gamma^* q}|^2 &= 4 \alpha_s \frac{1}{2} \frac{1-\epsilon}{2N} \tilde{\Gamma}(\beta-2\epsilon) \left\{ \frac{s}{-t} - \frac{-t}{s} - \frac{2Q^2(Q^2-u)}{s\epsilon} \right\}. \quad (5.5.12)
 \end{aligned}$$

On integrating over  $y$  these give respectively

$$\begin{aligned}
 \frac{d\sigma}{dQ^2 dy} &= -\frac{1}{\epsilon} \frac{\alpha_s}{2\pi} P_{q\bar{q}}(z) \left( \frac{\mu^2}{Q^2} \right)^\epsilon + \frac{\alpha_s}{2\pi} \frac{1}{2} \left[ (z^2 + (1-z)^2) \ln \frac{(1-z)^2}{z} - \frac{3z^2}{2} + z + \frac{3}{2} \right], \\
 -\frac{d\Delta\sigma}{dQ^2 dy} &= -\frac{1}{\epsilon} \frac{\alpha_s}{2\pi} \Delta P_{q\bar{q}}(z) \left( \frac{\mu^2}{Q^2} \right)^\epsilon + \frac{\alpha_s}{2\pi} \frac{1}{2} \left[ (2z-1) \ln \frac{(1-z)^2}{z} - \frac{3z^2}{2} + 3z - \frac{1}{2} - a(2z-1) \right], \quad (5.5.13)
 \end{aligned}$$

Here we see the expected term  $a(2z-1)$  which will precisely cancel the corresponding term in the deep-inelastic coefficient functions. Extracting the last of the required quantities,  $f_{g,DY}$  and  $\Delta f_{g,DY}$ , one has:

$$\begin{aligned}
 f_{g,DY} &= \frac{1}{2} \left[ (z^2 + (1-z)^2) \ln \frac{(1-z)^2}{z} - \frac{3z^2}{2} + z + \frac{3}{2} \right], \\
 \Delta f_{g,DY} &= \frac{1}{2} \left[ (2z-1) \ln \frac{(1-z)^2}{z} - \frac{3z^2}{2} + 3z - \frac{1}{2} - a(2z-1) \right], \quad (5.5.14)
 \end{aligned}$$

where, as usual, the singularity has been subtracted.

5.6. Numerical results for the helicity asymmetries in the Drell-Yan process

From the results given in the previous two sections one can derive the required differences: in the quark sector one has

$$2(f_{q,DY} - f_q) = \frac{4}{3} \left[ \frac{3}{(1-z)_+} + 2(1+z^2) \left( \frac{\ln(1-z)}{1-z} \right)_+ - 6 - 4z + \left(1 + \frac{4\pi^2}{3}\right) \delta(1-z) \right],$$

$$2(\Delta f_{q,DY} - \Delta f_q) = 2(f_{q,DY} - f_q) + \frac{4}{3}(2 + 2z), \quad (5.6.1)$$

and for the gluon contributions,

$$(f_{g,DY} - f_g) = \frac{1}{2} \left[ (z^2 + (1-z)^2) \ln(1-z) + \frac{9z^2}{2} - 5z + \frac{3}{2} \right],$$

$$(\Delta f_{g,DY} - \Delta f_g) = \frac{1}{2} \left[ (2z - 1) \ln(1-z) - \frac{3z^2}{2} + 3z - \frac{1}{2} \right]. \quad (5.6.2)$$

The important point to notice is that the large corrections from the delta function are equal in the two cross-sections  $d\sigma_{DY}$  and  $d\Delta\sigma_{DY}$  and thus in the asymmetry (the ratio of these two) the K-factor precisely cancels. Below, in Fig. 5.6.1, the moments of the above expressions (5.6.1 and 2) are plotted against  $n$ . As can be seen the remaining difference between the expressions for the spin-averaged and helicity-correlated cross-sections are truly small, about 10% for  $n = 2$  and decreasing rapidly with  $n$ .



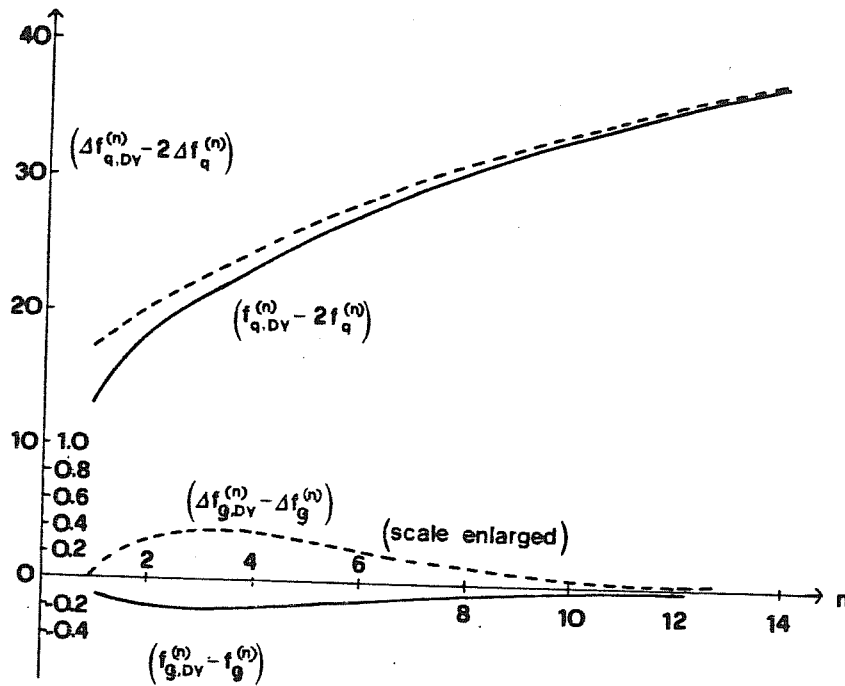


Fig. 5.6.1. Moments of the differences  $2(f_{qDY} - f_q)$  and  $(F_{gDY} - f_g)$ , solid lines  $Z(f_{q,DY} - f_q)$  and  $(f_{g,DY} - f_g)$ , broken lines. The gluonic terms are shown on an enlarged scale.

Using the parton distributions of appendix A4 the asymmetry has been calculated as a function of  $\tau$  for various values of centre-of-mass energy.

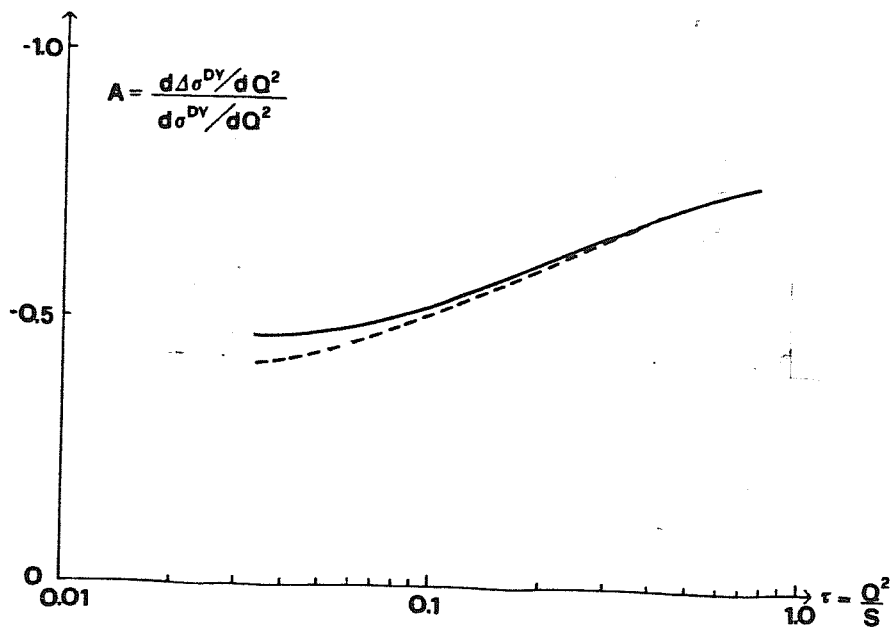


Fig. 5.6.2. The asymmetry  $\mathcal{A}_{LL}$  for the Drell-Yan process. Full calculation (solid line) and only the  $\delta$ -function corrections (dashed line).

From an experimental point-of-view a more useful quantity is the asymmetry with respect to the cross-section differential in Feynman  $x_F = 2q_z / \sqrt{s}$ . The authors of ref. [9] have calculated the spin-averaged part of the latter; they give the form for the quark contribution as

$$\begin{aligned} \frac{Q^2 d^2 \sigma}{dQ^2 dx_F} = & \frac{4\pi\alpha}{9S} \left\{ \frac{1}{\sqrt{x_F^2 + 4\tau}} \left[ \tilde{H}(x_1^0, x_2^0, t) \left[ 1 + \frac{\alpha_s(t)}{2\pi} \frac{4}{3} \left( 1 + \frac{4}{3}\pi^2 \right) \right] \right. \right. \\ & + \frac{\alpha_s(t)}{2\pi} \int_{x_1^0}^1 \frac{dx_2}{x_1} \tilde{H}(x_1, x_2^0, t) g\left(\frac{x_1^0}{x_1}\right) + \frac{\alpha_s(t)}{2\pi} \int_{x_2^0}^1 \frac{dx_2}{x_2} \tilde{H}(x_1^0, x_2, t) g\left(\frac{x_2^0}{x_2}\right) \\ & \left. \left. + \frac{\alpha_s(t)}{2\pi} \int_{x_1^0}^1 \frac{dx_1}{x_1} \int_{x_2^0}^1 \frac{dx_2}{x_2} \tilde{H}(x_1, x_2, t) f(x_1, x_2) \right. \right. \end{aligned} \quad (5.6.3)$$

where  $\tilde{H}(x_1, x_2, t) = \sum_i e_i^2 q_i^{[1]}(x_1, t) q_i^{[2]}(x_2, t)$ , the explicit forms of  $g$  and  $f$  can be found in the original paper. A similar expression is given for the gluon contribution. Thus the corrections for the asymmetry will come from the small differences in  $g$  and  $f$  between the spin-averaged and -correlated cross-sections.

So, provided  $\tau$  is not too small, to a good approximation one can calculate the asymmetry using only the first line of (5.6.3) and making the usual replacement  $q \rightarrow \Delta q$  etc. for the helicity part. The leading order result is given in Fig. 5.6.3 for the asymmetry

$$A_{LL} = \frac{Q^2 d^2 \Delta \sigma^{DY}}{dQ^2 dx_F} \bigg/ \frac{Q^2 d^2 \sigma^{DY}}{dQ^2 dx_F} \bigg|_{x_F=0} \quad (5.6.4)$$

where

$$\frac{Q^2 d^2 \Delta \sigma^{DY}}{dQ^2 dx_F} = \frac{4\pi\alpha}{9S} \frac{1}{\sqrt{x_F^2 + 4\tau}} \sum_i e_i^2 \Delta q_{\frac{1}{i}}^{[1]}(x_2, t) \Delta \bar{q}_{\frac{1}{i}}^{[2]}(x_2, t) \left[ 1 + \frac{\alpha_s(t)}{2\pi} \frac{4}{3} \left( 1 + \frac{4\pi^2}{3} \right) \right]. \quad (5.6.5)$$

This should provide a good guide to the asymmetry, despite the fact that the normalisation is increased by a factor of order 2 by the radiative corrections, that is the additional smearing in (5.6.3) is likely to be negligible.

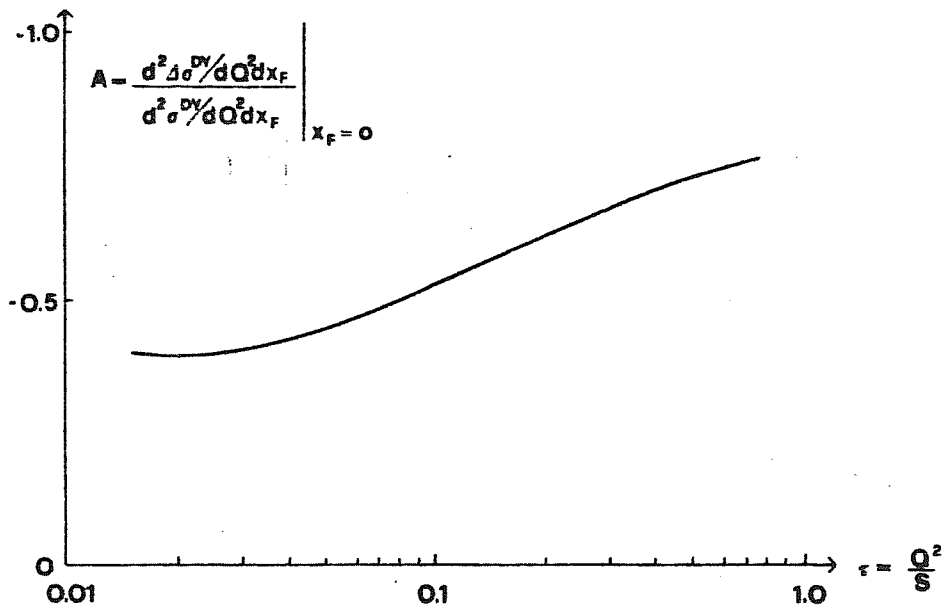


Fig. 5.6.3. Plot of the leading order asymmetry  $A_{LL} = (d^2 \Delta \sigma^{DY} / dQ^2 dx_F) / (d^2 \sigma^{DY} / dQ^2 dx_F) \Big|_{x_F = 0}$  against  $\tau$ .

References to chapter 5

- [1] G.T. Bodwin, S.J. Brodsky and G.P. Lepage, Phys. Rev. Lett. 47, 1799 (1981); SLAC reports SLAC-PUB-2787, 2860 (1981) and 2927 (1982).
- [2] W.W. Lindsay, D.A. Ross and C.T. Sachrajda, Phys. Lett. 117B, 105 (1982), Nucl. Phys. B214, 61 (1983).
- [3] J.C. Collins, D.A. Soper and G. Sterman, Phys. Lett. B109, 388 (1982); Stony Brook preprint ITP-SB-82-46.
- [4] R. Doria, J. Frenkel and J.C. Taylor, Nucl. Phys. B168, 93 (1980); D. Di'Lieto, S. Gendron, I.G. Halliday and C.T. Sachrajda, Nucl. Phys. B183, 223 (1981); A.H. Mueller, Columbia preprint CU-TP-213 (1981).
- [5] B. Humpert and W.L. van Neerven, Phys. Lett. 84B, 327 (1979).
- [6] F. Khalafi and P.V. Landshoff, Cambridge preprint DAMTP 81/23 (1981). F. Khalafi, Z. Phys. C11, 251 (1981).
- [7] P.V. Landshoff and W.J. Stirling, Z. Phys. C14, 251 (1982); F. Khalafi, Z. Phys. C14, 135 (1982); C18, 57 (1983).
- [8] C.T. Sachrajda and S. Yankielowicz in the Proc. of the 1979 Cargèse Summer Institute on Quarks and Leptons.
- [9] G. Altarelli, R.K. Ellis and G. Martinelli, Nucl. Phys. B157, 461 (1979); B143, 521 (1978), E: B146, 544 (1978).
- [10] K. Harada, T. Kaneko and N. Sakai, Nucl. Phys. B155, 169 (1979), E: B165, 545 (1980).  
J. Kubar-André and F.E. Paige, Phys. Rev. D19, 221 (1978).  
J. Abad and B. Humpert, Phys. Lett. 77B, 105 (1978); 80B, 286 (1979).  
For a discussion of higher order corrections for various processes besides Drell-Yan see also: W. Furmanski and R. Petronzio, Z. Phys. C11, 293 (1982).

- [11] P. Ratcliffe, Nucl. Phys. B223, 45 (1983).
- [12] S.L. Adler, Phys. Rev. 143, 1144 (1965).
- [13] T. Kodaira, S. Matsuda, K. Sasaki and T. Uematsu, Phys.Rev. D20, 627 (1979).
- [14] T. Kodaira, S. Matsuda, K. Sasaki and T. Uematsu, Nucl. Phys. B159 99 (1979).
- [15] N.S. Craigie and P. Ratcliffe, Z. Phys. C17, 43 (1983).
- [16] A.J. Buras, E.G. Floratos, D.A. Ross and C.T. Sachrajda, Nucl. Phys. B131, (1977).
- [17] For a proof of this see for example D. Gross in Methods in field theory. Les Houches 1975, Eds. R. Balian and J. Zinn-Justin, Chap. 4. Amsterdam: North Holland.

Chapter 6      Helicity asymmetries in higher power mechanisms

- 6.1      Bethe-Salpeter approach to the hadronic asymptotic wave function
- 6.2      Hyperon production at large angles in proton-proton collisions
- 6.3      The hard scattering kernel
- 6.4      Numerical results for transmitted asymmetries in  $\Delta$ -production

## 6.1 Bethe-Salpeter approach to the hadronic asymptotic wave function

In the subasymptotic region (for which typical momentum transfers or  $P_T$  are not much larger than hadronic mass scales) one expects higher power mechanisms to play a significant rôle in exclusive and semi-inclusive processes.

Due to the pioneering work of Lepage and Brodsky [1] many of these mechanisms are accessible to perturbative QCD. Lepage and Brodsky use light-cone perturbation theory and the light-cone gauge to derive evolution equations for the hadron distribution amplitudes  $\Phi(x_i, Q^2)$  which control the valence quark distributions in high-momentum-transfer reactions. These may be evaluated to any required order in  $\alpha_s(Q^2)$ . These amplitudes are then convoluted with a hard scattering kernel, which depends on the process under consideration and can be thought of as lining up the quarks to form the hadron.

The distribution amplitude  $\Phi$  is simply related to the hadronic wave function:

$$\Phi(x_i, Q^2) \propto \int^a [dk_{Ti}] \Psi(x_i, k_{Ti}) . \quad (6.1.1)$$

It contains the essential physics of that part of the hadronic wave function which affects exclusive channels with large momentum transfers. The distribution amplitude, clearly process independent, is only weakly dependent on  $Q^2$ , and this dependence is completely specified by an evolution equation which in leading order takes the form

$$Q^2 \frac{\partial}{\partial Q^2} \Phi(x_i, Q^2) = \frac{\alpha_s(Q^2)}{4\pi} \int_0^1 [dy] V(x_i, y_i) \Phi(y_i, Q^2), \quad (6.1.2)$$

where  $V$  can be computed from a single-gluon-exchange kernel. The general solution of this equation in the case of the proton is

$$\Phi(x_i, Q^2) = x_1 x_2 x_3 \sum_{n=0}^{\infty} a_n \left( \ln \frac{Q^2}{\Lambda^2} \right)^{\gamma_n} \tilde{\Phi}_n(x_i) . \quad (6.1.3)$$

Asymptotically the first term dominates:

$$\Phi(x_i, Q^2) \rightarrow C x_1 x_2 x_3 \left( \ln \frac{Q^2}{\Lambda^2} \right)^{-2/3\beta_0} . \quad (6.1.4)$$

The evolution equation is represent schematically in Fig. 6.1.1, where the terms not exhibited represent higher order  $\alpha_s$  corrections

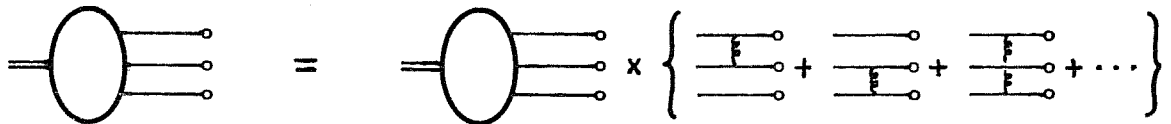


Fig. 6.1.1 Bound state equation for the baryonic three-quark wave function at large momenta.

By way of an example consider the electromagnetic form factor of a nucleon, given by

$$G_H(Q^2) = \int_0^1 [dx] [dy] \Phi^*(x_i, Q^2) T_H(x_i, y_i, Q^2) \Phi(y_i, Q^2) , \quad (6.1.5)$$

where the hard scattering amplitude is given by the set of diagrams in Fig. 6.1.2 (the contribution from the triple gluon coupling is absent as the colour factor is zero).

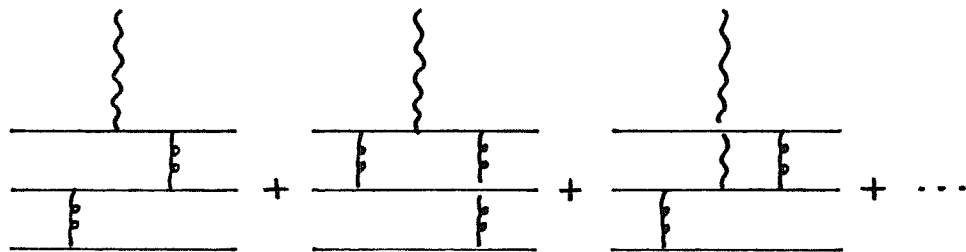


Fig. 6.1.2. Diagrams contributing to  $T_H$  for baryonic form factors.



Note that  $T_H$  is defined with its external legs on shell and is therefore both gauge and Lorentz invariant. The expression for  $G_M$  can thus be viewed pictorially as in Fig. 6.1.3. The rôle of the hard-scattering kernel of

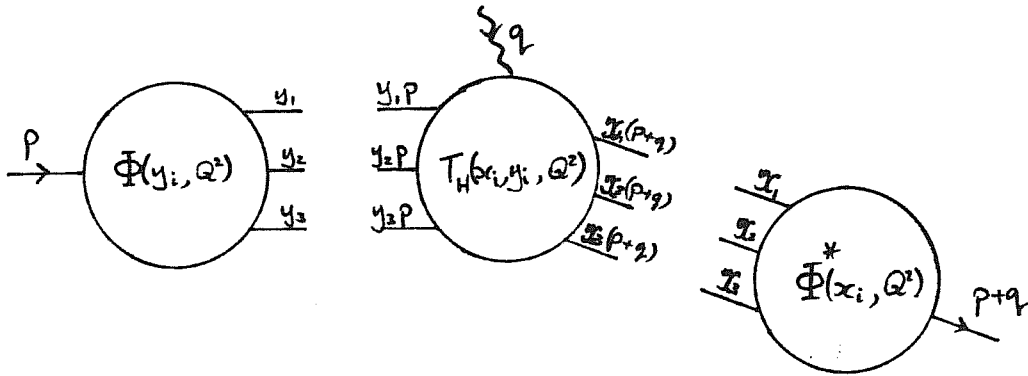


Fig. 6.1.3. The general structure of the proton's magnetic form factor at large  $Q^2$

redistributing the large momentum  $q$  between the quarks in order to realign them is clear. This also implies the gluons of Fig. 6.1.2 carry large momentum transfers  $\sim O(Q^2)$  thus justifying the use of perturbative QCD.

## 6.2 Hyperon production at large angles in proton-proton collisions

As already discussed in sect. 4.2 , measurements of single-spin asymmetries (or more precisely polarisation) of strange baryons produced in proton-proton collisions have produced startling results. While such effects are not readily accessible to perturbative QCD, as discussed in sect. 3.5 assuming the strange quark is produced essentially via a gluon-fusion mechanism one can obtain estimates of both the reflected and transmitted asymmetries. Such asymmetries should also be well accessible to experiment, in particular the UA6 experiment (see sect. 4.4) could, even without polarised proton beam, measure to a high degree of accuracy the transmitted asymmetry in  $\vec{p}p \rightarrow \vec{\Lambda}X$ .

For not very large values of  $p_T$  one expects that higher power mechanisms will play an important rôle. While it is often very difficult to ascertain the power-law behaviour with respect to  $p_T$  , helicity dependence tends to be strikingly large and can differ drastically from mechanism to mechanism and thus provide a valuable method of identifying the particular process at work.

One possible method for producing a  $\Lambda$  hyperon is by combining a diquark from one proton with a strange quark (produced by a gluon from the other proton) via a hard-scattering kernel similar to that described in the previous section [2] . This process is represented diagrammatically in Fig. 6.2.1, the blob is precisely the hard-scattering kernel.

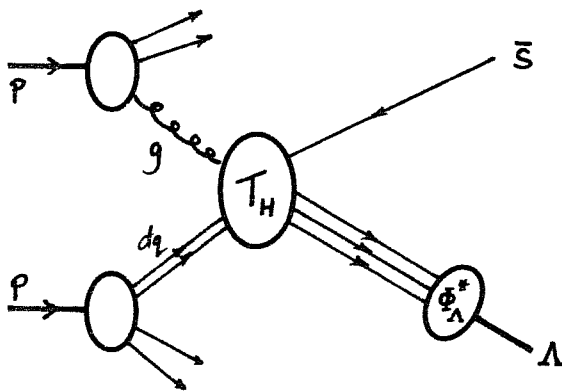


Fig. 6.2.1. A higher power mechanism for  $\Lambda$  production in  $pp$  collisions.

This picture motivates a simple description of the process, namely a pointlike effective interaction  $g + dq \rightarrow \Delta + \bar{s}$ , which could be understood in terms of gauge invariant effect Lagrangian:

$$\mathcal{L} = \bar{\Psi}_\Lambda \gamma_\mu \partial_\nu \varphi_{dq} F^{\mu\nu} \gamma_5, \quad (6.2.1)$$

where  $\varphi_{dq}$  is a spin-zero diquark (in the case of a vector diquark one would replace  $\partial_\nu \varphi_{dq} \rightarrow V_\nu$ ), which according to the leading quark rule of Blankenbecker, Brodsky and Gunion [3] should be the dominant contribution. Also recent work on the diquark content of the proton [4] has revealed that the spin-1 diquark is highly suppressed with respect to the spin-0 diquark. The derivative can act on any of the fields, however since  $\partial_\mu F^{\mu\nu} = 0$  (this is actually a higher dimension term) one only has two effective independent couplings. These can be conveniently chosen as two different helicity configurations and thus lead to non-interfering amplitudes. The choice of a spin-zero diquark means that the  $\Delta$  helicity is that of the s-quark, this allows the helicity dependent and independent cross-sections to be written in a particularly convenient factorised form:

$$E \frac{d\sigma^{++}}{d^3\vec{p}} = \sum_{i=\pm} \int_0^1 [dx_i] D_g^i(x_g) D_{dq}(x_1, x_2) \left| \int_0^1 [dy_i] T^i(x_j, y_i) \Phi(y_i) \right|^2, \quad (6.2.2)$$

and similarly for  $d\sigma^{+-}$ , where  $i$  indicates the helicity of the gluon relative to the proton and for  $T$  the helicity of the outgoing  $\Delta$  (or s-quark) relative to the incoming gluon. Note that this particular mechanism gives zero reflected asymmetry since the diquark is not polarised (a vector diquark on the other hand would lead to a non-vanishing initial-initial asymmetry).

The quantity to be calculated then is the hard scattering kernel  $T_H$  for the two helicity configurations, this is the subject of the next section.

### 6.3 The hard scattering kernel

A typical diagram to be considered is given in Fig. 6.3.1, in all there are 64 diagrams as one now has to include triple and even quartic gluon vertices.

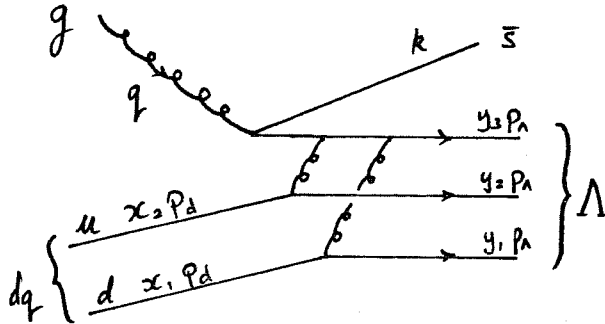


Fig. 6.3.1. A typical diagram contributing to the hard-scattering kernel  $T_H$ .

It is convenient to write the amplitude  $T_H$  in terms of the two helicity amplitudes mentioned and form factors:

$$T_H(q+dq \rightarrow \Lambda + \bar{s}) = F^+ \hat{T}^+ + F^- \hat{T}^- , \quad (6.3.1)$$

where the amplitudes  $\hat{T}^i$  are taken to be

$$\begin{aligned} \hat{T}^+ &= \frac{1}{\hat{\epsilon}} \bar{u}_\Lambda(p_\Lambda, h) \not{p}_d \gamma^\mu \not{q} v_{\bar{s}}(k) \epsilon_\mu(q, \lambda) , \\ \hat{T}^- &= \frac{1}{\hat{a}} \bar{u}_\Lambda(p_\Lambda, h) \not{q} \gamma^\mu \not{p}_d v_{\bar{s}}(k) \epsilon_\mu(q, \lambda) , \end{aligned} \quad (6.3.2)$$

$p_\Lambda$ ,  $p_d$ ,  $q$ ,  $k$  are the momenta of respectively the  $\Lambda$ , diquark, gluon, anti-strange quark,  $h$  and  $\lambda$  being  $\Lambda$  (or  $s$ -quark) and gluon helicities.

The subprocess Mandelstam variables are defined as

$$\hat{s} = (p_d + q)^2 , \quad \hat{t} = (p_d - p_\Lambda)^2 , \quad \hat{u} = (q - p_\Lambda)^2 . \quad (6.3.3)$$

The helicities of the incoming diquark are fixed by helicity conservation with respect to the outgoing quarks, similarly for the outgoing antistrange

quark. Thus these redundant helicity labels will be suppressed. Squaring these amplitudes up one has

$$|\hat{T}^\pm|^2 \propto \hat{S} \delta_{\lambda, \pm h}, \quad (6.3.4)$$

where the constant of proportionality will be absorbed into the definition of the  $F^i$ . Note that this separation between  $\hat{T}^i$  and  $F^i$  is quite arbitrary but in the form given is most convenient.

The structure functions actually decompose into further helicity components depending on the relative helicities of the quarks in the final state, similarly  $\Phi(y_i)$ , the baryonic amplitude has different helicity components.

As mentioned above there are 64 diagrams in all to be evaluated, these can be divided up into 13 classes, equivalent through interchanging vertices along single quark lines, these are listed below in Figs. 6.3.2, .3 and .4.

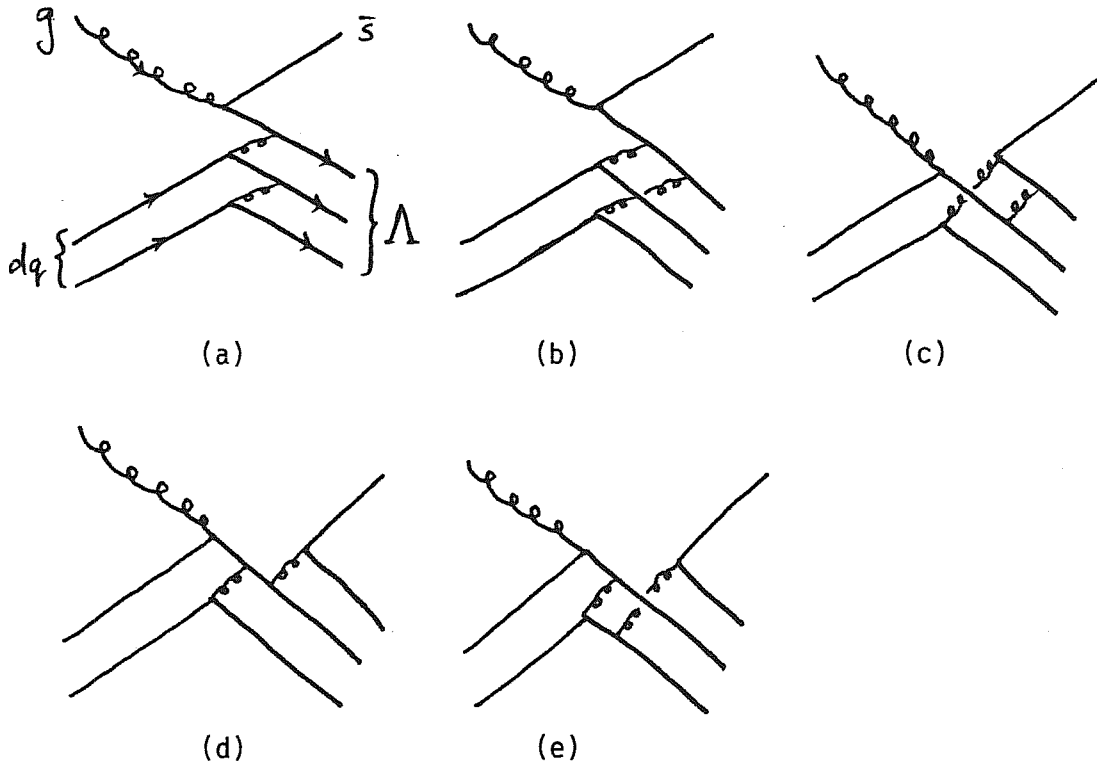


Fig. 6.3.2. QED type diagrams contributing to  $T_H$ . The total number of diagrams per type (include exchange of diquark lines) is: (a) 8, (b) 6, (c) 8, (d) 12, (e) 8.

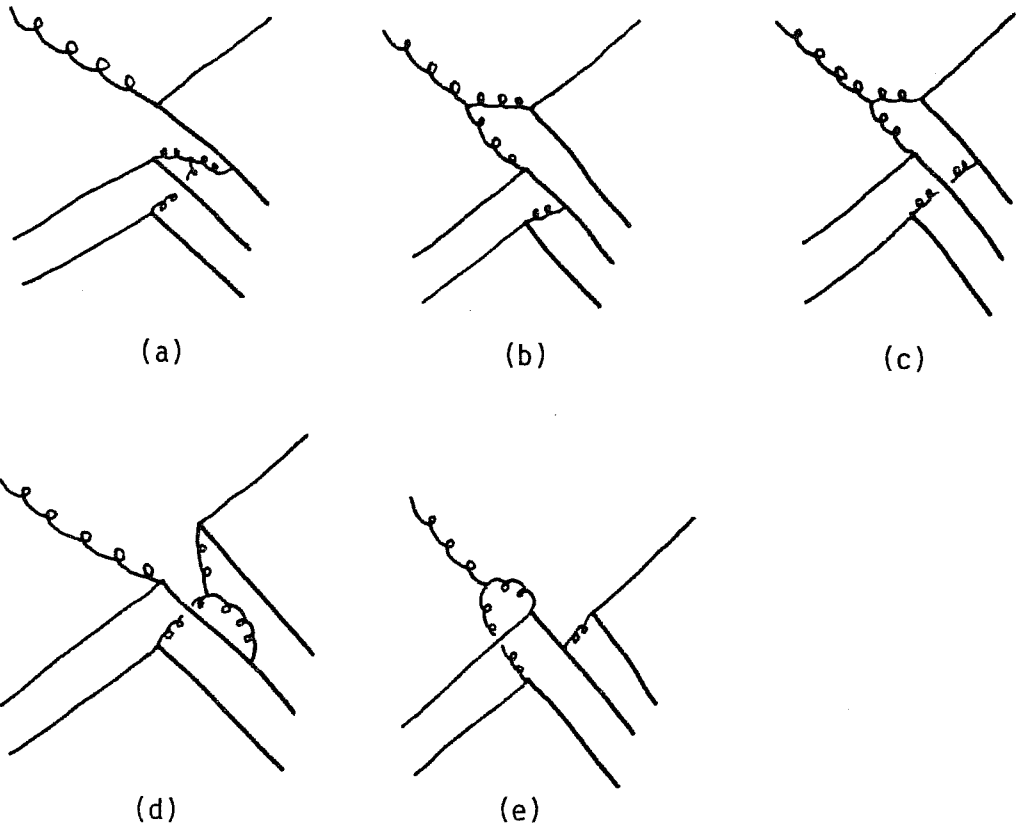


Fig. 6.3.3. Diagrams with one triple-gluon vertex contributing to  $T_H$ . The total number of diagrams per type is: (a) 2, (b) 4, (c) 4, (d) 4, (e) 4.

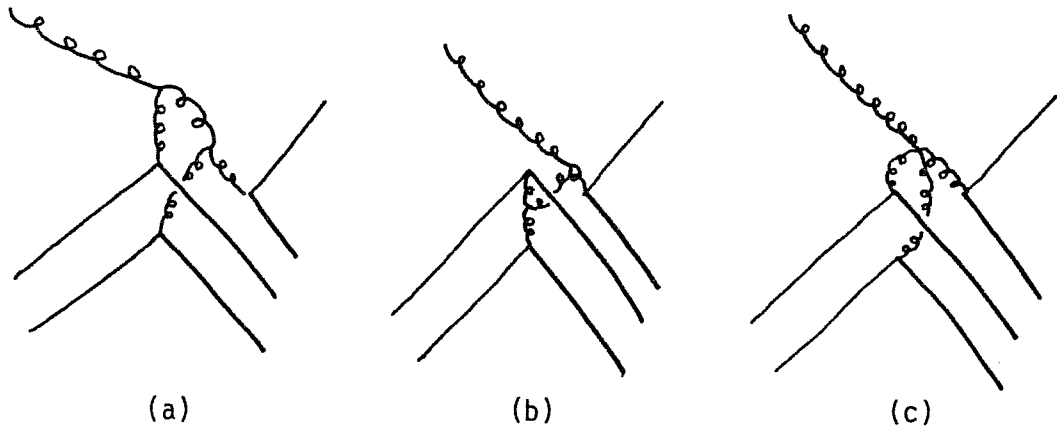


Fig. 6.3.4. Diagrams with two gluon vertices or one quartic vertex, with number of diagrams per type: (a) 2, (b) 1, (c) 1.

## 6.4 Numerical results for transmitted asymmetries in $\Delta$ -production

The large number of diagrams involved in this calculation, many of which contain pinch singularities, renders the exact evaluation of this process highly complicated. In order to obtain a reasonable estimate of the asymmetry following ref. [2] a subset of diagrams, namely those of Fig. 6.3.2(a) and (b), are considered. These t-like exchanges should give dominant contributions, the diagrams involving triple or quartic gluon couplings are generally suppressed by colour factors (the diagrams of Figs. 6.3.3(a) and 6.3.4(b) are in fact zero).

The individual helicity amplitudes can be evaluated using the various identities given in appendix A2 and the diagrams considered lead to the following

$$F^{(i)} = \frac{256\pi^2}{9} \frac{\alpha_s^2(\hat{s})}{\hat{u} \hat{t}^2} \int [dy] \left\{ \Phi_{\Lambda}^{+-+}(y_1, y_2, y_3) V^{+-i}(x_1, x_2, y_1, y_2, y_3) \right. \\ \left. + \Phi_{\Lambda}^{-++}(y_1, y_2, y_3) V^{-+i}(x_1, x_2, y_1, y_2, y_3) \right\}, \quad (6.4.1)$$

with

$$V^{+-+} = \frac{8x}{x_1 y_1 y_3 (1-y_3)} + \frac{4x^3 [(2-y_2)x - (1-y_2)x^-]}{x_1 x_2 y_1 y_2 y_3 [y_2 x x_1 - (1-y_2)x^- x_2]} + (1 \leftrightarrow 2),$$

$$V^{-++} = \frac{8x}{x_1 y_2 y_3 (1-y_3)} + \frac{4x [(1-y_2)(1-y_3)(x x_1 + x^- x_2) - y_3 x^- x_2]}{x_1 x_2 y_1 y_2 y_3 (1-y_2) [y_2 x x_1 - (1-y_2)x^- x_2]} + (1 \leftrightarrow 2),$$

$$V^{+--} = \text{zero},$$

$$V^{-+-} = - \frac{4x^2 x^- y_3}{x_2 y_1 y_2 (1-y_2) [y_2 x x_1 - (1-y_2)x^- x_2]} + (1 \leftrightarrow 2), \quad (6.4.2)$$

where  $\Phi_A^{\lambda_1 \lambda_2 \lambda_3}(y_1, y_2, y_3)$  refers to the wave function of the  $A$  with the  $u, d$  and  $s$  quarks carrying helicity  $\lambda_1, \lambda_2$  and  $\lambda_3$  and momentum fraction  $y_1, y_2$  and  $y_3$  respectively,  $x = x_1 + x_2$  is the total diquark momentum fraction and  $x_{\pm} = \frac{1}{2}(V(x_T^2 + x_F^2) \pm x_F)$ ,  $x_T$  and  $x_F$  are defined below. The contributions of the diagrams of Fig. 6.3.2(a) are the first terms of  $V^{++}$  and  $V^{-++}$ .

Two interesting points emerge from the calculation: firstly one notices that the graphs of Fig. 6.3.2(a) automatically select the spin-zero component of the diquark system and secondly the contributions of the diagrams in Fig. 6.3.2(b) do not have appreciably different asymmetries, in particular the contribution of the form factor  $V^{-+-}$  (corresponding to a helicity asymmetry of opposite sign) is negligible compared to the others. This strengthens the belief that the omitted diagrams should not significantly alter the asymmetry.

For the purpose of calculation, following ref [2], only the leading term in the asymptotic expansion for the proton wave-function (see Eqn. 6.1.4)  $\sim y_1 y_2 y_3$ , is considered and (since on the scale considered it is small) we neglect the logarithmic scale dependence. To facilitate the somewhat involved convolutions the diquark distribution may be taken to be a delta-function in the difference  $x_1 - x_2$ . Checks on the leading terms of (6.4.2) showed the cross-sections to be almost totally insensitive to the parameterisation of the diquark distribution with respect to this variable. Thus one has  $x_1 = x_2 = \frac{1}{2}x$ . And the two form factors become, on integrating over the  $y_i$

$$F^{(-)} = \frac{256 \pi^2}{9} \alpha_s^2(\hat{t}) \frac{1}{\hat{u} \hat{t}^2} \left\{ \frac{7}{4} - \frac{9x}{2(x+x^-)} - \frac{9x^2}{2(x+x^-)^2} \ln \frac{x^-}{x} \right\},$$

$$F^{(+)} = \frac{256 \pi^2}{9} \alpha_s^2(\hat{t}) \frac{1}{\hat{u} \hat{t}^2} \left\{ \frac{x^-}{2(x+x^-)} + \frac{x x^-}{2(x+x^-)^2} \ln \frac{x^-}{x} \right\} \left[ \frac{\hat{u}}{\hat{t}} \right]. \quad (6.4.3)$$

Examining these two expressions one sees that, for  $x_F > 0$ ,  $|F^{(+)}|^2 \ll |F^{(-)}|^2$ . In fact the ratio of the two form factors, for wave-functions that are largest near  $y_1 \approx y_2 \approx y_3$ , is less than  $10^{-4}$ . This again supports the belief that the diagrams considered dominate the process.



Thus one sees that the helicity structure is driven by the subprocess couplings which, including colour factors etc., are

$$|\hat{T}^{(-)}|^2 = \alpha_s(\hat{t}) \frac{2\hat{s}}{3} \delta_{h\bar{\lambda}} ,$$

$$|\hat{T}^{(+)}|^2 = \alpha_s(\hat{t}) \frac{2\hat{s}}{3} \delta_{h\lambda} , \quad (6.4.4)$$

and the helicity distribution of the gluons.

Hence the transmitted asymmetry for the whole process is of the form

$$A_{LL}^{if}(\vec{p} \rightarrow \vec{\Lambda} X) = \frac{\int P.S. \left\{ D_{dq}^{(B)}(x) \Delta g^{(A)}(x_g) \left[ |F^{(+)}|^2 - |F^{(-)}|^2 \right] \hat{s} + (A \leftrightarrow B) \right\}}{\int P.S. \left\{ D_{dq}^{(B)}(x) g^{(A)}(x_g) \left[ |F^{(+)}|^2 + |F^{(-)}|^2 \right] \hat{s} + (A \leftrightarrow B) \right\}} , \quad (6.4.5)$$

where the parton phase-space integral is given by

$$\int P.S. = \int_0^1 dx_g \int_0^1 dx \frac{\hat{s}}{\pi} \delta(\hat{s} + \hat{t} + \hat{u}) , \quad (6.4.6)$$

where  $\hat{s} = x x_g s$ ,  $\hat{t} = x t$  and  $\hat{u} = x_g u$ , with the hadronic variables  $t = (p_A - p_{\Lambda})^2$ ,  $u = (p_B - p_{\Lambda})^2$ . One also has the following relationships between the variables of the process:

$$t = -x^+ s , \quad u = -x^- s$$

$$x_F = \frac{2p_{\Lambda}}{\sqrt{s}} , \quad x_T = \frac{2p_{\Lambda T}}{\sqrt{s}} , \quad (6.4.7)$$

where  $p_{A\parallel}$  and  $p_{A\perp}$  are the components of the  $A$  momentum parallel and perpendicular to the beam axis.

In principle one could examine the deep question of factorisation of the diquark distribution in QCD, through which this distribution could be extracted from other processes. However the asymmetry is fairly insensitive to the detailed form of the diquark distribution. Note that in calculating the overall power behaviour of the cross-section one must take into account that this distribution is accompanied by a factor  $M^2/s$ , where  $M^2$  is the mass-squared dimension associated with the matrix element of the corresponding twist-4 operator. Since the wave-function also has the dimension of mass-squared, it is easy to see that the mechanism considered here scales like  $E d\sigma/d^3p \sim p_T^{-10}$  in accordance with the power-law counting rules of Brodsky et al [6].

In order to make an estimate of the asymmetry the following choice of distributions was used in [2]:

$$\begin{aligned} x D_{dq}(x) &\propto (1-x)^3, \\ x g(x) &\propto (1-x)^4. \end{aligned} \tag{6.4.8}$$

These will change with  $p_T^2$  and although the overall normalisation depends crucially on these choices, the asymmetry is rather insensitive to the specific form chosen. One may therefore neglect the scale-breaking behaviour of the parton distributions. However the asymmetry does depend strongly on the ratio  $\Delta g(x)/g(x)$  which was taken to be  $x(5x-2)/3$  for the leading-quark-gluon-bremsstrahlung model [5] and  $1/3x(2-x)/[1+(1-x)^2]$  in the SU(6) conservative model, see sect. 3.4(a).

The asymmetries for this mechanism are shown below in Fig. 6.4.1. In Fig. 6.4.1(a) the effect of including only the dominant graphs of Fig. 6.3.2(a). One sees that the other diagrams are only important for small angles, at  $90^\circ$  their inclusion is almost negligible over the whole range. Thus one might

expect that the remaining uncalculated diagrams will become important for small trigger angles and large  $x_T$ .

In Fig. 6.4.1(b) the mechanism is compared with the asymptotically leading  $p_T^{-4}$  mechanism due to the subprocess  $gg \rightarrow s\bar{s}$ . It is important to notice the opposite sign (the scale is inverted) and completely different shape. The change of sign can be understood from helicity conservation.

Finally in Fig. 6.4.1(c) the different inputs for  $\Delta g(x)$  are compared. It is clear that this particular mechanism depends critically on the extent to which hard gluons carry the parent proton helicity, which confirms the conclusion of [5], namely that the transmitted helicity in  $pp \rightarrow \Delta + X$  is a sensitive way of studying the question.

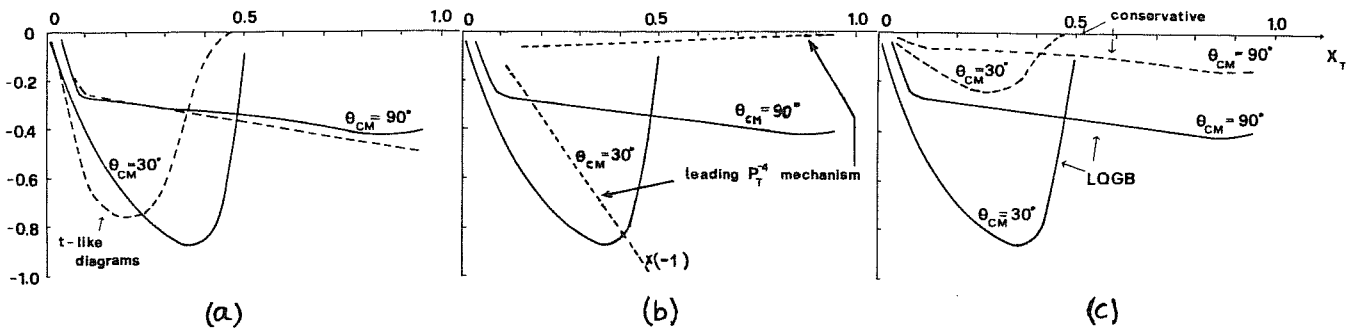


Fig. 6.4.1. (a) Asymmetry using all graphs calculated (solid curve) and only the leading  $t$ -like diagrams (dashed curve), (b) comparison with the leading  $p_T^{-4}$  mechanism (dashed curve with scale inverted), (c) comparison between the gluon bremsstrahlung and SU(6) conservative (dashed curve) models.

To end this section let us make a few remarks on normalisation. Characteristically, when one produces a hadron directly the price to pay is a higher power of  $\alpha_s/p_T^2$ . With current expectations of  $\Delta \approx 100\text{-}200$  MeV, at

first sight, one might expect such mechanisms to be unimportant in any region. A similar situation holds for direct meson production which is further suppressed by a factor  $F_{\pi}^2/P_T^2$ . However there are a number of ways this could be substantially compensated without affecting unduly the helicity asymmetry:

(i) The large number of diagrams involved, 64, typical of higher power mechanisms could considerably increase the overall normalisation. For proton-proton elastic scattering there are over 3,000 diagrams.

(ii) The  $\Lambda$  seen experimentally can be the decay product of directly produced  $\Lambda^*$  or  $\Sigma^*$  resonances. Typically the two-body decays  $B^* \rightarrow \Lambda \pi$  will be strongly favoured [6]. This will slightly soften the  $\Lambda$  spectrum, but again increase the inclusive  $\Lambda$  cross-section. For larger  $x_T$  the helicity will be transmitted to the  $\Lambda$  and consequently the basic asymmetry predictions should remain unaltered.

(iii) Finally one could imagine that QCD radiative corrections might have a considerable effect on the process. The analysis of chapter 5 suggests that while increasing the cross-section they may not affect the asymmetry.

In conclusion then while one must admit that higher power corrections give at the moment only a qualitative description of normalisation, the asymmetry predictions can be expected to be quantitatively correct and thus provide a very valuable signature to the understanding of the production process.

REFERENCES TO CHAPTER 6

- [1] G.P. Lepage and S.J. Brodsky, Phys. Rev. D22, 2157 (1980). For an alternative approach based on the short distance expansion of a product of three quark fields in the wave function see also: K. Tesima, Tokyo preprint UT-368 (1981).  
N.S. Craigie, V.K. Dobrev and I.T. Todorov, Trieste preprints IC/83/35 and 39.  
S.J. Brodsky, Y. Frischman, G.P. Lepage and S. Sachrajda, Phys. Lett. 91B, 239 (1980).
- [2] N.S. Craigie and P. Ratcliffe, Z. Phys. C17, 47 (1983).
- [3] R. Blankenbecler, S.J. Brodsky and J.F. Gunion, Phys. Rev. D6, 2652 (1972).
- [4] S. Fredriksson, M. Jandel and T. Larsson, Z. Phys. C14, 35 (1982); C19, 53 (1983).
- [5] See ref. [15] chapter. 3.
- [6] N.S. Craigie, Phys. Rep. 47, 1 (1978).

Chapter 7    On the problem of transverse-spin asymmetries in QCD perturbation theory

- 7.1    Introduction to transverse spin
- 7.2    The standard OPE approach
- 7.3    Some difficulties and criticisms of the standard approach
- 7.4    Spectator interaction effects
- 7.5    General comments and conclusions

## 7.1 Introduction to transverse spin

The description of transverse spin within the framework of perturbative QCD has been considered by various authors [1,2,3,4,5] , apart from the experimental interest (see sect. 4.3) this aspect of the spin properties of hadrons is also an important testing ground for many of the fundamental theoretical ideas underlying our understanding of high-energy hadronic physics.

It has been long known that transverse spin is governed by a twist-three operator in the Wilson light-cone expansion [1] . Thus access to the relevant structure function  $\mathcal{G}_2$  (see sect. 2.1) will allow a test of the applicability of standard techniques and ideas to higher-twist effects, in particular the extension of the factorisation theorem to the inclusion of the latter [6] . Another interesting point is the appearance of a further twist-three operator proportional to the quark mass [2] . This new operator mixes with the original twist-three operator [3] giving rise to a contribution proportional to  $m/M$  where  $m$  is the quark mass and  $M$  some hadronic mass scale (and therefore non-perturbative) such as the transverse momentum cut-off for example. Transverse spin has also been discussed in the context of the cut-vertex method [4] , this permits the derivation of evolution equations valid also for the light-like vertices of massive lepton-pair production or  $e^+e^-$  annihilation. The cut-vertex analysis leads to an interesting interpretation of the quark-mass effect in the parton model. This effect comes from considering the usual set of ladder diagrams with all vertical quark lines effectively massless except for one, from which precisely the mass term is taken.

There also exist results which throw some doubt on the validity of the above purely perturbative approaches [5] . Discrepancies essentially due to a lack of gauge invariance lead to the consideration of the rôle of spectator interactions along the lines of the model discussed in sect. 5.2. The results of this work (to be discussed shortly ) essentially throw into doubt the gauge invariance of the operator renormalisation and the neglect of spectator contributions (i.e. bound-state effects).

## 7.2 The standard OPE approach

As discussed in sect. 2.1 spin effects in deep-inelastic scattering are governed by the antisymmetric part of the Fourier transform of the commutator of two electromagnetic currents sandwiched between nucleon states of definite spin, in terms of the structure functions  $\mathcal{G}_1$  and  $\mathcal{G}_2$  this is expanded as

$$W_{\mu\nu}^A = -\epsilon_{\mu\nu\rho\sigma} \frac{q^\rho M}{2P \cdot q} \left\{ \frac{q \cdot s}{P \cdot q} p^\sigma \mathcal{G}_1 + \left[ s^\sigma - \frac{q \cdot s}{P \cdot q} p^\sigma \right] \mathcal{G}_2 \right\}. \quad (7.2.1)$$

Recall the redefinition of  $\mathcal{G}_1$  and  $\mathcal{G}_2$  with respect to the usual structure functions  $g_1$  and  $g_2$  3 :

$$\mathcal{G}_1 = -2g_1, \quad \mathcal{G}_2 = -2(g_1 + g_2). \quad (7.2.2)$$

These definitions separate out the transverse and parallel components of  $s$  as can be seen by defining  $s^\nu = s_{\parallel}^\nu + s_{\perp}^\nu$  with  $q \cdot s_{\perp}^\nu = 0$ . Since  $s_{\parallel}^\nu \propto p^\nu$  this means we can write

$$s_{\parallel}^\sigma = \frac{q \cdot s}{P \cdot q} p^\sigma, \quad s_{\perp}^\sigma = s^\sigma - \frac{q \cdot s}{P \cdot q} p^\sigma. \quad (7.2.3)$$

Thus the form factor  $\mathcal{G}_2$  is explicitly responsible for the dependence on the transverse-spin degree-of-freedom of hadrons.

The Fourier transform of the time-ordered product of currents can be written as

$$\int d^4z e^{iq \cdot z} T(J_\mu(\frac{z}{2}) J_\nu(-\frac{z}{2}))^A = -\epsilon_{\mu\nu\rho\sigma} q^\rho \sum_{n \text{ odd}} \left(\frac{2}{Q^2}\right)^n q_{\mu_1} \dots q_{\mu_{n-1}} C_{A,2}^n \mathcal{O}_{A,2}^{\sigma\mu_1 \dots \mu_{n-1}} \\ - \left[ \epsilon_{\mu\nu\rho\sigma} q_\lambda + \epsilon_{\mu\nu\lambda\rho} q_\sigma \right] q^\rho \sum_{n \text{ odd}} \left(\frac{2}{Q^2}\right)^n q_{\mu_1} \dots q_{\mu_{n-2}} C_{A,3}^n \mathcal{O}_{A,3}^{\lambda\sigma\mu_1 \dots \mu_{n-2}}, \quad (7.2.4)$$



where the coefficient  $C_{A,2}^n$  and  $C_{A,3}^n$  of the twist-two and -three operators respectively are functions of  $\alpha_s$  and  $Q^2$ .

One then assumes that the matrix elements of the operators between nucleon states exist and thus one has, for states of momentum  $p^\nu$  and spin  $s^\nu$  :

$$\langle p,s | \mathcal{O}_{A,2}^{\sigma\mu_1 \dots \mu_{n-1}} | p,s \rangle = a_n \mathcal{P} (s^\sigma p^{\mu_1} \dots p^{\mu_{n-1}}) , \quad (7.2.5)$$

$$\langle p,s | \mathcal{O}^{\lambda\sigma\mu_1 \dots \mu_{n-2}} | p,s \rangle = b_n \frac{1}{2} (s^\sigma p^\lambda - s^\lambda p^\sigma) p^{\mu_1} \dots p^{\mu_{n-2}} ,$$

where  $\mathcal{P}$  denotes symmetrisation over the indices  $\sigma\mu_1 \dots \mu_{n-1}$ . Using these definitions one then obtains the standard moment sum rules for  $\mathcal{G}_1$  and  $\mathcal{G}_2$  (n odd only):

$$\begin{aligned} \mathcal{G}_1^n(Q^2) &= \int_0^1 dx x^{n-1} \mathcal{G}_1(x, Q^2) = a_n C_{A,2}^n(Q^2, \alpha_s) , \\ \mathcal{G}_2^n(Q^2) &= \int_0^1 dx x^{n-1} \mathcal{G}_2(x, Q^2) = \frac{1}{n} a_n C_{A,2}^n(Q^2, \alpha_s) + b_n C_{A,3}^n(Q^2, \alpha_s) . \end{aligned} \quad (7.2.6)$$

Notice in particular that the anomalous dimension matrix is not diagonalised by this choice of  $\mathcal{G}_1$  and  $\mathcal{G}_2$ , this would require the redefinition of the structure function  $\mathcal{G}_2$  by

$$\tilde{\mathcal{G}}_2^n(Q^2) = \mathcal{G}_2^n(Q^2) - \frac{1}{n} \mathcal{G}_1^n(Q^2) , \quad (7.2.7)$$

which, inverting the moments, gives [7] :

$$\tilde{\mathcal{G}}_2(x, Q^2) = \mathcal{G}_2(x, Q^2) - \int_x^1 \frac{dy}{y} \mathcal{G}_1^n(y, Q^2) . \quad (7.2.8)$$

The leading non-singlet operators contributing to  $\mathcal{O}_{A,2}$  are twist-two (as already mentioned in sect. 2.1) and are

$$\mathcal{O}_{A,2}^{\sigma\mu_1 \dots \mu_{n-1}} = i^{n-1} \mathcal{P} \bar{\Psi} \gamma_\sigma \gamma^{\mu_1} \dots \gamma^{\mu_{n-1}} \Psi . \quad (7.2.9)$$

The leading, twist-three, operators contributing to  $\mathcal{O}_{A,3}$  are

$$\mathcal{O}_{A,3}^{\lambda\sigma\mu_1\dots\mu_{n-2}} = i^{\pi-1} \mathcal{S}' \bar{\Psi} \gamma_5 \gamma^\lambda \gamma^\sigma \mathcal{D}^{\mu_1} \dots \mathcal{D}^{\mu_{n-2}} \Psi, \quad (7.2.10)$$

where  $\mathcal{S}'$  denotes symmetrisation on the indices  $\sigma\mu_1\dots\mu_{n-2}$  followed by anti-symmetrisation on  $\lambda\sigma$ . Throughout this chapter only the non-singlet sector will be considered, although of course a complete analysis would also necessarily include the more complicated flavour-singlet sector.

The reduction in spin of the operator through antisymmetrisation of two indices allows a further operator (still twist-three) to enter, namely

$$\mathcal{O}'_{A,3}{}^{\lambda\sigma\mu_1\dots\mu_{n-2}} = i^{\pi-1} \mathcal{S}' m \bar{\Psi} \gamma_5 \gamma^\lambda \gamma^\sigma \mathcal{D}^{\mu_1} \dots \mathcal{D}^{\mu_{n-2}} \Psi, \quad (7.2.11)$$

where the correct dimensions are maintained by explicit inclusion of a factor  $m$  (the quark mass) which is the only dimensional object available at this level.

As mentioned above the contribution of this operator is clearly proportional to  $m/M$ , and thus in particular disappears smoothly in the chiral limit. This operator however plays no rôle in the analysis of this chapter (but see later comments), although its presence underlines an important point in respect of transverse spin: the proton carries transverse spin by virtue of its own mass, independently of the quark masses (these two though must be intimately related through chiral symmetry breaking). In any case the two operators give quite distinct contributions and therefore in the context of perturbative QCD (if valid in this case), it is legitimate to consider the zero quark-mass limit (i.e. to simply neglect this contribution).

The standard calculation of the operator renormalisation (see sect. 2.2) gives the following anomalous dimensions [1,3]:

$$\begin{aligned} \gamma_{A,2}^{(n)} &= g^2 2 C_2(R) \left\{ 1 - \frac{2}{n(n+1)} + \sum_i^n 4/j \right\}, \\ \gamma_{A,3}^{(m)} &= g^2 2 C_2(R) \left\{ 1 - \frac{2}{n} + \frac{n-2}{n-1} \sum 2/j \right\}, \end{aligned} \quad (7.2.12)$$

for which one derives the high-energy behaviour of the two structure functions. Use of the cut-vertex technique provides the same results [4] and the approach of Altarelli and Parisi allows a parton model interpretation in terms of a spin-projector:

$$\mathcal{P}_{(p,s)} = a(x) \not{p} + b(x) m + c(x) \gamma_5 \not{p} + d(x) \gamma_5 [\not{p}, \not{p}] , \quad (7.2.13)$$

where  $a(x)$  etc. are distribution functions.



the infra-red singularity of the ladder diagram, although of course it remains in the wave-function renormalisation coefficient. Thus the anomalous dimensions are singular.

The third method [10] uses the covariant Feynman gauge and application of the so-called collinear Ward identities to the non-factorising diagrams to put them into the same form as the ladder diagrams. It is instructive to see how this works. Consider the diagrams contributing to  $W_{\mu\nu}$  (see Fig. 7.3.2) where the gluon connected to the blob does not connect to the external leg.

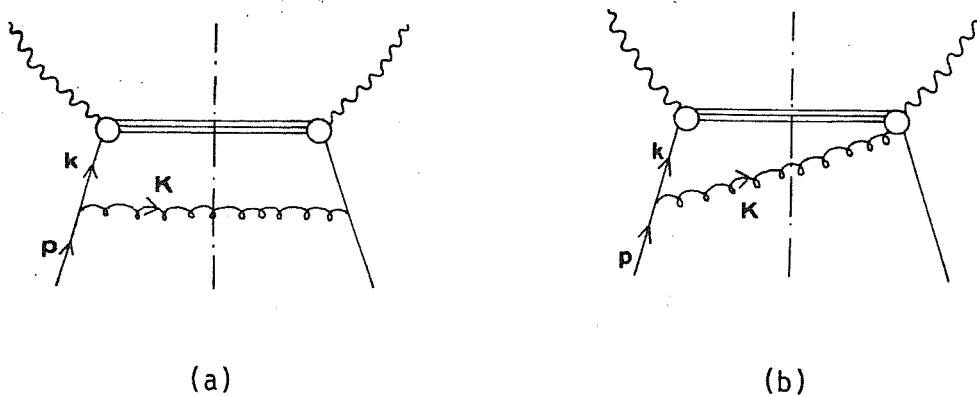


Fig. 7.3.2. Diagrams contributing to  $W_{\mu\nu}$  in a covariant gauge.

With an external projector  $\not{p}$  (or  $\gamma_5 \not{p}$ ) acting on the gluon-quark vertex in Fig. 7.3.2(b) gives

$$\not{p} \gamma^\mu k \sim \not{p} 2k^\mu \sim \not{p} 2K^\mu \frac{\alpha}{1-\alpha}, \quad (7.3.1)$$

where  $K = p-k$  and the leading logarithmic approximation has been applied to write  $k \sim \alpha p$  in the numerator. Via the collinear Ward identities one then shows (invoking Block-Nordsieck cancellation) that  $K^\mu$  contracted into the blob reduces Fig. 7.3.2(b) to the factorising form of Fig. 7.3.2(a). It is clear that on external projector  $\gamma_5 \not{p}$  cannot produce the same simplification.

To try and uncover the origin of these discrepancies let us examine more closely the application of the Wilson expansion and the calculation of the corresponding anomalous dimensions. The accepted approach is to calculate the operator renormalisation sandwiched between hypothetical quark states. However

for free quarks (therefore on mass-shell) the operator  $\mathcal{O}_{A,3}$  vanishes identically, for zero quark mass. This is simply the statement that massless fermions on shell only have two spin states: positive or negative helicity and cannot carry transverse spin. Giving the quarks a mass does not resolve this problem as now we only have the contribution corresponding to the massive operator and its mixing with the first. Thus one is forced to consider off-shell quarks (as indeed is implicit in all the calculation for transverse spin in the literature) and not surprisingly the problem of gauge invariance arise.

To understand this physically it is instructive to consider what a complete calculation would involve. Consider the time-ordered product of two currents inserted into a hadron, see Fig. 7.3.3(a). The full order  $\alpha_s$  corrections would involve those diagrams in Fig. 7.3.3.(b).

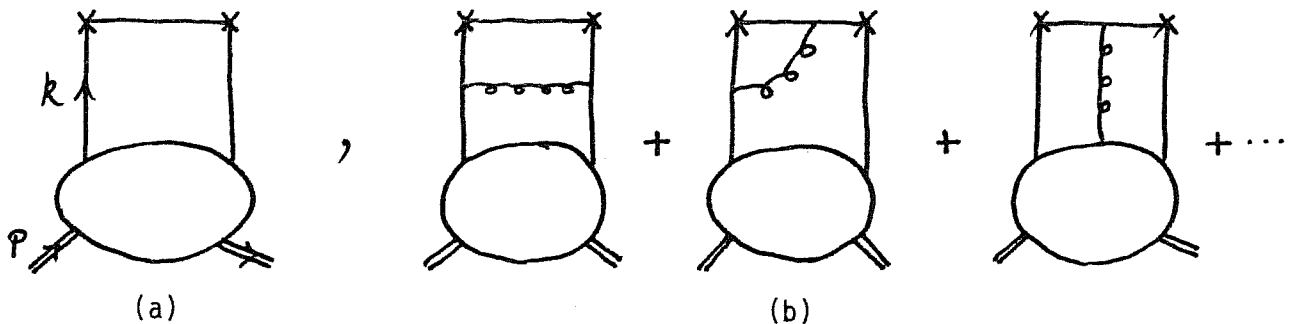


Fig. 7.3.3. Diagrams contributing to  $T_{\mu\nu}$  : (a) Lowest order (b) Order  $\alpha_s$  corrections.

All but the last diagram are familiar. The general belief is that the gluon entering the blob does not enter in the leading logarithmic approximation. Indeed as discussed in sec. 5.2 it has been shown that this diagram (as far as twist-two is concerned) gives no large logarithm and even the next-to-leading logarithmic contribution is identical to that obtained by standard on-shell methods when summed over all diagrams. In the case of transverse spin where one is dealing precisely with an off-shell (or bound-state) effect it might be

expected that details of the bound state via spectator interactions should be important and lead to a Green's function dependent behaviour.

Before going on in the next section to a calculation of the spectator contributions, a comment on a possible further operator which could change the picture somewhat although probably not to the extent required. The symmetry conventionally imposed on the indices of the operator  $\mathcal{O}_{A,3}^{\lambda\sigma\mu_1\cdots\mu_{n-2}}$  excludes a possible contribution, namely:

$$i^{n-1} \mathcal{Y}' \bar{\Psi} \gamma_5 \mathcal{D}^\lambda \mathcal{D}^\sigma \gamma^{\mu_1} \mathcal{D}^{\mu_2} \dots \mathcal{D}^{\mu_{n-2}} \Psi. \quad (7.3.2)$$

While this, in part, contains the usual operator it also contains a piece proportional to  $[\mathcal{D}^\lambda, \mathcal{D}^\sigma] \approx igF^{\lambda\sigma}$ . The new piece could be isolated by defining an operator proportional to the coupling constant:

$$i^n \mathcal{Y}' \bar{\Psi} \gamma_5 \mathcal{D}^{\mu_1} \dots \mathcal{D}^{\mu_{\ell-1}} gF^{\lambda\sigma} \mathcal{D}^{\mu_{\ell+1}} \dots \mathcal{D}^{\mu_{n-2}} \Psi, \quad (7.3.3.)$$

where  $\ell = 1, \dots, n-2$  to include the different operators generated by the different possible positions of the  $F^{\mu\nu}$ . The fact that this operator is proportional to  $g$  means that its coefficient function in the Wilson expansion is undetermined to leading order.

The importance of this new operator has been considered in refs. 12,13. The authors of the latter also recognise the problem of considering on-shell external particles for calculating the renormalisation constants and instead use the transition from a quark state to a quark plus gluon state. However they do not give any calculational details and it is not clear how they decided on the correct combination of the new order  $g$  operator with the original twist-three operator. Moreover the result they obtain, they only calculate for their operator are in complete disagreement with the results obtained in 5 using the effective Lagrangian model to be presented in the following section.

The fact that the coefficient function is not easily distinguishable may unfortunately be a simple reflection of the lack of factorisation of the high and low energy regions for transverse spin, in other words the anomalous dimensions and coefficients functions are somehow tangled up.



## 7.4 Spectator interaction effects

In order to take into account in some measure the fact that quarks are off mass-shell due to their being bound in a hadron, a calculation was performed in ref [5] using a simple model for the proton.

The simplest model which incorporates transverse spin is a spin- $\frac{1}{2}$  proton with an effective pointlike interaction with a spin- $\frac{1}{2}$  quark and scalar diquark according to the effective Lagrangian:

$$\mathcal{L}_{\text{eff}} = \lambda (\bar{\Psi}_q \varphi_{dq} \Psi_p + \text{h.c.}) + \text{kinetic terms} \quad (7.4.1)$$

The quark and diquark are both contained in the usual representation of the colour gauge group algebra. The new Feynman rules are given in Fig. 7.4.1. There is also a "seagull" vertex for the diquark, however to order  $\alpha_s$  it only enters in a tadpole contribution to the diquark self-energy which in dimensional regularisation gives zero contribution [14]. The quark and diquark propagator

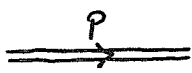
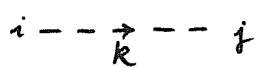
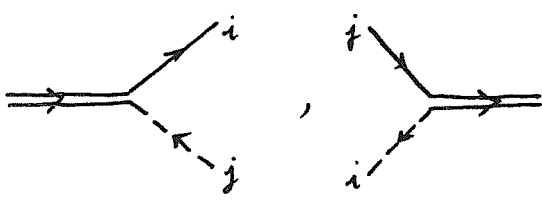
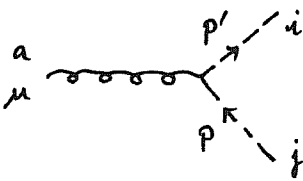
proton propagator		: $i (\not{P} - M)^{-1}$ ,
diquark propagator		: $i \delta_{ij} k^{-2}$ ,
		: $\lambda \delta_{ij}$
		: $-ig \tau_{ij}^a (p+p')^\mu$

Fig. 7.4.1. Feynman rules for the effective Lagrangian (7.4.1).

are considered in the massless limit, as the object of the calculation is only

the behaviour of the operator  $\mathcal{O}_{A,3}$ . This Lagrangian is explicitly gauge invariant thus the calculations may be performed in any gauge, the most convenient being the Feynman gauge.

The spin projector for the external hadron lines is now the usual  $\mathbb{P} = \frac{1}{2}(\not{p} + M)(1 + \gamma_5 \not{S})$ , where  $M$  is the effective elementary hadronic mass. The piece  $\not{p} + M$  projects out the spin-averaged part of  $W_{\mu\nu}$  and  $\not{p} \gamma_5 \not{S}$  relates to the massive operator  $\mathcal{O}'_{A,3}$ . The remaining piece  $M \not{S}$  may be decomposed as above into  $M \not{S}$  and  $M \not{S}_T$ . For comparison the calculation will be performed for those two pieces in parallel.

The basic diagram (zeroth order in  $\alpha_s$ ) is the simple box diagram shown in Fig. 7.4.2. This diagram:

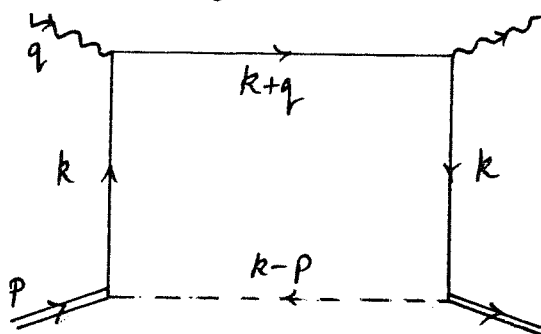


Fig. 7.4.2. The basic diagram for deep-inelastic scattering in the simple model.

leads to the following integral (for one quark flavour).

$$-\frac{3}{2} e^2 \lambda^2 \int [dk] \frac{\text{tr} [\mathbb{P} \not{k} \gamma^\mu (\not{k} + \not{q}) \gamma^\nu \not{k}]}{(k^2)^2 (k+q)^2 (k-p)^2}, \quad (7.4.2)$$

where  $p$  is the external hadron momentum and  $q$  that of the virtual photon, the loop-momentum integral  $[dk]$  is defined as in appendix A.3 for the  $\overline{\text{MS}}$  scheme. The integral in (7.4.2) is ultra-violet convergent by power counting and thus the number of dimensions may be set equal to four. However, as written, it is infra-red singular. This divergence could be controlled in a straightforward manner by the introduction of masses for the various particles. To leading

logarithmic order it is sufficient and more convenient to introduce an infra-red cut-off which for simplicity may be chosen as  $|k^2| \geq M^2$ .

Inspection of the integral reveals that the region contributing the large logarithm (here  $\ln Q^2/M^2$ ) is just  $M^2 \leq k^2 \leq Q^2$ . Thus the simplest procedure is to expand the denominators in the following way:

$$(k+q)^{-2} (k-p)^{-2} = -Q^{-2} k^{-2} \sum_{m=0}^{\infty} \left( \frac{2k \cdot q + k^2}{Q^2} \right)^m \sum_{n=0}^{\infty} \left( \frac{2k \cdot p - M^2}{k^2} \right)^n \quad (7.4.3)$$

The small terms  $k^2/Q^2$  and  $M^2/k^2$  kill the large logarithm, thus with  $D = 4$  one obtains for the spin-dependent part,  $M^2$ , of  $\mathbb{P}$ :

$$I^{\mu\nu} = \int_{M^2}^{Q^2} \frac{[dk]}{k^4} \frac{1}{q^2} \frac{\text{tr}[\gamma_5 \not{k} \gamma^\mu (\not{k} + \not{q}) \gamma^\nu \not{k}]}{k^2} \sum_{m=0}^{\infty} \left( \frac{2k \cdot q}{Q^2} \right)^m \left( \frac{2k \cdot p}{k^2} \right)^n \quad (7.4.4)$$

Now the large logarithm comes from  $\int [dk] k^{-4}$  therefore one need only take the part zeroth order in  $k^2$  from the rest of the integrand. Moreover any term proportional to  $M^2$  may be discarded as it implies a higher-power contribution.

Application of the symmetric integration formula (A3.7) with  $D = 4$  shows that the vectors contracted with  $k^\mu$  become contracted among themselves. Thus in particular, power counting reveals that the term in  $k^2/Q^2$  in (7.4.4) would lead to  $M^2/Q^2$  and is therefore to be discarded.  $I^{\mu\nu}$  is now reduced to

$$I^{\mu\nu} = \frac{i}{(4\pi)^2} \ln \frac{Q^2}{M^2} \sum_{m=0}^{\infty} \frac{1}{(m+2)! 2^{m+1}} \frac{1}{q^2} \left\{ \text{tr}[\gamma_5 \not{q} \gamma^\alpha \gamma^\mu \not{q} \gamma^\nu \gamma_\alpha] \left( \frac{-4p \cdot q}{q^2} \right)^m m! \right. \\ \left. + \text{tr}[\gamma_5 \not{q} (\not{p} \gamma^\mu \not{q} \gamma^\nu + \not{q} \gamma^\mu \not{q} \gamma^\nu \not{p})] \left( \frac{-4p \cdot q}{q^2} \right)^m m \cdot m! \frac{1}{p \cdot q} \right\} \quad (7.4.5)$$

taking traces and substituting  $x = Q^2/2p \cdot q$  one finally obtains:

$$-\frac{3}{4} \frac{e^2 \lambda^2}{(4\pi)^2} \ln \frac{Q^2}{M^2} \frac{1}{p \cdot q} \epsilon^{\mu\nu\lambda\sigma} q_\lambda \sum_{n=0}^{\infty} \left(\frac{1}{x}\right)^n \frac{1}{n+1} \left\{ S_\sigma - \left(1 - \frac{1}{x}\right) \left(\frac{q \cdot S}{p \cdot q}\right) p_\sigma \right\}. \quad (7.4.6)$$

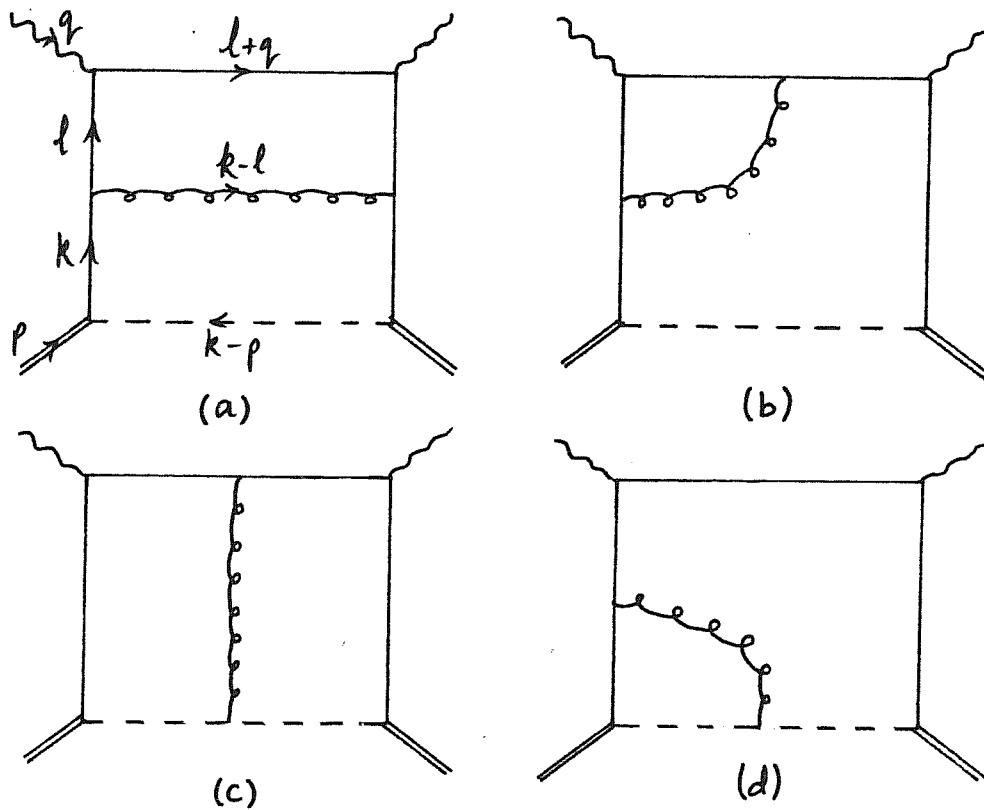
Adding the crossed diagram (for which  $\mu \leftrightarrow \nu$  and  $q \rightarrow -q$ ,  $x \rightarrow -x$ ) and decomposing  $S^\mu$  one readily obtains, to zeroth order in  $\alpha_s$  for the moments of the structure functions:

$$\mathcal{G}_1^{(n)} = 3 \frac{e^2 \lambda^2}{(4\pi)^2} \ln \frac{Q^2}{M^2} \cdot \frac{1}{n(n+1)} \quad ; \quad n = 1, 3, 5, \dots$$

$$\mathcal{G}_2^{(n)} = 3 \frac{e^2 \lambda^2}{(4\pi)^2} \ln \frac{Q^2}{M^2} \cdot \frac{1}{n+1} \quad ; \quad n = 1, 3, 5, \dots \quad (7.4.7)$$

In keeping with general parton model principles diagrams which involve direct photon-hadron or photon-diquark couplings since these in some sense correspond to even higher twist contributions. Here they are only artifacts of the model which could be distorted by considering alternatively a zero-charge hadron (a neutron for example) or diquark (in an integral charge quark model). In any case the inclusion of such terms although altering some details does not have any bearing on the main conclusions.

To order  $\alpha_s$  the two-loop diagrams of Fig. 7.4.3 are to be evaluated. In order to illustrate certain points it is useful to perform the calculation by stages. Considering for the moment only active-active quark contributions, the diagrams in Fig. 7.4.3(a) and (b) may be evaluated by computing first the top loop which corresponds to the usual calculation with off-shell legs. Then the effect of including the bottom loop can be seen separately.



+ self energy contributions

Fig. 7.4.3. Diagrams contributing in order  $\alpha_s$  to  $\mathcal{G}_1$  and  $\mathcal{G}_2$ .

The ladder graph of Fig. 7.4.3 is ultra-violet convergent thus using the technique outlined above a straightforward calculation in the Feynman gauge yields

$$\frac{\alpha_s}{2\pi} C_2(R) \ln \frac{Q^2}{|k^2|} i\epsilon^{\mu\nu\lambda\sigma} q_\lambda \gamma_5 2 \sum_{\substack{n=1 \\ \text{odd}}}^{\infty} \omega^n \left\{ \gamma_\sigma \left( \frac{-1}{n+1} \right) + \frac{k_\sigma q_\rho}{k \cdot q} \left( \frac{2}{n+1} - \frac{1}{n} \right) \right\}, \quad (7.4.8)$$

for the top loop, where  $w = 2k \cdot q / Q^2$  and the coupling constant a colour factor for the basic diagram are not included.

The diagram of Fig. 7.4.3 (b) is a little more complicated as it is ultra-violet divergent so that one must also include the region  $|k^2| \geq Q^2$ . Nevertheless it is still relatively straightforward, by expanding denominators according to the region, to obtain (including mirror partner):

$$\frac{\alpha_s}{4\pi} C_2(R) \frac{1}{(4\pi)^2} \ln \left| \frac{q^2}{k^2} \right| \left\{ \frac{-i\epsilon}{k \cdot q} q_\sigma \gamma_\sigma \gamma_\mu \gamma_\nu \gamma_\rho - \frac{i\epsilon}{(k \cdot q)^2} q_\sigma k_\rho \gamma_\sigma \gamma_\mu \gamma_\nu \gamma_\rho \right\} 2 \sum_{\substack{n=1 \\ \text{odd}}}^n \omega^n \sum_{j=2}^n \frac{1}{j}, \quad (7.4.9)$$

for the region  $M^2 \leq k^2 \leq Q^2$  and

$$\frac{\alpha_s}{4\pi} C_2(R) \frac{1}{(4\pi)^2} \left[ \frac{2}{\epsilon} - \ln \frac{Q^2}{\mu^2} \right] \frac{i\epsilon}{k \cdot q} q_\sigma \gamma_\sigma \gamma_\mu \gamma_\nu \gamma_\rho 2 \sum_{\substack{n=1 \\ \text{odd}}}^n \omega^n, \quad (7.4.10)$$

for the ultra-violet region. These results are in complete agreement with those of ref. [3]. Including the fermion self-energy graphs and taking note of the combinatorics in eq. (7.2.6) one obtains the anomalous dimensions (7.2.12). However the corresponding coefficient of  $\omega^n$  for  $\mathcal{G}_2$  is  $1 - \frac{2}{n+1} + \sum_{j=2}^n \frac{2}{j}$ .

In order to facilitate the comparison with the full calculation the top-loop contributions to the coefficients of  $\omega^n$  in  $\mathcal{G}_1$  and  $\mathcal{G}_2$  are listed below (note that they are zero for  $n$  even). Ladder contributions of Fig. 7.4.3(a):

$$\begin{aligned} \mathcal{G}_1 &: \frac{-2}{n(n+1)} \\ \mathcal{G}_2 &: \frac{-2}{n+1} \end{aligned} \quad (7.4.11)$$

Vertex contributions of Fig. 7.4.3(b) plus mirror diagram:

$$\begin{aligned} \mathcal{G}_1 &: \sum_{j=2}^n \frac{4}{j} \\ \mathcal{G}_2 &: \sum_{j=2}^n \frac{2}{j} \end{aligned} \quad (7.4.12)$$

where the ultra violet contributions have been omitted, they are in any case not  $n$ -dependent.

To complete the computation of these diagrams one must now include the bottom loop. The procedure is as before and, although more tedious, the calculations are still fairly straightforward; one now requires large logarithms from both loops. For clarity of presentation below are listed the coefficients of  $(1/x)^n$  for  $\mathcal{G}_1$  and  $\mathcal{G}_2$  with the factors  $\frac{1}{n(n+1)}$  and  $\frac{1}{n+1}$ , corresponding to the lowest order graph (see 7.4.7), factored out. Again the  $n$ -independent ultra-violet contribution is omitted and will be included later. Full ladder contribution of Fig. 7.4.3(a):

$$\begin{aligned} \mathcal{G}_1 & : \frac{-2}{n(n+1)} , \\ \mathcal{G}_2 & : \frac{2}{n+1} - 2 . \end{aligned} \tag{7.4.13}$$

Full vertex contribution of Fig. 7.4.3(b), plus mirror:

$$\begin{aligned} \mathcal{G}_1 & : \sum_{j=2}^n \frac{4}{j} , \\ \mathcal{G}_2 & : \frac{n-1}{n} \sum_{j=2}^n \frac{2}{j} . \end{aligned} \tag{7.4.14}$$

Already a definite mutation of the factors for  $\mathcal{G}_2$  is evident, while, as was expected, the factors for  $\mathcal{G}_1$  remain unchanged.

Finally the spectator contributions are to be evaluated, by way of example the computation is outlined below for the graph of Fig. 7.4.3(d). The integral to be evaluated is:

$$i \int [dk][dl] \text{tr} [\gamma_5 \not{k} \gamma^\mu (k+q) \gamma^\nu \not{k} \gamma^\alpha \not{l}] \frac{(k+l-2p)_\alpha}{k^2 l^2 (k+q)^2 (k-l)^2 (k-p)^2 (l-p)^2} . \tag{7.4.15}$$

Firstly note that there is an ultra-violet divergence, which in this case is rather easy to extract as it comes purely from the  $l_\alpha$  in  $(k+l-2p)_\alpha$ . Therefore this part of the integral reduces to

$$i \int [dk][dl] \text{tr} [\gamma_5 \not{k} \gamma^\mu (\not{k} + \not{q}) \gamma^\nu \not{k}] \frac{1}{k^4 (k+q)^2 (k-p)^2 (l-k)^2 (l-p)^2} \quad (7.4.16)$$

The  $l$ -integral is then trivial and gives

$$\frac{-i}{(4\pi)^2} \frac{1}{\epsilon} \left[ \frac{-(k-p)^2}{\mu^2} \right]^{-\epsilon} \quad (7.4.17)$$

Expanding in powers of  $\epsilon$ , subtracting the pole and keeping only the logarithm one has

$$\frac{i}{(4\pi)^2} \ln \left| \frac{k^2}{\mu^2} \right| \quad (7.4.18)$$

The  $k$ -integral is finite and setting  $D = 4$  one obtains the same integral as (7.4.4) with an additional factor of  $\ln |k^2|$ .

The remaining part of (7.4.15) is ultra-violet finite. Consider first the  $l$ -integral (in four dimensions):

$$\int [dl] \frac{l^2}{l^2 (l-k)^2 (l-p)^2} \quad (7.4.19)$$

To obtain a large logarithm one need only consider the region  $M^2 \ll |l^2| \ll |k^2|$  and so expanding the denominators accordingly one has

$$(7.4.19) = \frac{i}{(4\pi)^2} \frac{1}{k^2} \ln \left| \frac{k^2}{\mu^2} \right| \sum_{m=0}^{\infty} \left( \frac{2p \cdot k}{k^2} \right)^m \frac{1}{m+2} \quad (7.4.20)$$

Again the  $M^2/l^2$  is to be ignored as too is the term  $l^2/k^2$  since this will give  $p^2$  on symmetric integration. For certain other graphs this latter term is removed by considering the effect of extra powers of  $1/k^2$  on the  $k$ -integral.



Power counting and symmetric integration then give for the  $l$ -integral

$$\frac{i}{(4\pi)^2} \frac{1}{l^2} \ln \frac{|k^2|}{M^2} \not{\epsilon} \sum_{m=0}^{\infty} \left( \frac{2p \cdot k}{k^2} \right)^m \frac{1}{m+2}, \quad (7.4.21)$$

thus for the  $k$ -integral one is left with

$$\int \frac{[dk]}{k^4} \ln \frac{|k^2|}{M^2} \text{tr} [\not{\epsilon} \not{\epsilon} \not{\gamma}^\mu (k+q) \not{\gamma}^\nu k] (k-p)^{-2} (k+q)^{-2} \left( \frac{2p \cdot k}{k^2} \right)^m. \quad (7.4.22)$$

There are two points worth mentioning here: firstly from the sum in (7.4.21) one notes already the appearance of the typical  $\sum 1/j$  term and secondly the presence of the  $\not{\epsilon}$  in (7.4.22) implies that only the transverse-spin structure function receives a contribution since  $s_{\mu} \sim p$  and thus the contribution to  $\mathcal{G}_1$  is suppressed by  $M^2/Q^2$ .

The  $k$ -integral may now be evaluated by expanding the denominators and restricting, as usual, to the region  $M^2 \leq |k^2| \leq Q^2$ . Note also that the term  $k$  from  $(k+q)$  produces either higher power corrections or does not contribute to the structure functions  $\mathcal{G}_1$  and  $\mathcal{G}_2$ . Symmetric integration then gives for the hadronic vertex contribution of Fig. 7.4.3(d).

$$\begin{aligned} \mathcal{G}_1 & : \quad \text{zero}, \\ \mathcal{G}_2 & : \quad \frac{n+1}{n} \sum_{j=2}^n \frac{1}{j}. \end{aligned} \quad (7.4.23)$$

Similarly for the remaining top-quark-spectator contribution of Fig. 7.4.3(c) one obtains

$$\begin{aligned} \mathcal{G}_1 & : \quad \text{zero}, \\ \mathcal{G}_2 & : \quad \frac{n-3}{n} \sum_{j=2}^n \frac{1}{j} - \frac{2(n-1)}{n^2}. \end{aligned} \quad (7.4.24)$$

The total ultra-violet contribution (including self-energies) is

$$\mathcal{G}_1 : 1 , \tag{7.4.25}$$

$$\mathcal{G}_2 : 1 .$$

Thus the complete answer is:

$$\mathcal{G}_1 : 1 - \frac{2}{n(n+1)} + \sum_{j=2}^n \frac{4}{j} ,$$

$$\mathcal{G}_2 : 1 - \frac{2}{n(n+1)} + \frac{n-1}{n} \sum_{j=2}^{n-1} \frac{4}{j} \tag{7.4.26}$$

For convenience the above results are listed in table 7-I. Thus for  $\mathcal{G}_1$  the usual result is recovered while for  $\mathcal{G}_2$  the result is considerably modified. In particular the dominant piece, going as  $\ln(n)$  for large  $n$  has now a coefficient 4 in place of the original 2.

Diagram	$S_{//}$		$S_{\perp}$	
	U.V.	I.R.	U.V.	I.R.
Fig. 7.4.3(a)	0	$-\frac{2}{n(n+1)}$	0	$\frac{-2}{n(n+1)} - \frac{2(n-1)}{n}$
2 x Fig. 7.4.3 (b)	0	$\sum_{j=2}^n 4/j$	0	$\frac{(n-1)}{n} \sum_{j=2}^n 2/j$
Fig. 7.4.3(c)	0	0	0	$\frac{(-3)}{n} \sum_{j=2}^n 1/j - \frac{2(n-1)}{n}$
2 x Fig. 7.4.3 (d)	-1	0	-1	$\frac{(n+1)}{n} \sum_{j=2}^n 1/j$
Self Energies	2	0	2	0
Total	$1 - \frac{2}{n(n+1)} + \sum_{j=2}^n 4/j$		$1 - \frac{2}{n(n+1)} + \frac{(n-1)}{n} \sum_{j=2}^n 4/j$	

Table 7-I: the contributions of the different order  $\alpha_s$  diagrams to the coefficient  $(\frac{1}{x})^n$  in  $\mathcal{G}_1$  and  $\mathcal{G}_2$  calculated in the Feynman gauge.

## 7.5 General comments and conclusions

A few comments are in order before proceeding to any conclusions. Earlier attention was focused on the Wilson expansion approach. If one applies the model to the calculation of the operator renormalisation, although rather more tedious (due to the fact that all integrals are ultra-violet divergent), it is not difficult to show that while the spectator contributions are zero for  $\mathcal{O}_{A,2}$  the same is not true for  $\mathcal{O}_{A,3}$ . This is yet a further indication of the apparent failure of the operator approach to take into account spectator interactions when bound states are involved.

The calculations in the axial gauge are much more complicated (there appear to be two structures which propagate through the ladder graphs as opposed to simply  $\not{V}$  or  $\gamma_5 \not{V}$  in the twist-two case), however a cursory examination seems to suggest that while spectator interactions remain, gluons coupling to the top quark-rung still give zero contribution. Thus some kind of iterative structure, albeit very complex, might survive to produce a Bethe-Salpeter evolution equation. However it remains to be seen whether this would be Green's function independent and thus lead to universally defined parton distributions.

The inevitable conclusion to which one is drawn is that, at least in the case when the leading operators are the twist-three operators governing transverse-spin effects, the standard Wilson approach is not applicable. The operator-product expansion might be salvaged in this case by use of another technique of calculating the anomalous dimensions. This consists in finding another operator (well understood) to which the operator in question couples, then one can perform the calculations for the vacuum expectation value of the product, using the well-known property that the renormalisation constants factor out.

The question is raised by this analysis of what, if anything, distinguishes the case of transverse spin from the use of the Wilson expansion in general for Green's functions involving non-perturbative bound states; a question which it is clear requires a deeper examination. These remarks may also have a direct bearing on the existence of a generalised factorisation theorem for higher-twist as conjectured by Politzer [6]. In particular, in the light of these results it is difficult to see how the mass-singularity approach (see Ellis et al ref. [6]) could deal with problems of a non-perturbative origin.

## References to Chapter 7

- [1] M.A. Ahmed and G.G. Ross, Nucl. Phys. B56, 385 (1975); ref. [4] chap. 2.  
H. Ito, Prog. Theor. Phys. 54, 555 (1975).  
K. Sasaki, Prog. Theor. Phys. 54, 1816 (1975).  
J. Kodaira, S. Matsuda, T. Muta, K. Sasaki and T. Uematsu, Phys. Rev. D20, 627 (1979).  
J. Kodaira, Nucl. Phys. B165, 129 (1980).
- [2] G. Altarelli and S. Muzzeto, preprint LPTENS 79/27 (1979).
- [3] J. Kodaira, S. Matsuda, K. Sasaki and T. Uematsu, Nucl. Phys. B159, 99 (1979).
- [4] I. Antoniadis and C. Kounas, Ecole Polytechnique preprint A399.0580 (1980); Phys. Rev. D24, 505 (1981).
- [5] P. Ratcliffe, SISSA-Trieste preprint 5/83/E.P. (1983).
- [6] H.D. Politzer, Nucl. Phys. B172, 349 (1980).  
R.K. Ellis, W. Furmanski and R. Petronzio, CERN preprints TH.3254 (1982); TH 3301 (1982).
- [7] S. Wandzura and F. Wilczek, Phys. Lett. 72B, 195 (1977).  
S. Wandzura, Nucl. Phys. B122, 412 (1977).
- [8] See ref. [7] chapter 2.
- [9] See ref. [8] chapter 2.
- [10] D. Amati et al. ref [7] chapter 2.
- [11] See for example N.S. Craigie and H.F. Jones ref. [7] , chapter 2.
- [12] A.P. Bukhovstov, E.A. Kyrayev and L.N. Lipatov, Sov.Phys., JETP 37, 406 (1983).
- [13] E.V. Shuryak and A. Vainstein, Nucl. Phys. B201, 141 (1982).
- [14] G. Leibbrandt, Rev. Mod. Phys. 47, 849 (1975).

Chapter 8      Helicity asymmetries as a test of supersymmetric QCD  
interactions

- 8.1    A brief review of supersymmetry theory
- 8.2    General phenomenological implications of supersymmetry
- 8.3    Helicity asymmetries in supersymmetric particle production

## 8.1 A brief review of supersymmetry

Recently with the realisation [1] that supersymmetry may solve the "fine tuning" problem [2] of grand unified theories, there has been increasing interest in the phenomenological implications of such an extension to the present theoretical framework. Since the superpartners of the known particles should in general necessarily have masses below 1 TeV they may be accessible to future and even present experiments. In this section the basic relevant theoretical considerations involved in supersymmetric theories are discussed.

Supersymmetry is a symmetry between Bosonic and Fermionic degrees of freedom related through a supersymmetry transformation. The Lagrangian for a supersymmetric Yang-Mills gauge theory can be expressed as

$$\mathcal{L}_{\text{susy}} = \mathcal{L}_{\text{gauge}}(A, \lambda, D) + \mathcal{L}_{\text{matter}}(\Psi, \phi, A, F) + \mathcal{L}_{\text{Higgs}} \quad (8.1.1)$$

where the pure gauge-sector particles:  $A$  (spin-1),  $\lambda$  (spin- $\frac{1}{2}$ ) and  $D$  (auxiliary field) are in the adjoint representation of the gauge group and those of the matter sector  $\Psi$  (spin- $\frac{1}{2}$ ),  $\phi$  (spin-0) and  $F$  (auxiliary field) are in the regular representation. The invariance of  $\mathcal{L}_{\text{susy}}$  under the supersymmetry transformations:

$$\begin{aligned} \delta A_\mu^a &\sim \bar{\epsilon} \gamma_\mu \lambda^a, \\ \delta \lambda^a &\sim \epsilon (\sigma_{\mu\nu} F^{\mu\nu a} + D^a), \\ \delta D^a &\sim \bar{\epsilon} (\not{\partial} \lambda)^a, \\ \delta q_i &\sim \epsilon (\not{\partial} \phi)_i, \\ \delta \phi_i &\sim \bar{\epsilon} q_i, \\ \delta F_i &\sim \bar{\epsilon} \not{\partial} q_i, \end{aligned} \quad (8.1.2)$$



has the important implication that quadratic and logarithmic divergences associated with loop corrections to the masses in the theory cancel between fermionic and bosonic loop contributions. The point is that self energy diagrams like that of Fig. 8.1.1(a) have a partner with a fermion loop, Fig. 8.1.1(b) which gives a minus sign and the supersymmetry invariance guarantees the right couplings for the two diagrams to cancel.

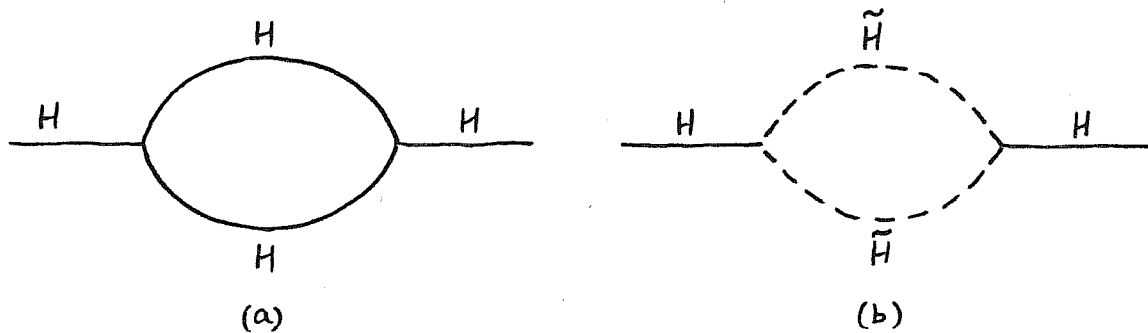


Fig. 8.1.1: (a) typical self energy with logarithmic divergence cancelled by the partner graph (b).

If unbroken supersymmetry implies a set of superpartners to the known particles with identical masses, then since these are not observed such a theory must be broken. However even in the broken theory it is in general very difficult to give a mass to the colour octet of spin- $\frac{1}{2}$  gluinos owing to the presence of a continuous R-invariance [3]. This problem can be avoided by considering a spontaneously broken supergravity theory, R-invariance is then necessarily broken by the mass of the Majorana spin-3/2 gravitino [4], so that the gluino (and also the photino) can acquire a mass.

Thus if one considers the gauge group  $SU(3)_{\text{col}} \times SU(2) \times U(1)$  with a supersymmetric Higgs sector which induces the breakdown of electroweak at a scale  $m_{3/2}$  (the gravitino mass) and induces a splitting of  $W^\pm$  and  $Z^0$  gauge bosons and the  $W^\pm$  and  $Z^0$  gauginos at the same scale, various radiative effects can give masses to the gluino and photino.

In this way, in going through the various stages of symmetry breaking, the masses acquired by the different particles all get related to one mass-scale, in a large class of theories [4,5] this latter is indeed the gravitino mass. Thus typically one obtains mass relations for the  $W^\pm$  and  $Z^0$  bosons of the form

$$m_{W^\pm, Z^0} \sim \left(\frac{e}{\lambda}\right) m_{3/2}, \quad (8.1.3)$$

where  $\lambda$  is a Yukawa coupling. If one assumes that  $e$  and  $\lambda$  are comparable in magnitude then the gravitino mass cannot be much larger than the  $W^\pm$  and  $Z^0$  masses.

The spin-zero partners to the leptons and quarks, namely sleptons ( $\tilde{l}$ ) and squarks ( $\tilde{q}$ ), acquire tree-level masses of order  $m_{3/2}$  with splitting (due to mixing) proportional to their respective fermion counterpart masses. Thus slepton and squark masses are generally thought to lie somewhat above those of the weak bosons.

In the gauge fermion sector the photino ( $\tilde{\gamma}$ ) and gluino ( $\tilde{g}$ ), massless at the tree-level, become massive through radiative corrections. These masses are proportional to their relative gauge couplings:

$$m_{\tilde{\gamma}} \sim \frac{\alpha}{2\pi} m_{3/2} \sim \text{a few GeV}$$

$$m_{\tilde{g}} \sim \frac{\alpha_s}{2\pi} m_{3/2} \sim \text{a few GeV} \quad (8.1.4)$$

In other theories [6] with different schemes of supersymmetry breaking one can arrive at very large masses (of order or greater than  $m_W$ ) for the gauge fermions. Therefore an urgent problem is to derive experimental limits on these masses in order to select the correct form of supersymmetric theory and breaking scheme.

The above mass-parameters represent the only unfixed quantities of the theory relevant to strong interaction phenomenology at present energies, the couplings being analogous to those of the standard theory. All effects of gravitation are limited to mass terms, recently it has been shown that in a class of  $SU(3) \times SU(2) \times U(1)$  locally supersymmetric models no sizeable gravitational radiative effects exist at the one-loop level [7], although one-loop diagrams exist involving virtual gravitino exchange use of the harmonic gauge  $\gamma^\mu \psi_\mu = 0$  reduces the contribution to just two diagrams whose quadratically divergent parts precisely cancel.

Thus the phenomenological consequences of a supersymmetric version of QCD can be ascertained by the inclusion in the usual calculation of hard scattering kernels the contributions from supersymmetric particle production in the usual way. The necessary Feynman rules can be derived from the standard supersymmetric Lagrangian with the inclusion of the relevant mass terms for the squarks and gluinos. For  $N = 1$  supersymmetry (Majorana gluinos) the Lagrangian takes the form

$$\begin{aligned}
\mathcal{L}_{SQCD} = & \mathcal{L}_{QCD} + \frac{i}{2} \bar{\lambda}^a \mathcal{D}^{ab} \lambda^b \\
& + (\mathcal{D} \tilde{q}_s)^\dagger (\mathcal{D} \tilde{q}_s) + (\mathcal{D} \tilde{q}_p)^\dagger (\mathcal{D} \tilde{q}_p) \\
& + g\sqrt{2} \left\{ \bar{\lambda}^a (\tilde{q}_{s,i}^\dagger - \tilde{q}_{p,i}^\dagger \gamma_5) \tau_{ij}^a q_j + h.c. \right\} \\
& + (\text{quadratic squark term}) + (\text{mass terms}).
\end{aligned} \tag{8.1.5}$$

Here the covariant derivative acting on the gluino field,  $\lambda^a$ , takes the usual form for gauge fields, namely

$$\mathcal{D}_\mu^{ab} = \delta^{ab} \partial_\mu - ig f^{abc} A_\mu^c, \tag{8.1.6}$$

and acting on the squark fields,  $q_s$  and  $q_p$ , is the same as that for quarks. The colour octet indices  $a, b$  run over 1 to 8 and the triplet  $i, j$  over 1 to 3, flavour indices have been suppressed.

The scalar and pseudoscalar combinations,  $q_s$  and  $q_p$ , of the more usual  $s$  and  $t$  scalar partners to the left- and right-handed quarks respectively, are given in terms of the latter by

$$\begin{aligned}\tilde{q}_s &= \frac{-i}{\sqrt{2}} (s + t), \\ \tilde{q}_p &= \frac{-i}{\sqrt{2}} (s - t).\end{aligned}\tag{8.1.7}$$

Note that this representation diagonalises the scalar mass-matrix [4].

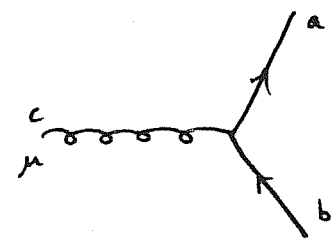
The coupling constant  $g$ , structure constants  $f^{abc}$  and regular representation matrices  $\tau_{ij}^a$  are as for standard QCD.

The Feynman rules derived from the above Lagrangian then give the usual form of massive spin-zero and spin- $\frac{1}{2}$  propagators for the squarks and gluinos respectively, namely

$$\begin{aligned}\text{squark propagator } & j \text{ --- } \xrightarrow{p} \text{ --- } i & : & i \delta_{ij} (p^2 - m_{\tilde{q}}^2)^{-1}, \\ \text{gluino propagator } & a \text{ --- } \xrightarrow{k} \text{ --- } b & : & -i \delta^{ab} \frac{k + m_{\tilde{g}}}{k^2 - m_{\tilde{g}}^2}\end{aligned}\tag{8.1.8}$$

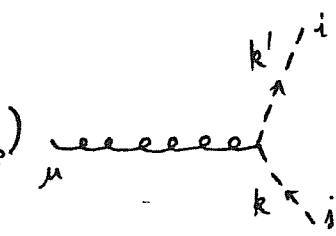
Several new vertices appear, the triple vertices of interest here are the following:

$g\tilde{g}\tilde{g}$  vertex



:  $g f^{abc} \gamma_\mu$ ,

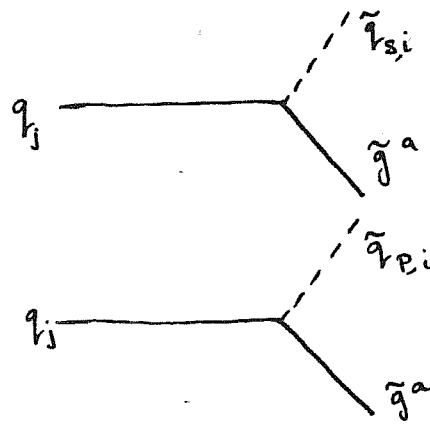
$g\tilde{q}\tilde{q}$  vertex ( $\tilde{q}_s$  or  $\tilde{q}_p$ )



:  $ig \tau_{ij}^a (k+k')_\mu$ ,

(8.1.9)

$q\tilde{q}\tilde{q}$  vertices



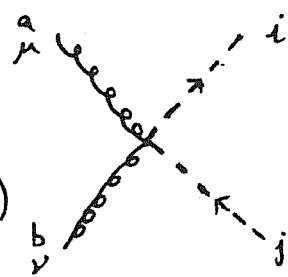
:  $ig \tau_{ij}^a$ ,

:  $-ig \tau_{ij}^a \gamma_5$ .

The hermitean conjugate of the last two (i.e. for the antiparticles) is identical with the exception that the minus sign for the pseudoscalar case is dropped.

There are also new four-point vertices present, of which only the gluon-gluon-squark-squark vertex is required in this chapter:

$gg\tilde{q}\tilde{q}$  vertex ( $\tilde{q}_s$  or  $\tilde{q}_p$ )



:  $ig^2 \{ \tau^a, \tau^b \}_{ij} g_{\mu\nu}$ .

(8.1.10)

Note that for  $N = 1$  supersymmetry the gluinos are Majorana particles; in calculations this is accounted for by using Dirac spinors and multiplying the gluino production cross-sections by a factor  $\frac{1}{2}$ . In the  $N = 2$  case gluinos are Dirac particles.

## 8.2 General phenomenological implications of supersymmetry

Assuming the previously discussed supersymmetric partner particle masses lie within the experimentally accessible range how would the presence of such particles manifest itself? For the purpose of this discussion let us for the moment restrict the considerations to proton-(anti)proton collisions, the situation being analogous for  $ep$  and  $e^+e^-$  scattering.

Above the, as yet unknown, threshold for supersymmetric particle production one expects to produce gluinos and squarks with strong interaction cross-sections which would then give rise to hadronic jets. However the decay of the supersymmetry partners is governed by the multiplicative conservation of an R-parity [8] which is given by

$$R = (-1)^{F - 3B - L}, \quad (8.2.1)$$

where F, B and L are fermion, baryon and lepton number respectively. Thus the gluino and squarks have odd R-parity and can therefore only decay into states containing at least one R-odd particle. In the "D-type" models discussed in the previous section in which the gluino is considerably lighter than the squarks the most likely decay modes for the gluino are  $\tilde{g} \rightarrow g + \tilde{G}$  ( $\tilde{G}$  a Goldstino) or the three-body decay  $\tilde{g} \rightarrow q\bar{q} + \tilde{\gamma}$  via

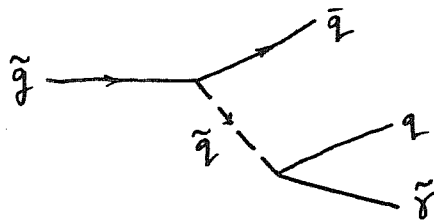


Fig. 8.2.1. Three-body decay mode of the gluino:  $\tilde{g} \rightarrow q\bar{q} + \tilde{\gamma}$ .

with a lifetime  $c\tau \sim 1$  cm. The squarks also decay rapidly to  $q + \tilde{G}$ .

Both the photino and Goldstino are essentially non-interacting and therefore would escape detection in a normal experiment. Thus the signature for a supersymmetry event is an imbalance in transverse momentum and missing momentum out of the plane. To make use of this it is convenient to define the quantity [9]:

$$x_E = \frac{-\vec{p}_T \cdot \vec{p}'_T}{|\vec{p}_T|^2}, \quad (8.2.2)$$

where  $p_T$  is the sum of transverse momenta in one hemisphere and  $p'_T$  that of the opposite hemisphere. For a normal QCD event  $x_E = 1$  but is different for missing energy events. Using various cuts on  $x_E$  and the total transverse momenta the authors of ref. [9] showed in a Monte-Carlo simulation that a reasonable signal could be obtained from about  $10^6$  events. The only background after the missing  $p_T$  cuts (which reduce the signal to some  $10^3$  events) comes from heavy quark production. Above threshold the cross-section  $\sigma(gg \rightarrow \tilde{g}\tilde{g}) \sim 10 \sigma(gg \rightarrow Q\bar{Q})$  owing essentially to colour factors, taking into account the 10% leptonic branching ratio for  $Q \rightarrow l \nu X$  one sees that this background is very small and maybe still further reduced by applying a lepton veto.

The present limits on the gluino mass are set by beam dump experiments, the lower bound being around 2 GeV [10]. The absence of new thresholds at PETRA provides a lower limit for the squark masses of about 17 GeV [11].

Recently the enhancement of the one-jet cross-section in  $p\bar{p}$  reactions has been considered as a signal [12]. There are two important reasons to expect the jet cross-section to be larger owing to the existence of gluinos and squarks:

- i) new production channels open,
- ii) the running coupling constant increases.

The authors of [12] considered the effect of gluinos with mass 2 GeV and squarks of 17 GeV mass at collider energies ( $\sqrt{s} = 540$  GeV). They found



that the effect is always small if one neglects squarks but that their inclusion leads to a very large enhancement, of order 2 for  $p_T = 80$  GeV at  $\theta = 90^\circ$  and is an increasing function of the transverse momentum  $p_T$ .

As a final comment on the present limits on gauge fermion masses it is interesting to note that the cosmological constraints on the photino mass [13], suggest this to be about 2 GeV which coincides with the typical predictions of the D-type models, see eqn. (8.1.2).

### 8.3 Helicity asymmetries in supersymmetric particle production

If one recalls that the important feature of supersymmetric theories is that all fermions get bosonic partners and vice-versa a further signal suggests itself, namely the helicity asymmetry. At high energies the dominant subprocess contributing to  $pp \rightarrow \text{jet}+X$  at sufficiently small  $p_T$  is gluon production from gluon fusion, as we have already seen in chapter 3 the helicity asymmetry (initial-initial) for this process is very large and positive. The corresponding dominant supersymmetric process is gluino production, again from gluon fusion. Since the gluinos are fermions with similar couplings to quarks (barring colour factors) the analysis of chapter 3 now tells us that the asymmetry is precisely -1 for this partonic subprocess.

Following the analysis presented in ref. 14 where the various new partonic cross-sections were evaluated as functions of the gluino and squark masses, the full expressions are given below the asymmetries being plotted against  $\theta_{\text{cm}}$  in Fig. 8.3.1 for various values of  $R = 4m^2/s = m^2/E_{\text{beam}}^2$ . It is convenient to use slightly modified  $t$  and  $u$  variables:

$$t' = -2 p_1 \cdot k_1 \quad , \quad (8.3.1a)$$

$$u' = -2 p_1 \cdot k_2 \quad ,$$

with  $p_i(k_i)$  the incoming (outgoing) momenta (thus  $s + t' + u' = 0$ ) for the first three processes below and, for the fourth:

$$t' = -2 p_1 \cdot k_1 + \Delta \quad ,$$

$$u' = -2 p_1 \cdot k_2 + \Delta \quad , \quad (8.3.1b)$$

with  $\Delta = M^2 - m^2$ , where  $M$  and  $m$  are the squark and gluino masses respectively.

(i)  $gg \rightarrow \tilde{g}\tilde{g}$

$$\frac{d\hat{\sigma}}{dt} = \frac{\pi\alpha_s^2}{s^2} \frac{9}{4} \left[ 1 - \frac{t'u'}{s^2} \right] \left[ \frac{t'}{u'} + \frac{u'}{t'} + \frac{4m^2s}{t'u'} \left( 1 - \frac{m^2s}{t'u'} \right) \right],$$

$$\frac{d\Delta\hat{\sigma}}{dt} = -\frac{\pi\alpha_s^2}{s^2} \frac{9}{4} \left[ 1 - \frac{t'u'}{s^2} \right] \left[ \frac{t'}{u'} + \frac{u'}{t'} \right] \left[ 1 - \frac{2m^2s}{t'u'} \right]. \quad (8.3.2)$$

(ii)  $gq \rightarrow \tilde{g}q$

$$\begin{aligned} \frac{d\hat{\sigma}}{dt} = \frac{\pi\alpha_s^2}{s^2} \frac{1}{2} & \left[ \frac{(u'+2\Delta)}{t'} - \frac{4(t'-2\Delta)}{9s} + \frac{8\Delta}{9u'} \right. \\ & \left. + \Delta \left( \frac{2m^2}{t'^2} + \frac{8M^2}{9u'^2} + \frac{(M^2+m^2)}{t'u'} \right) - \frac{\Delta^2}{s} \left( \frac{1}{t'} + \frac{1}{9u'} \right) \right], \end{aligned} \quad (8.3.3)$$

$$\frac{d\Delta\hat{\sigma}}{dt} = -\frac{\pi\alpha_s^2}{s^2} \frac{1}{2} \left[ \frac{(u'+2\Delta)}{t'} - \frac{4(t'-2\Delta)}{9s} + \frac{8M^2}{9u'} - \frac{2sm^2}{t'^2} \right].$$

(iii)  $gg \rightarrow \tilde{q}\tilde{q}$

$$\frac{d\hat{\sigma}}{dt} = \frac{\pi\alpha_s^2}{s^2} \frac{1}{24} \left[ -\frac{9t'u'}{s^2} + 8M^4 \left( \frac{1}{t'^2} + \frac{1}{u'^2} - \frac{M^2+4s}{4M^2t'u'} \right) + \frac{18M^2}{s} + 4 \right],$$

$$\frac{d\Delta\hat{\sigma}}{dt} = -\frac{\pi\alpha_s^2}{s^2} \frac{1}{24} \left[ -\frac{9t'u'}{s^2} + \frac{18M^2}{s} - 4 - \frac{8M^2s}{t'u'} \right] \quad (8.3.4)$$

(iv)  $\underline{q_\alpha q_\beta \rightarrow \tilde{q}_I \tilde{q}_J}$  ( $\alpha, \beta$  refer to flavour I, J to scalar or pseudoscalar combinations)

$$\frac{d\hat{\sigma}}{dt} = \frac{\pi\alpha_s^2}{s^2} \frac{1}{9} \left\{ \left[ 1 - \frac{\Delta^2}{t'u'} \right] \left[ \frac{u'}{t'} + \delta_{\alpha\beta} \left( \frac{t'}{u'} + \frac{2}{3} \epsilon_{IJ} \right) \right] - \frac{4}{3} \frac{m^2 s}{t'u'} \delta_{\alpha\beta} \delta_{IJ} \right\},$$

$$\begin{aligned} \frac{d\Delta\hat{\sigma}}{dt} = & - \frac{\pi\alpha_s^2}{s^2} \frac{1}{9} \left\{ \left[ 1 - \frac{\Delta^2}{t'u'} \right] \left[ \frac{u'}{t'} + \delta_{\alpha\beta} \left( \frac{t'}{u'} + \frac{2}{3} \epsilon_{IJ} \right) \right] \right. \\ & \left. - \frac{2m^2 s}{t'u'} \left[ \frac{u'}{t'} + \delta_{\alpha\beta} \left( \frac{t'}{u'} + \frac{2}{3} (\delta_{IJ} - 1) \right) \right] \right\}. \end{aligned} \quad (8.3.5)$$

where  $\epsilon_{IJ} = 1$  for  $I = J$  and  $-1$  for  $I \neq J$ . The spin-averaged cross-sections are in complete agreement with those given in refs. [10] (erratum) and [12].

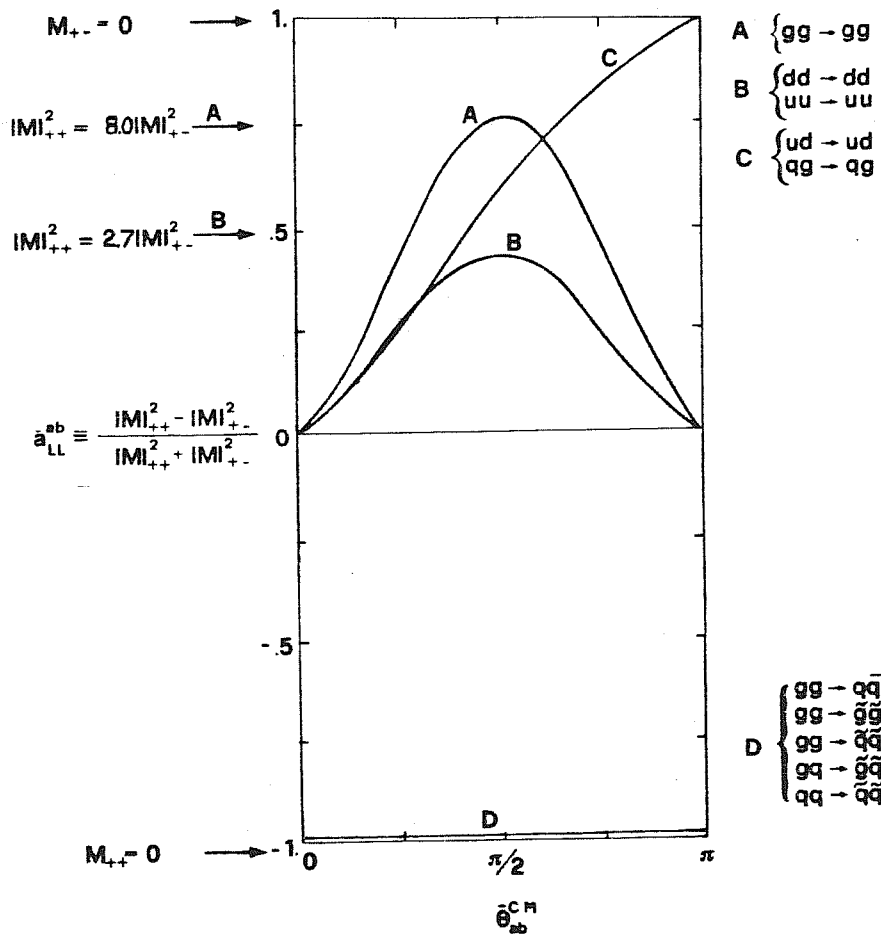


Fig. 8.3.2. Partonic helicity asymmetries in the limit of zero gluino and squark masses for the processes  $gg \rightarrow \tilde{g}\tilde{g}$ ,  $gq \rightarrow \tilde{g}\tilde{q}$ ,  $gg \rightarrow \tilde{q}\tilde{q}$  and  $qq \rightarrow \tilde{q}\tilde{q}$  compared with the corresponding asymmetries for the standard QCD processes  $gg \rightarrow gg$ ,  $gq \rightarrow gq$ ,  $gg \rightarrow q\bar{q}$  and  $qq \rightarrow qq$ .

In the limit  $m^2/s \rightarrow 0$  all asymmetries are -1 which is to be contrasted with the large positive asymmetries which vary with  $\theta_{CM}$  of the corresponding standard QCD processes, see Fig. 8.3.2 above and Table 8 - I following.

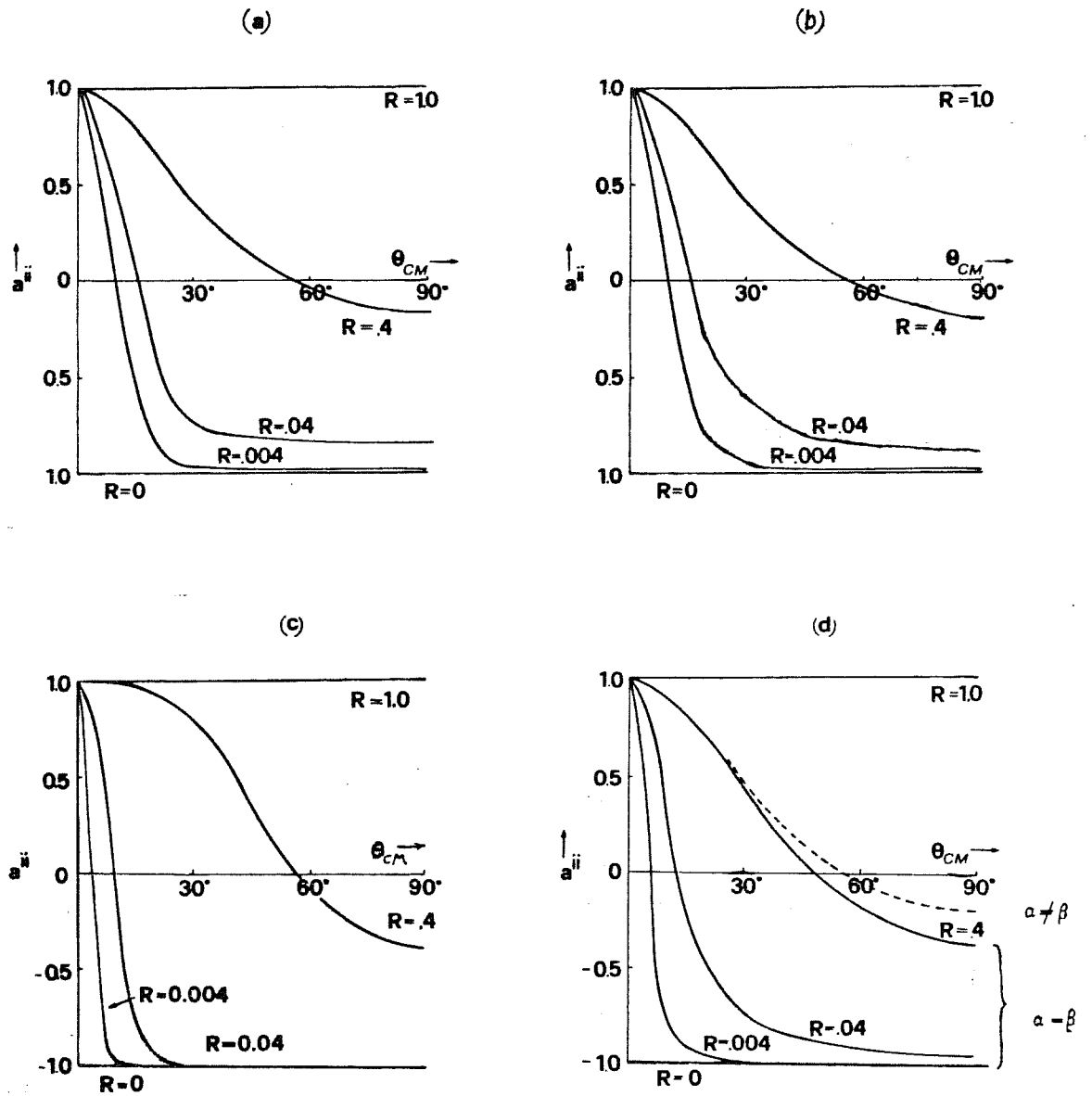


Fig. 8.3.1. Helicity asymmetries of hard parton cross-sections for the production of supersymmetric particles ( $R = 4m^2/s$ ):

(a)  $gg \rightarrow \tilde{g}\tilde{g}$ , (b)  $gq \rightarrow \tilde{g}\tilde{q} (M = m)$ , (c)  $gg \rightarrow \tilde{q}\tilde{q} (M = m)$ ,

(d)  $\sum_{I,J} q q \rightarrow \tilde{q}_I \tilde{q}_J (M = m)$ .

Table 8-I

$ab \rightarrow \tilde{a}\tilde{b}(ab)$	$d\hat{\sigma}/dt \left( \frac{\pi\alpha_S^2}{s^2} \right)$	$a_{ii}$
$gg \rightarrow \tilde{g}\tilde{g}$	$\frac{9}{4} \left( 1 - \frac{tu}{s^2} \right) \left( \frac{t}{u} + \frac{u}{t} \right)$	-1
$gg \rightarrow gg$	$\frac{9}{4} \left( \frac{s^2}{tu} \right)^2 \left( 1 - \frac{tu}{s^2} \right)^3$	$\frac{(2s^2 - tu)tu}{(s^2 - tu)^2}$
$gq \rightarrow \tilde{g}\tilde{q}$	$\frac{1}{2} \left\{ \frac{u}{t} - \frac{4}{9} \frac{t}{s} \right\}$	-1
$gq \rightarrow gq$	$\left( 1 + \frac{u^2}{s^2} \right) \left( \frac{s^2}{t^2} - \frac{4}{9} \frac{s}{u} \right)$	$\frac{(s^2 - u^2)}{(s^2 + u^2)}$
$gg \rightarrow \tilde{q}\tilde{q}$	$\frac{1}{24} \left( 4 - \frac{9tu}{s^2} \right)$	-1
$gg \rightarrow q\bar{q}$	$\frac{1}{6} \left( \frac{u}{t} + \frac{t}{u} \right) \left( 1 - \frac{9}{4} \frac{tu}{s^2} \right)$	-1
$q_\alpha q_\beta \rightarrow \tilde{q}_I \tilde{q}_J$	$\frac{1}{9} \left[ \frac{u}{t} + \delta_{\alpha\beta} \left( \frac{t}{u} + \frac{2}{3} \epsilon_{IJ} \right) \right]$	-1
$q_\alpha q_\beta \rightarrow q_\alpha q_\beta$	$\frac{4}{9} \left[ \frac{s^2 + u^2}{t^2} + \delta_{\alpha\beta} \left( \frac{s^2 + t^2}{u^2} - \frac{2}{3} \frac{s^2}{tu} \right) \right]$	$\frac{\left[ \frac{(s^2 - u^2)}{t^2} + \delta_{\alpha\beta} \left( \frac{s^2 - t^2}{u^2} - \frac{2}{3} \frac{s^2}{tu} \right) \right]}{\left[ \frac{(s^2 + u^2)}{t^2} + \delta_{\alpha\beta} \left( \frac{s^2 + t^2}{u^2} - \frac{2}{3} \frac{s^2}{tu} \right) \right]}$

Partonic cross-sections and asymmetries for supersymmetric processes compared with usual QCD processes. Indices  $\alpha, \beta$  refer to quark flavours and  $I, J$  refer to scalar or pseudoscalar squarks with  $\epsilon_{IJ} = 1$  ( $I = J$ ) or  $-1$  ( $I \neq J$ ).

One might worry that for not particularly small  $R$  (i.e. close above threshold) the small  $\theta_{cm}$  region of positive asymmetry could wash out the effect at the hadronic level when convoluted with parton distributions. In Fig. 8.3.3 the  $pp(\bar{p})$  cross-section asymmetry corresponding to the subprocess  $gg \rightarrow \tilde{g}\tilde{g}$  (dominant at these energies) is plotted again as a function of  $m/E_{beam}$ . One sees that even very close above the production threshold one still has a negative asymmetry for large enough  $x_T$ . The reason is essentially that the partonic  $x$  integrals are cut off below about  $m/E_{beam}$ . However there is still a change of sign in the asymmetry as one approaches the threshold (from above), thus apart from the change in sign one expects on going from normal events to those with missing energy there is also an energy dependence of the sign in purely supersymmetric QCD events.

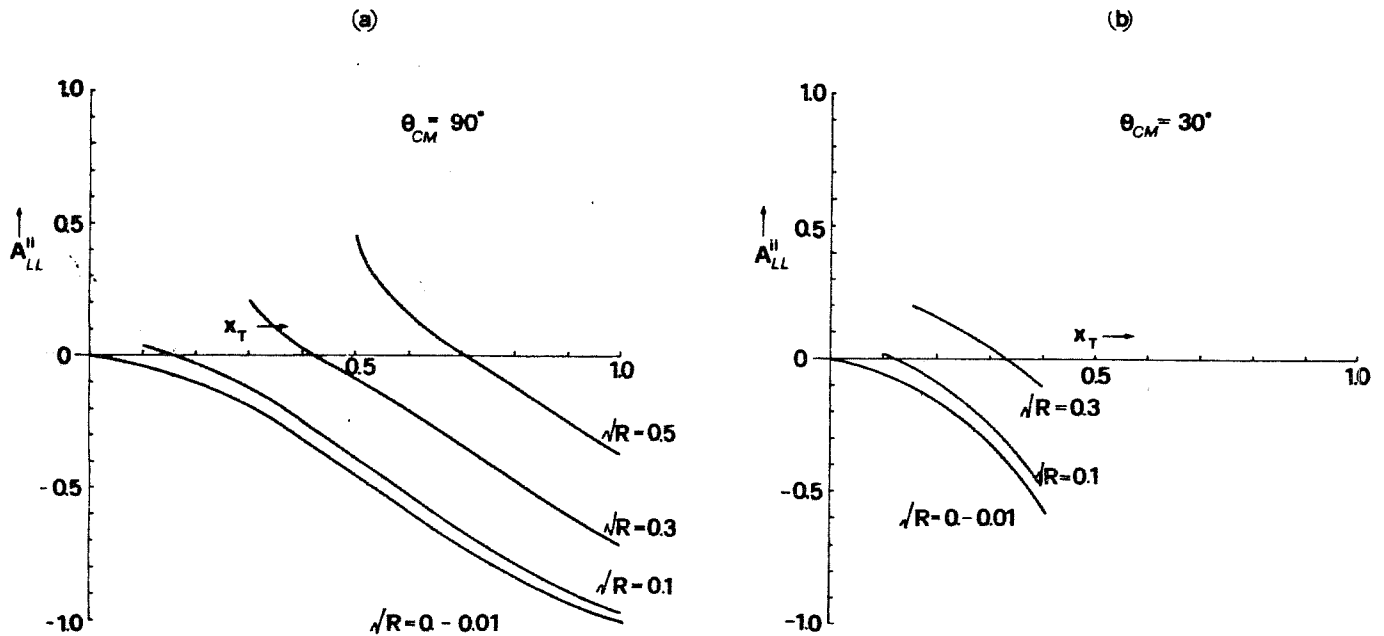


Fig. 8.3.3. Helicity asymmetry for  $pp \rightarrow \tilde{g}\tilde{g}X$  for different values of  $\sqrt{R} = m/E_{beam}$  plotted against  $x_T$  for (a)  $\theta_{cm} = 90^\circ$  and (b)  $\theta_{cm} = 30^\circ$ .



In conclusion then one sees that, if missing energy events are found in  $pp(\bar{p})$  collisions involving high transverse-momentum jets, a helicity asymmetry measurement would provide a good check as to whether or not these events were due to the production of new heavy spin- $\frac{1}{2}$  degrees of freedom, namely gluinos.

References to Chapter 8

- [1] H. Georgi and S. Dimopoulos, Nucl. Phys. B193, 150 (1981). N. Sakai, N. Sakai, Z. Phys. C11, 153 (1982).  
E. Witten, Nucl. Phys. B188, 513 (1981).  
M. Dine, W. Fischler and M. Srednicki, Nucl. Phys. B189, 575 (1981).  
S. Dimopoulos and S. Raby, Nucl. Phys. B192, 353 (1981).
- [2] E. Gildener and S. Weinberg, Phys. Rev. D13, 3333 (1976).  
E. Gildener, Phys. Rev. D14, 1667 (1976).
- [3] P. Fayet, Phys. Lett. 78B, 417 (1978).
- [4] E. Cremmer, P. Fayet and L. Girardello, Paris preprint LPTENS 82/30 (1982).
- [5] R. Arnowitt, A.H. Chamseddine and P. Nath, Phys. Rev. Lett. 49, 870 (1982).  
E. Cremmer, S. Ferrara, L. Girardello and A. van Proyen, CERN preprints TH-3312, -3348 (1982).  
S. Ferrara, L. Girardello and H.P. Nilles, CERN preprint TH-3494 (1982).
- [6] L.E. Ibáñez and G.G. Ross, Phys. Lett. 110B, 215 (1982).  
M. Dine and W. Fischler, Phys. Lett. 110B, 227 (1982).  
L. Alvarez-Gaume, M. Claudson and M.B. Wise, Harvard preprint HUTP 81/A063(1981)  
C.R. Nappi and B.A. Ovrut, Phys. Lett. 113B, 175 (1982).  
J. Ellis, L.E. Ibáñez and G.G. Ross, CERN preprint TH-3382 (1982).
- [7] R. Barbieri, L. Girardello and A. Masiero, Padova preprint IFPD 6/83 (1983).
- [8] A. Salam and J. Strathdee, Nucl. Phys. B87, 85 (1975).  
P. Fayet, Nucl. Phys. B90, 104 (1975).  
G. Farrar and P. Fayet, Phys. Lett. 76B, 575 (1978).  
G. Farrar and S. Weinberg, Rutgers/Texas preprint RU-82-38 (1982).
- [9] S.H. Aronson et al., Brookhaven preprint (1982).

- [10] G.L. Kane and J.P. Leveille, Phys. Lett. 112B, 227 (1982).  
P.R. Harrison and C.H. Llewellyn Smith, Nucl. Phys. B213, 223 (1983);  
Erratum (to appear in Nucl. Phys.)
- [11] D.P. Barber et al., Phys. Rev. Lett. 45, 1904 (1980).  
CELLO Collaboration, DESY preprint 82-021 (1982).
- [12] I. Antoniadis, L. Baulieu and F. Delduc, Paris preprint LPTHE 83.10 (1983).
- [13] H. Goldberg, Northeastern Univ. preprint NUBn.2592 Rev. (1983).
- [14] N.S. Craigie, K. Hidaka and P. Ratcliffe, Trieste Preprint IC/83/43  
(1983)(to appear in Phys. Lett. B).

Chapter 9

Single-spin asymmetries in QCD

9.1 Introduction to single-spin asymmetries in QCD

9.2 The calculation of single-spin asymmetries in the Drell-Yan process

## 9.1 Introduction to single-spin asymmetries

A brief discussion has already been given in chapter 4 of some of the surprising and still unexplained single-spin phenomena which occur in high energy particle interactions. In this chapter the theoretical predictions for single-spin asymmetries in the Drell-Yan process are reviewed [1].

First of all let us recall that although strong interactions are parity conserving (barring weak interference effects) one can in principle produce asymmetries using only one polarisation by considering the correlation between the kinematical configuration of say the final particles and the spin of an initial particle.

In the leading order however the Drell-yan process admits of no single-spin dependence since no imaginary (absorptive) phase is associated with the parton probability distributions. This leading order prediction then provides a useful null test of QCD which is not dependent on the parton distributions themselves.

It is well-known however, that loops (and indeed only loops) can generate an imaginary part, thus looking at higher order effects one can hope to discover some single-spin dependence. It turns out that one has to go to order  $\alpha_s^2$ , the reason being that apart from one factor of  $\alpha_s$  coming from the loop one also requires  $Q_T$  of the lepton pair to be non-zero for kinematical reasons; this implies emission of a real gluon for example which gives another factor of  $\alpha_s$ .

The situation envisaged here is precisely that of the planned experiments at CERN and FNAL (see chapter 4) so it is important to have clear QCD predictions for such effects.

One is considering then the spin dependence of the differential cross-section:

$$\frac{d\sigma}{d^4Q d\Omega} (\vec{A}B \rightarrow \mu^+ \mu^- X) , \quad (9.1.1)$$

where  $Q^\mu$  is the lepton pair 4-momentum and  $\Omega$  their angles in a given frame, A and B are two suitable hadrons ( $p\pi$  or  $p\bar{p}$  for example). Describing the process in terms of the usual leptonic and hadronic tensors

$$e^2 W^{\mu\nu} = \int d^4x e^{iQ \cdot x} \langle p_A, s_A, p_B | J^{(\mu)} J^{(\nu)} | p_A, s_A, p_B \rangle , \quad (9.1.2)$$

$$L^{\mu\nu} = -2Q^2 \left( g^{\mu\nu} - \frac{Q^\mu Q^\nu}{Q^2} - \frac{k^\mu k^\nu}{k^2} \right) ,$$

where  $k$  is the difference between the lepton momenta  $k_1$  and  $k_2$ . One obtains

$$\frac{d\sigma}{d^4Q d\Omega} = \frac{\alpha^2}{2(2\pi)^4} \frac{1}{Q^2 s} \left( \delta^{ij} - \frac{k_1^i k_1^j}{k_1^2} \right) W_{ij} , \quad (9.1.3)$$

in the lepton pair rest-frame. In order to define the angles  $\vartheta$  and  $\varphi$  in this frame it is convenient to construct the following basis [2].

$$Z^\mu = P_A^\mu Q \cdot P_B - P_B^\mu Q \cdot P_A ,$$

$$X^\mu = P_A^\mu Q^2 Z \cdot P_B - P_B^\mu Q^2 Z \cdot P_A + Q^\mu (Q \cdot P_B Z \cdot P_A - Q \cdot P_A Z \cdot P_B) , \quad (9.1.4)$$

$$Y^\mu = \epsilon^{\mu\nu\rho\sigma} P_{A\nu} P_{B\rho} Q_\sigma .$$

The differential cross-section for  $Q_T \neq 0$  may be written in the form [2]

$$\begin{aligned}
\frac{d\sigma}{d^4Q d\Omega} &= \frac{\alpha^2}{2(2\pi)^4} \frac{1}{Q^2 s} \left\{ 2(W_{0,0} + Y.S_A T_{0,0}) \right. \\
&+ \frac{1}{3} \left[ (1 - 3\cos^2\theta)(W_{2,0} + Y.S_A T_{2,0}) \right] \\
&+ \sin 2\theta \cos \varphi (W_{2,1} + Y.S_A T_{2,1}) \\
&+ \frac{1}{2} \left[ \sin^2\theta \cos 2\varphi (W_{2,2} + Y.S_A T_{2,2}) \right] \\
&+ \sin 2\theta \sin \varphi (X.S_A T_{2,-1}^T + Z.S_A T_{2,-1}^L) \\
&+ \sin^2 2\theta \sin 2\varphi (X.S_A T_{2,-2}^T + Z.S_A T_{2,-2}^L) \left. \right\}
\end{aligned} \tag{9.1.5}$$

where the polarisation of hadron B has been averaged over. It is clear from the above that to define the angle  $\varphi$  one must keep  $Q_T \neq 0$ . QCD power counting then tells us that

$$\begin{aligned}
W_{2,2}, T_{2,2}, T_{2,-2}^L, T_{2,-2}^T &\propto \frac{Q_T^2}{\hat{s}}, \\
W_{2,1}, T_{2,1}, T_{2,-1}^L, T_{2,-1}^T &\propto \frac{Q_T}{\sqrt{\hat{s}}},
\end{aligned} \tag{9.1.6}$$

when compared with  $W_{00}$ . Moreover transverse spin effects, as discussed in chapter 7 are suppressed by a further power of  $\sqrt{\hat{s}}$  so that  $T_{2,1}$  and  $T_{2,-1}^T$  should be small. Thus the term most likely to provide a large effect at the lowest non-trivial order (i.e. at order  $\alpha_s^2$  for  $q\bar{q}$  annihilation) is the helicity term  $T_{2,-1}^L$ .

## 9.2 The calculation of single-spin asymmetries in the Drell-Yan process

To calculate  $T_{2,-1}^L$  one requires the imaginary part of the interference between Born graphs, Fig. 9.2.1(a) and higher order graphs, e.g. Figs. 9.2.1(b)-(d), the authors of [1] claim that these are indeed the only graphs with an imaginary part contributing. Typically then one has to evaluate integrals of the form

$$\text{Im} \frac{1}{i} \int d^D l \frac{(1, l^\mu, l^\mu l^\nu, l^\mu l^\nu l^\rho)}{l^2(p-l)^2(Q-r-l)^2(l+r)^2} \quad (9.2.1)$$

using dimensional regularisation  $D = 4 - 2\epsilon$ . At the partonic subprocess level the resulting expression, which is the coefficient of  $\delta((p+r-Q)^2)$ , may be cast into the form

$$\text{Z.S.}_A \hat{T}_{2,-1}^L = 2\pi^2 e_q^2 \alpha_s^2 \frac{C_2(R)}{N_c} \left[ C_2(R) - \frac{1}{2} C_2(A) \right] \quad (9.2.2)$$

$$\times \left[ A \left( \frac{1}{\epsilon} - \ln \frac{Q^2}{\mu^2} \right) + B \ln \frac{\hat{s}}{Q^2} + C \ln \left( 1 + \frac{Q_T^2}{Q^2} \right) + D \ln \left( \frac{Q \cdot P}{Q \cdot T} \right) + E \right] .$$

As a first check on the calculation the coefficient A of the infra-red singularity should be zero since an imaginary divergence would not be factorisable into the parton distributions in the usual manner, rendering QCD unapplicable. This the authors of [1] find and they give the other coefficients as

$$B = -C = \frac{-2\Delta Q^4}{\hat{s} Q_T^3 \sqrt{Q^2 + Q_T^2}} ,$$

$$D = \frac{Q^2 [Q^2 (\hat{s} - Q^2) + 2Q_T^2 \hat{s}]}{\hat{s} Q_T^3 \sqrt{Q^2 + Q_T^2}} ,$$



$$\begin{aligned}
E = & -\Delta \left[ \hat{s}^2 (13Q^2 + 9Q_T^2) - 12\hat{s} (Q^4 + 4Q^2Q_T^2 + 3Q_T^4) \right. \\
& \left. - Q^2 (Q^4 - 15Q^2Q_T^2 - 12Q_T^4) \right] \\
& \times \left[ \hat{s} Q_T (\hat{s} - Q^2) (Q^2 + Q_T^2) \sqrt{Q^2 + Q_T^2} \right]^{-1},
\end{aligned} \tag{9.2.3}$$

with  $\Delta = Q.p - Q.r$ ,  $\ln(Q.r/Q.p)$  being twice the rapidity of the pair in the subprocess c.m. system. A close examination of the expression for  $T_{2,-1}^L$  shows that it does indeed vanish like  $Q_T/\sqrt{s}$  consistent with eqn. (9.1.6).

One can now define an integrated asymmetry  $\mathcal{A}_L$  for the physical process by

$$\mathcal{A}_L = \frac{\int_0^1 d\cos\Theta \left[ \int_0^\pi d\varphi - \int_0^{2\pi} d\varphi \right] d\sigma^+ / d^4Q d\Omega}{\int_0^1 d\cos\Theta \left[ \int_0^\pi d\varphi + \int_0^{2\pi} d\varphi \right] d\sigma / d^4Q d\Omega}, \tag{9.2.4}$$

where  $d\sigma^+$  indicates a positive helicity proton A, since  $\mathcal{A}_L$  is linear in the proton helicity  $d\sigma^+$  and  $\frac{1}{2}(d\sigma^+ - d\sigma^-)$  are entirely equivalent. From expression (9.1.5) it is straightforward to show that

$$\mathcal{A}_L = \frac{2Z.S_A T_{2,-1}^L}{3\pi W_{0,0}}. \tag{9.2.5}$$

And defining  $\mathcal{a}_L$ , the subprocess asymmetry, in the obvious way modifying (9.2.4), one obtains a similar expression for  $\mathcal{a}_L$  in terms of  $T_{2,-1}^L$ .

In Fig. 9.2.1 the subprocess asymmetry is plotted as a function of the lepton-pair transverse momentum  $Q_T$  for  $Q^2 = 25 \text{ GeV}^2$ ,  $s = 200$  and  $400 \text{ GeV}^2$ , and the photon rapidity  $y > 0$ . The asymmetry is rather small owing essentially to the colour factor  $(C_2(R) - N_C/2) = -1/6$  for  $SU(3)$ . Infact  $(C_2(R) - N_C/2)/(N_C/2) = -1/9$ ,

that is a suppression of roughly one order of magnitude owing to a coincidental partial cancellation of colour factors.

Summarising the result of the complete order  $\alpha_s^2$  calculation in the limit  $s \rightarrow \infty$  with  $Q^2/s, Q_T^2/s, y$  held fixed one obtains the estimate

$$|\mathcal{A}_L| \approx \left| C_2(R) - \frac{1}{2}N_c \right| \frac{\alpha_s^2 \left\langle \left( \frac{Q_T}{\sqrt{s}} \right) \lambda_q(x) q(x) \bar{q}(x) \right\rangle}{\alpha_s \langle q(x) \bar{q}(x) \rangle} \sim 5\alpha_s \% \quad (9.2.6)$$

where the brackets indicate partonic variable convolutions. Numerically integrating this result using the  $NA_3$  parton distributions and  $\lambda_q(x) = 0.94\sqrt{x}$ , see section 4.3, the authors obtain  $\mathcal{A}_L = -2.2\alpha_s\%$  ( $1.8\alpha_s\%$ ) at  $Q^2 = 25 \text{ GeV}^2, Q_T = 4$  (3) GeV and  $y = 1$  for  $\pi^+p$  experiments at  $\sqrt{s} = 27 \text{ GeV}$ .

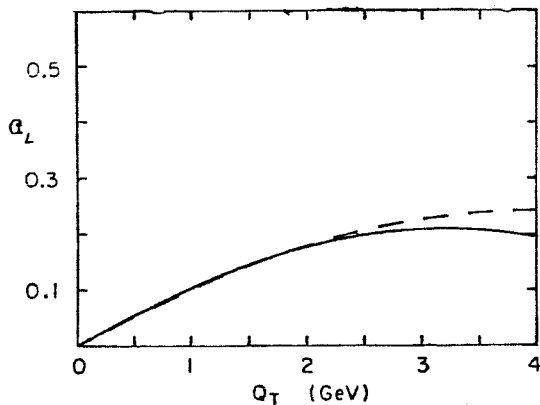


Fig. 9.2.1. The asymmetry at the sub-process level, as defined in eq. (9.2.4), in units of  $(2C_2(R) - N_c) \alpha_s(Q^2)$  for  $s=200 \text{ GeV}^2$  (full curve) and  $s=400 \text{ GeV}^2$  (dashed curve).

In conclusion then the null result for  $\mathcal{A}_L$  in the naive Drell-Yan model is not altered substantially at  $O(\alpha_s^2)$  in QCD owing to a fortuitous cancellation of colour factors for the  $q\bar{q}$  annihilation process. The competing QCD Compton process would have a colour factor  $2N_c$  in place of that of eq. (9.2.6) which might compensate the valence suppression of this channel, however it is unlikely to alter the asymmetry by more than a few  $\alpha_s\%$ .

References to chapter 9

- [1] B. Pire and J.P. Ralston
- [2] J.C. Collins and D.A. Soper, Phys. Rev. D16, 2219 (1977).  
J.P. Ralston and D.A. Soper, Nucl. Phys. B152, 109 (1979).

## APPENDIX A1

### Colour gauge group algebra

The algebra of the colour gauge group,  $SU(3)_{col}$ , is defined by the structure constants  $f^{abc}$  of the group which fix the commutation relations of its representations.

$$[\tau^a, \tau^b]_{ij} = i f^{abc} \tau^c_{ij} . \quad (A1.1)$$

For the fermion (regular) representation of the group the matrices  $\tau^a$  are just the usual Gell-Mann 3x3 matrices ( $a = 1, \dots, 8$ ). However for generality the following formulae are given for the group  $SU(N)$ , whence the fermion representation consists of  $(N^2 - 1)$   $N \times N$  matrices. The element of the group will be represented by the indices  $a, b, \dots, e$  running over  $1, \dots, (N^2 - 1)$ , while the suffices  $i, j, \dots, n$  running over  $1, \dots, N$  will indicate the matrix element in the representation. Thus we have for summation over repeated indices (always assumed):

$$\delta^{aa} = N^2 - 1 , \quad (A1.2)$$

$$\delta_{ii} = N . \quad (A1.3)$$

The fermion representation matrices then obey the following relation:

$$\tau^a_{ij} \tau^a_{kl} = \frac{1}{2} (\delta_{il} \delta_{jk} - \frac{1}{N} \delta_{ij} \delta_{kl}) . \quad (A1.4)$$

The following equations define the Casimirs or invariants of the group representation:

$$\tau_{ij}^a \tau_{jk}^a = C_2(R) \delta_{ik} \quad , \quad (\text{A1.5})$$

$$\tau_{ij}^a \tau_{jk}^b = T(R) \delta^{ab} \quad . \quad (\text{A1.6})$$

For SU(N) these two Casimirs are given by:

$$C_2(R) = (N^2 - 1) / 2N \quad , \quad (\text{A1.7})$$

$$T(R) = \frac{1}{2} \quad (\text{for each fermion type}) \quad . \quad (\text{A1.8})$$

The following set of traces are useful in evaluating various matrix elements involving particles in the fermion representation:

$$T_2(R) = \text{tr}[\tau^a \tau^a] = \frac{1}{2} (N^2 - 1) \quad , \quad (\text{A1.9})$$

$$T_4(R) = \text{tr}[\tau^a \tau^a \tau^b \tau^b] = (N^2 - 1)^2 / 4N \quad , \quad (\text{A1.10})$$

$$T_4'(R) = \text{tr}[\tau^a \tau^b \tau^a \tau^b] = -(N^2 - 1) / 4N \quad , \quad (\text{A1.11})$$

$$T_{22}(R) = \text{tr}[\tau^a \tau^b] \text{tr}[\tau^a \tau^b] = \frac{1}{4} (N^2 - 1) \quad . \quad (\text{A1.12})$$

The totally antisymmetric structure constants  $f^{abc}$  also satisfy the commutation relations: define a matrix representation  $(F^a)_{bc}$  by

$$(F^a)_{bc} = -i f^{abc} \quad , \quad (\text{A1.13})$$

and one can rewrite the Bianchi identities in the following form,

$$[F^a, F^b] = i f^{abc} F^c \quad . \quad (\text{A1.14})$$

Now one has the Casimir  $C_2(A) = N$  defined by

$$\text{tr} [F^a \cdot F^b] = C_2(A) \delta^{ab} , \quad (\text{A1.15})$$

and the following set of traces:

$$T_2(A) = \text{tr} [F^a F^a] = N(N^2 - 1) , \quad (\text{A1.16})$$

$$T_4(A) = \text{tr} [F^a F^a F^b F^b] = N^2(N^2 - 1) , \quad (\text{A1.17})$$

$$T'_4(A) = \text{tr} [F^a F^b F^a F^b] = \frac{1}{2} N^2(N^2 - 1) , \quad (\text{A1.18})$$

$$T_{22}(A) = \text{tr} [F^a F^b] \text{tr} [F^a F^b] = N^2(N^2 - 1) . \quad (\text{A1.19})$$

The commutation relations (A1.1) may be expressed in diagrammatic form as

$$\text{Diagrammatic equation (A1.20)} \quad (\text{A1.20})$$

This allows the colour factor multiplying, for example, the s-channel amplitude shown here to be expressed in terms of those for the t- and u-channels. This in turn permits the full amplitude to be expressed in a very compact form.

Similarly one can decompose the s-channel colour factor for four-gluon scattering into its t- and u-channel components according to:

Diagram (A1.21) shows a four-gluon vertex on the left, which is equal to the difference between two diagrams on the right. The first diagram on the right is a box diagram with a vertical internal gluon line. The second diagram on the right is a box diagram with a vertical internal gluon line and a four-gluon vertex on the right side.

$$\text{Four-gluon vertex} = \text{Box diagram} - \text{Box diagram with vertex} \quad (A1.21)$$

Finally the colour factor for the four-gluon vertex is automatically given in terms of those for the s-, t- and u-channels according to

Diagram (A1.22) shows a four-gluon vertex on the left, which is equal to the sum of three diagrams on the right. The first diagram on the right is a four-gluon vertex. The second diagram on the right is a box diagram with a vertical internal gluon line. The third diagram on the right is a box diagram with a vertical internal gluon line and a four-gluon vertex on the right side.

$$\text{Four-gluon vertex} = \text{Four-gluon vertex} + \text{Box diagram} + \text{Box diagram with vertex} \quad (A1.22)$$

each term on the right-hand side here has however, its own separate kinematical factor.

A more complete set of identities may be found in appendix B of ref[1].

## APPENIDX A2

### Dirac spinor and spin projector identities

In this appendix a list is given of useful formulae and identities applicable to calculations of hard scattering cross-sections where masses may be neglected. It is convenient to begin with the spin projector for external (massless) gauge particles as this will be adopted for identities involving spinors.

For the following discussion it will be useful to consider a particular reference frame, the final results being written in Lorentz covariant form will however be independent of the frame chosen. Consider a gauge particle (photon or gluon) with four-momentum  $q^\mu$  ( $q^2 = 0$ ) then we adopt the frame in which the components of  $q$  are given by:

$$q^\mu \propto (1, 0, 0, 1) . \quad (\text{A2.1})$$

The spin projector  $\xi^\mu(q, \lambda)$  for the state with helicity  $\lambda$  obeys the following conditions:

$$\xi^2 = 0 , \quad (\text{A2.2})$$

$$q \cdot \xi = 0 . \quad (\text{A2.3})$$

In order to fix the gauge one further condition is required and this is usually chosen to be:

$$\eta \cdot \xi = 0 , \quad (\text{A2.4})$$

where the light-like vector is



$$\eta^\mu = (1, 0, 0, -1) . \quad (\text{A2.5})$$

The spin projector must then necessarily be of the form:

$$\xi^\mu = \frac{1}{\sqrt{2}} (0, -\lambda, i, 0) , \quad (\text{A2.6})$$

where the factor  $\frac{1}{\sqrt{2}}$  is for normalisation purposes. One can then construct in a straightforward manner a covariant form for  $\xi^\mu$  by making use of one other arbitrary light-like vector  $\eta'^\mu$ , and we have eqn. (1.4.10) [2]:

$$\begin{aligned} \xi^\mu(q, \lambda; \eta, \eta') &= \frac{1}{2} [\eta \cdot \eta' q^\mu + q \cdot \eta' \eta^\mu - q \cdot \eta \eta'^\mu \\ &\quad + i \lambda \epsilon^{\mu\rho\sigma\kappa} q_\rho \eta_\sigma \eta'_\kappa] / \sqrt{(\eta \cdot \eta' q \cdot \eta q \cdot \eta')} . \end{aligned} \quad (\text{A2.7})$$

As defined  $\xi^\mu$  automatically satisfies certain symmetry conditions (parity and charge conjugation):

$$\begin{aligned} \xi^{\mu*}(q, \lambda; \eta, \eta') &= \xi^\mu(q, -\lambda; \eta, \eta') \\ &= \xi^\mu(\eta, \lambda; q, \eta') . \end{aligned} \quad (\text{A2.8})$$

Contracting this expression with  $\gamma_\mu$  and applying the well-known Chisholm identity [3]:

$$\gamma^\mu \gamma^\nu \gamma^\kappa = g^{\mu\nu} \gamma^\kappa - g^{\mu\kappa} \gamma^\nu + g^{\nu\kappa} \gamma^\mu + i \epsilon^{\mu\nu\kappa\rho} \gamma_5 \gamma_\rho , \quad (\text{A2.9})$$

one obtains

$$\begin{aligned} \not{q} &= \frac{1}{4} \left[ \not{\eta} \not{\eta}' \not{q} (1 + \lambda \gamma_5) + \not{q} \not{\eta}' \not{\eta} (1 - \lambda \gamma_5) \right] \\ &\quad \times (\eta \cdot \eta' q \cdot \eta q \cdot \eta')^{-\frac{1}{2}}. \end{aligned} \quad (\text{A2.10})$$

For a spin- $\frac{1}{2}$  particle moving in the z-direction the Dirac spinors may be written in the form:

$$u = \begin{pmatrix} \sqrt{E+m} \chi \\ \sqrt{E-m} \sigma_3 \chi \end{pmatrix} \quad \text{and} \quad v = \begin{pmatrix} \sqrt{E-m} \sigma_3 \chi \\ \sqrt{E+m} \chi \end{pmatrix}, \quad (\text{A2.11})$$

where  $E$  and  $m$  are the energy and mass and  $\chi$  is a two component spinor:  $\begin{pmatrix} 1 \\ 0 \end{pmatrix}$  for positive helicity and  $\begin{pmatrix} 0 \\ 1 \end{pmatrix}$  for negative. By considering the spinors for particles moving in the negative Z-direction, then one finds that the current  $\bar{u}_1 \gamma^\mu u_2$ , with  $u_1$  ( $\bar{u}_2$ ) moving in the positive (negative) Z-directions, is proportional to the expression on the right-hand side of equation (A2.6). Squaring up the current and this expression it is a straightforward matter to extract the normalisation factor and one obtains:

$$\bar{u}(p_2, h_2) \gamma^\mu u(p_1, h_1) = 2 \sqrt{p_1 \cdot p_2} \xi^\mu(p_1, h_1; p_2, \eta) \delta_{h_1 h_2} \quad (\text{A2.12})$$

In using this identity care is needed to use the same vector  $\eta$  in different amplitudes contributing to the same process (for example as in sections 3.2(a) and (b)), since although the cross-section is naturally independent of  $\eta$  the individual amplitudes are not. For larger (odd) numbers of matrices one uses the Chisholm identity (A2.8) to reduce the product to one matrix, with a possible  $\gamma_5$  which may be removed by using  $\gamma_5 u(p_1, h_1) = h_1 u(p_1, h_1)$ . The corresponding identities for currents involving antispinors are easily obtained for (A2.12)

by noting that one can always choose a basis in which  $v(p,h) = u(p, -h)$  etc.

Since in the chapter on supersymmetry it is necessary to consider scalar couplings which give rise to strings with an even number of matrices it will be useful to have similar simple identities for  $\bar{u}_2 u_1$  and  $\bar{u}_2 \sigma^{\mu\nu} u_1$ . The first of these is obtained immediately since the only scalar quantity available is  $p_1 \cdot p_2$  and squaring the expression gives the following identity:

$$\bar{u}(p_2, h_2) u(p_1, h_1) = \sqrt{p_1 \cdot p_2} \delta_{h_1 h_2} \quad . \quad (A2.13)$$

Notice now helicity is flipped rather than conserved. The second of the even matrix expressions also has to be a spin-flip amplitude and thus multiplying by (A2.13) and using the standard trace trick one readily obtains:

$$\bar{u}(p_2, h_2) \sigma^{\mu\nu} u(p_1, h_1) = \frac{i\sqrt{2}}{\sqrt{p_1 \cdot p_2}} \left[ p_2^\mu p_1^\nu - p_1^\nu p_2^\mu + i h_1 \epsilon^{\mu\nu\sigma\kappa} \frac{p_{1\sigma} p_{2\kappa}}{p_1 \cdot p_2} \right] \delta_{h_1 \bar{h}_2} \quad (A2.14)$$

where the definition of  $\sigma^{\mu\nu}$  is, as usual:

$$\sigma^{\mu\nu} = \frac{i}{2} [\gamma^\mu, \gamma^\nu] \quad . \quad (A2.15)$$

To conclude this appendix on simplifying techniques for Dirac spinor algebra, it should be pointed out that while these identities simplify quite considerably the evaluation of amplitudes involving one or two fermion lines with few matrices (and indeed the evaluation of the  $m$  terms of the amplitude as opposed to the  $m^2$  of the full cross-section), once the number of fermion lines and exchanges increases to five or six (as in the Born approximation for exclusive meson-nucleon or nucleon-nucleon scattering ref. [4]) then the large numbers of terms generated by repeated use of the Chisholm identity and the

and the large numbers of Feynman diagrams ( $10^4 - 10^5$ ) renders such calculations effectively impossible.

Recently however, a new and more powerful technique has been developed [5] to permit calculations to be performed for such processes as those mentioned above. The method is based on a reduced  $2 \times 2$  representation in which spinors are written in two component form:

$$\psi = \begin{pmatrix} \psi_+ \\ \psi_- \end{pmatrix}, \quad (\text{A2.16})$$

taking advantage of the Weyl representation of the Dirac matrices in terms of the  $2 \times 2$  Pauli matrices:

$$\gamma_5 = \begin{pmatrix} 1 & 0 \\ 0 & -1 \end{pmatrix}, \quad \gamma_0 = \begin{pmatrix} 0 & 1 \\ 1 & 0 \end{pmatrix}, \quad \gamma^i = \begin{pmatrix} 0 & \sigma^i \\ -\sigma^i & 0 \end{pmatrix}. \quad (\text{A2.17})$$

Defining  $\gamma_{\pm}^{\mu}$  and  $\not{p}_{\pm}$  by

$$\gamma^{\mu} = \begin{pmatrix} 0 & \gamma_{+}^{\mu} \\ \gamma_{-}^{\mu} & 0 \end{pmatrix} \quad \text{and} \quad \not{p} = \begin{pmatrix} 0 & \not{p}_{+} \\ \not{p}_{-} & 0 \end{pmatrix}, \quad (\text{A2.18})$$

a string of the form:

$$\bar{\psi}_f \gamma^{\mu_1} \not{p}_a \gamma^{\mu_2} \not{p}_b \dots \gamma^{\mu_n} \left( \frac{1 \pm \gamma_5}{2} \right) \psi_i, \quad (\text{A2.19})$$

becomes:

$$\psi_{f\pm}^{\dagger} \gamma_{\mp}^{\mu_1} \not{p}_{a\pm} \gamma_{\mp}^{\mu_2} \not{p}_{b\pm} \dots \gamma_{\mp}^{\mu_n} \psi_{i\pm}, \quad (\text{A2.20})$$

for an odd number of gamma-matrices and for an even number:

$$\psi_{f\mp}^{\dagger} \gamma_{\pm}^{\mu_1} \not{p}_{a\mp} \gamma_{\pm}^{\mu_2} \not{p}_{b\mp} \dots \gamma_{\pm}^{\mu_n} \psi_{i\mp}. \quad (\text{A2.21})$$

The reduction of such a string to one or two matrices is accomplished by use of the very simple Fierz identity:

$$\begin{aligned} (\gamma_{\mu+})_{ij} (\gamma_{-}^{\mu})_{kl} &= 2 \delta_{il} \delta_{jk} , \\ (\gamma_{\mu\pm})_{ij} (\gamma_{\pm}^{\mu})_{kl} &= 2 (\delta_{ij} \delta_{kl} - \delta_{il} \delta_{jk}) , \end{aligned} \quad (\text{A2.22})$$

where in the second expression summation over the two components  $\pm$  is understood.

Any two component spinor  $u_i$  can be written as a linear combination of

$$|s_0\rangle = \begin{pmatrix} 0 \\ 1 \end{pmatrix} \quad \text{and} \quad |s_{\pm}\rangle = \begin{pmatrix} 1 \\ 0 \end{pmatrix} , \quad (\text{A2.23})$$

and similarly  $\not{x}$  can be written as a linear combination of  $|s_0\rangle \langle s_0|$  etc. Thus after reduction via the Fierz identity the resulting strings are readily evaluated in terms of overlaps.

This technique was used by the authors of ref [5] to evaluate some 35,640 diagrams contributing to exclusive nucleon-nucleon scattering (i.e. six fermion lines exchanging five gluons) in less than one hour on a VAX.

## APPENDIX A3

### Dimensional regularisation and D dimensional integrals

The method of dimensional regularisation [6] has been described in many texts [7], thus here only a brief motivation for and explanation of its use will be given followed by a list of useful formulae for typical D-dimensional integrals encountered in evaluating Feynman diagrams containing loops.

A typical loop integral to be performed after simplification by various tricks such as Feynman parameterisation of numerators, shifting of loop momenta, symmetric integration etc., is of the form (when Wick rotated into Euclidean space):

$$(\mu^2)^{2-D/2} \int \frac{d^D k (k^2)^r}{(k^2 + M^2)^s} = \frac{(\mu^2)^{2-D/2}}{(4\pi)^{D/2}} \frac{\Gamma(r+D/2) \Gamma(s-r-D/2)}{\Gamma(D/2) \Gamma(s) (M^2)^{s-r-D/2}} \quad (\text{A3.1})$$

where  $M^2$  is in general a function of particle masses and external momenta, the term  $(\mu^2)^{2-D/2}$  with  $\mu$  of dimension  $[\text{mass}]^1$  ensures the coupling constant remains dimensionless and  $d^D k = d^D k / (2\pi)^D$ . Now the function  $\Gamma(n+1) = n!$  has poles for  $n$  a negative integer thus for  $r \geq s - D/2$  and  $D = 4$  the above integral is (ultra-violet) singular. However setting  $D = 4 - 2\epsilon$  renders the expression finite and performing a Laurent expansion in  $\epsilon$  permits the isolation of the singularity in the form of a  $1/\epsilon$  pole.

Notice also that for  $s > r + D/2$  the vanishing of  $M^2$  will also induce a singularity. In general  $M^2$  contains Feynman parameters over which an integration must be performed and the singularity (of the infra-red type) appears again as a gamma function pole. Thus the dimensional regularisation scheme also removes the I.R. singularities, but care must be taken in renormalisation not to confuse the two; only U.V. singularities contribute to the renormalisation constant whereas the various I.R. singularity cancellation theorems guarantee the disappearance of these under certain conditions.

By way of an example let us consider the following integral (again in Euclidean space):

$$I = (\mu^2)^{2-D/2} \int \frac{d^D k}{(k^2 + M^2)^2} = \frac{1}{(4\pi)^2} \left( \frac{4\pi\mu}{M^2} \right)^\epsilon \Gamma(\epsilon) . \quad (\text{A3.2})$$

Now the expansion of  $\Gamma(\epsilon)$  near  $\epsilon = 0$  is given by

$$\begin{aligned} \Gamma(\epsilon) &= \frac{1}{\epsilon} \Gamma(1+\epsilon) \\ &= \frac{1}{\epsilon} - \gamma_E + O(\epsilon) \end{aligned} \quad (\text{A3.3})$$

where  $\gamma_E$ , coming from the expansion of  $\Gamma(1+\epsilon)$ , is the Euler gamma  $\gamma_E = 0.5772 \dots$ . Thus one obtains, on expanding the term  $(4\pi\mu^2/M^2)^\epsilon$  :

$$I = \frac{1}{(4\pi)^2} \left[ \frac{1}{\epsilon} + \ln 4\pi - \gamma_E + \ln \frac{\mu^2}{M^2} + O(\epsilon) \right] . \quad (\text{A3.4})$$

The origin of the  $\ln 4\pi - \gamma_E$  is now clear and the modification of the measure (1.4.12) leads to the following in place of (A3.1):

$$\int \frac{[dk] (k^2)^r}{(k^2 + M^2)^s} = \frac{1}{(4\pi)^2} \left( \frac{\mu^2}{M^2} \right)^\epsilon \frac{\Gamma(r+D/2) \Gamma(s-r-D/2)}{\Gamma(D/2) \Gamma(s) \Gamma(3-D/2)} (M^2)^{r+2-s} \quad (\text{A3.5})$$

where the  $(\mu^2)^\epsilon$  has been absorbed into the definition of  $[dk]$ . This is now valid for the  $\overline{\text{MS}}$  scheme [8] up to one loop (in higher loops more complicated constant terms arise).

The expression (A3.5) has also been extended to the case where the axial gauge is adopted and one has numerators of the type  $\eta \cdot k$  [9]. One simplified form is then (in Minkowski space):

$$\int \frac{d^D k}{(k^2 - M^2)^s (k \cdot \eta)^a} = (-1)^{s+a} i \pi^{(D+1)/2} \frac{(M^2)^{D/2 - s - a/2}}{(\eta^2)^{a/2}} \frac{\Gamma(s + a/2 - D/2)}{\Gamma(s) \Gamma((a+1)/2)} \quad (A3.6)$$

More complicated integrals are given in [9] in terms of hypergeometric functions.

In general, before arriving at the form of the integral given above, the integrand contains a number of factors  $k^\alpha$  with indices uncontracted these are reduced to products of  $g^{\alpha\beta}$  and  $(k^2)^r$  by use of the symmetric integration formula:

$$\begin{aligned} I_{(r)}^{\mu_1 \mu_2 \dots \mu_{2r}} &= \int d^D k f(k^2) k^{\mu_1} k^{\mu_2} \dots k^{\mu_{2r}} \\ &\triangleq \frac{\int d^D k f(k^2) (k^2)^r (\sum g^{\mu_1 \mu_2} g^{\mu_3 \mu_4} \dots g^{\mu_{2r-1} \mu_{2r}})}{D(D+2) \dots (D+2r-2)}, \end{aligned} \quad (A3.7)$$

where the sum is over all distinct permutation of the indices  $\mu_1 \mu_2 \dots \mu_{2r}$ . For an odd product of  $k^\alpha$  (i.e.  $k^{\mu_1} k^{\mu_2} \dots k^{\mu_{2r-1}}$ ) the integral is clearly zero. In four dimensions the denominator  $D(D+2) \dots (D+2r-2)$  reduces to  $(r+1)! 2^r$ .

The identity (A3.6) is straightforward to derive: denote

$$G_{(r)}^{\mu_1 \mu_2 \dots \mu_{2r}} = \sum_{\text{perms}} g^{\mu_1 \mu_2} g^{\mu_3 \mu_4} \dots g^{\mu_{2r-1} \mu_{2r}} \quad (A3.8)$$

Then the following identity is trivial by inspection,

$$g_{\mu_1 \mu_2} G_{(r)}^{\mu_1 \mu_2 \dots \mu_{2r}} = (D+2r-2) G_{(r-1)}^{\mu_3 \mu_4 \dots \mu_{2r}} \quad (A3.9)$$

Now

$$\begin{aligned} I_{(r)}^{\mu_1 \mu_2 \dots \mu_{2r}} g_{\mu_1 \mu_2} &= \int d^D k f(k^2) k^2 k^{\mu_3} k^{\mu_4} \dots k^{\mu_{2r}} \\ &= k^2 I_{(r-1)}^{\mu_3 \mu_4 \dots \mu_{2r}} \end{aligned} \quad (A3.10)$$



Clearly  $I_{(r)}^{\mu_1 \mu_2 \dots \mu_{2r}}$  is proportional to  $(k^2)^r G_{(r)}^{\mu_1 \mu_2 \dots \mu_{2r}}$  by symmetry. Therefore writing

$$I_{(r)}^{\mu_1 \dots \mu_{2r}} = N_{(r)} d^D k f(k^2) (k^2)^r G_{(r)}^{\mu_1 \dots \mu_{2r}}, \quad (\text{A3.11})$$

contracting with  $g_{\mu_1 \mu_2}$ , applying (A3.8) and (A3.9) gives

$$N_{(r-1)} = N_{(r)} (D + 2r - 2), \quad (\text{A3.12})$$

hence (A3.6).

In chapter 7 use is made of the following expression for angle independent integrands, in particular for finite (although this is not necessary) integrals:

$$\int d^D k = \frac{\pi^{D/2}}{\Gamma(D/2)} \int k^{D-2} dk^2. \quad (\text{A3.13})$$

The above is in the MS scheme with the modification to  $\overline{\text{MS}}$  as already described.

The expansions for the Euler gamma and beta functions around integer values are as follows:

$$\Gamma(n+\epsilon) = \Gamma(n) \left[ 1 + \epsilon (S_n - \gamma_E) + O(\epsilon^2) \right], \quad (\text{A3.14})$$

$$B(m+\epsilon, n+\epsilon) = B(m, n) \left[ 1 + \epsilon (S_m + S_n - S_{m+n}) + O(\epsilon^2) \right], \quad (\text{A3.15})$$

where  $S_n = \sum_{j=1}^{n-1} 1/j$  and  $B(n, m) = \Gamma(n)\Gamma(m)/\Gamma(n+m)$ . The Euler beta function occurs frequently from the Feynman parameter integrals since

$$\int_0^1 x^{m-1} (1-x)^n dx = B(m, n). \quad (\text{A3.16})$$

For two denominators the Feynman integral is [10]

$$a^{-m} b^{-n} = B(m,n)^{-1} \int_0^1 dx x^{m-1} (1-x)^{n-1} [ax + b(1-x)]^{-(m+n)}, \quad (\text{A3.17})$$

which generalises to

$$\prod_{i=1}^m a_i^{-n_i} = \frac{\Gamma(\sum_1^m n_i)}{\prod_1^m (\Gamma n_i)} \int_0^1 \frac{\prod_1^m (dx_i x_i^{n_i-1}) \delta(1 - \sum_1^m x_i)}{[\sum_1^m a_i x_i]^{\sum_1^m n_i}}. \quad (\text{A3.18})$$

A much discussed problem in dimensional regularisation is the treatment of  $\gamma_5$  (or equivalently  $\epsilon_{\mu\nu\rho\sigma}$ ) in a non-integer number of dimensions [11, 12]. This problem is intimately connected with the axial vector anomalies of which the Adler-Bell-Jackiw anomaly is a particular case. Thus, as pointed out in reference [12] the choice of which Ward identities clash (dictated by physical circumstances) is essentially equivalent to a choice of definition of  $\gamma_5$ .

In the literature there are essentially two different prescriptions for dealing with the  $\gamma_5$  in D (non-integer) dimensions. The first due to 't Hooft and Veltman [6] is given by

$$\gamma_5 = i \gamma^0 \gamma^1 \gamma^2 \gamma^3, \quad (\text{A3.19})$$

with the following properties

$$\begin{aligned} \gamma_5^2 &= 1, \\ \{\gamma_5, \gamma^\mu\} &= 0 : \mu = 0, 1, 2, 3, \\ [\gamma_5, \gamma^\mu] &= 0 : \mu = 4, \dots, D-1 \end{aligned} \quad (\text{A3.20})$$

Other methods/equivalent to this can be found in reference [11]. This prescription although well defined requires the inclusion of extra counter terms to

cancel the spurious anomalies introduced into Ward identities which are really free of essential anomalies.

A second prescription [12] consists in a mathematically ill-defined  $\gamma_5$  whose properties alone are fixed according to

$$\begin{aligned} \gamma_5^2 &= 1, \\ \{\gamma_5, \gamma^\mu\} &= 0 \quad : \quad \mu = 0, 1, \dots, D-1 \end{aligned} \quad (\text{A3.21})$$

It is clear that this prescription will automatically satisfy the relevant Ward identities for loops with an even number of  $\gamma_5$  matrices. The canonical Ward identities are derived by formal manipulations which of course assume the naïve Dirac algebra including  $\{\gamma_5, \gamma^\mu\} = 0$ . For loops with odd numbers of  $\gamma_5$  matrices, precisely the case of the ABJ anomaly, this prescription leads to a polynomial ambiguity, that of the ABJ anomaly.

To see how this arises consider the trace  $\text{Tr}(\gamma_5 \gamma^\mu \gamma^\nu \gamma^\rho \gamma^\sigma \gamma_\alpha \gamma^\alpha)$  using the prescription of (A3.21), one obtains

$$\text{tr}(\gamma_5 \gamma^\mu \gamma^\nu \gamma^\rho \gamma^\sigma \gamma_\alpha \gamma^\alpha) = 4i D \epsilon^{\mu\nu\rho\sigma}, \quad (\text{A3.22})$$

unless one anticommutes one of the  $\gamma_\alpha$  past the other  $\gamma$ -matrices after which one obtains

$$\text{tr}(\gamma_5 \gamma^\mu \gamma^\nu \gamma^\rho \gamma^\sigma \gamma_\alpha \gamma^\alpha) = 4i(8-D) \epsilon^{\mu\nu\rho\sigma}. \quad (\text{A3.23})$$

The two results only agree for  $D = 4$ . Following [12] one can accept this ambiguity and define the trace to be

$$\text{tr}(\gamma_5 \gamma^\mu \gamma^\nu \gamma^\rho \gamma^\sigma \gamma_\alpha \gamma^\alpha) = 4i [D + 2b(4-D)] \epsilon^{\mu\nu\rho\sigma}, \quad (\text{A3.24})$$

where  $b$  is an arbitrary parameter to be fixed in any particular case by appealing to the relevant anomaly.

In chapter 5 where the constant terms (in part resulting from  $1/\epsilon$  pole multiplying an  $O(\epsilon)$  term) are important this method is adopted in evaluation of traces involving  $\gamma_5$ . There the problem also involves the use of  $\epsilon^{\mu\nu\rho\sigma}$  to project out the required Lorentz structures. One could of course avoid this problem entirely by use of the Chisholm identity (A2.9) in reverse to eliminate the presence of the external  $\epsilon$ -tensor. However the resulting expressions would be more complex to deal with and the final answer would be identical. Thus in the spirit of (and consistent with) [12] let us define the following contraction of  $\epsilon$ -tensors:

$$\epsilon^{\mu\nu\rho\sigma} \epsilon_{\mu\nu\lambda\kappa} = 2! (1 + a\epsilon) (\delta_{\kappa}^{\rho} \delta_{\lambda}^{\sigma} - \delta_{\lambda}^{\rho} \delta_{\kappa}^{\sigma}), \quad (\text{A3.25})$$

where, as before,  $a$  represents the ambiguity.

It is particularly convenient to adopt the method of dimensional reduction whereby traces are computed in 4 dimensions with external indices uncontracted. The latter are then contracted (after suitable rearrangement into standard tensor forms) with  $D$ -dimensional spin projectors. This is in some sense the converse of the procedure described above but is entirely equivalent. The point is that the same ambiguity  $a\epsilon$  occurs for both the deep-inelastic and Drell-Yan processes and (as is shown explicitly in Chapter 5) cancels from the final expression.

A note of warning however in connection with the expression resulting from the traces: the ambiguity manifests itself in the case of the  $\epsilon$ -tensor though the identity

$$\epsilon^{\mu\nu\rho\sigma} g^{\lambda\kappa} = \epsilon^{\mu\nu\rho\lambda} g^{\sigma\kappa} + \epsilon^{\mu\nu\lambda\sigma} g^{\rho\kappa} + \epsilon^{\mu\lambda\rho\sigma} g^{\nu\kappa} + \epsilon^{\lambda\nu\rho\sigma} g^{\mu\kappa}, \quad (\text{A3.26})$$

which when contracted with  $g_{\lambda\kappa}$  in  $D$  dimensions leads to a discrepancy of  $O(\epsilon)$ . Using a programme such as Schoonschip it is straightforward via this

identity to ensure all resulting expressions take the desired tensor form before contraction of the external indices.

APPENDIX A4

Parton distribution parameterisation and  $Q^2$ -evolution

For the purposes of discussion the following starting parton distributions for the proton [14] taken from the data for  $Q_0^2 = 1.8 \text{ GeV}^2$  [15] have been used. For the valence quarks

$$x u_v(x) + x d_v(x) = \frac{3}{B(\eta_1, 1+\eta_2)} x^{\eta_1} (1-x)^{\eta_2} , \quad (\text{A.4.1})$$

$$x d_v(x) = \frac{1}{B(\eta_3, 1+\eta_4)} x^{\eta_3} (1-x)^{\eta_4} .$$

The appearance of the beta function is necessary to satisfy the sum rule for the valence content of the proton:

$$\langle u_v(x) \rangle = 2 \quad (\text{A.4.2})$$

$$\langle d_v(x) \rangle = 1$$

Fits with the data given

$$\eta_1 = 0.7 \quad , \quad \eta_2 = 2.6 \quad (\text{A.4.3})$$

$$\eta_3 = 0.85 \quad , \quad \eta_4 = 3.35$$

The momentum fraction carried by the valence quarks is then

$$\langle x u_v \rangle + \langle x d_v \rangle \approx 0.488 . \quad (\text{A.4.4})$$

For the sea and gluon distributions the following have been used:

$$\begin{aligned}
 x s(x) &= 0.1467 (1-x)^7 : \text{SU}(3) \text{ symmetric,} \\
 x c(x) &= 0 \\
 x g(x) &= 2.412 (1-x)^5
 \end{aligned}
 \tag{A4.5}$$

where  $s(x)$  is the charmed sea contribution. Writing the total sea contribution as  $\Sigma(x) = 6 s(x) + 2 c(x)$  one has the following for the momentum fraction of the proton attributed to the sea and gluon content.

$$\begin{aligned}
 \langle x \Sigma \rangle &\approx 0.11 , \\
 \langle x g \rangle &\approx 0.402 .
 \end{aligned}
 \tag{A4.6}$$

Except in the comparisons for different models a slightly modified version of the Carlitz-Kaur distributions has been used in which the sea is permitted to carry some helicity. Thus for the valence distributions:

$$\begin{aligned}
 \Delta u_v(x) &= (u_v(x) - \frac{2}{3} d_v(x)) \cos(2\theta) , \\
 \Delta d_v(x) &= -\frac{1}{3} d_v(x) \cos(2\theta) ,
 \end{aligned}
 \tag{A4.7}$$

with the depletion factor:

$$\cos(2\theta) = [1 + 0.052 (1-x)^2 / 1x]^{-1} .
 \tag{A4.8}$$

Using the simple parameterisation based on a bremsstrahlung picture described in section 3.4(a) the following estimates for the non-valence spin content of the proton.

$$\begin{aligned}
\Delta s(x) &= 0.0158 (1-x)^7 (2-x), \\
\Delta c(x) &= 0, \\
\Delta g(x) &= 0.267 (1-x)^5 (2-x).
\end{aligned}
\tag{A4.9}$$

The normalisation is fixed by the  $\langle J_Z \rangle$  sum rule (3.4.3), with  $\langle L_Z \rangle = 0$ .

The above distributions are all valid for  $Q_0^2 = 1.8 \text{ GeV}^2$ , for other values of  $Q^2$  they must be evolved according to the Altarelli-Parisi master equations (2.2.9). As already remarked in section 2.2 it is a fairly straightforward matter to integrate these numerically. In ref 14 the spin-averaged distributions were parameterised by writing  $\eta_1 = \eta_1 + \eta_1' \bar{s}$  etc. in equations A4.1 (and similarly for the sea and gluon densities), where  $\bar{s} = \ln [\ln(Q^2/\Lambda^2) - \ln(Q_0^2/\Lambda^2)]$ . The  $\eta_i'$  being obtained by fitting the moments (known precisely for all  $Q^2$  via eqn. (2.1.18) and its singlet extension) for various  $\bar{s}$ . This gives a parameterisation good to within 2% for a large range of  $x$  and for values of  $\bar{s}$  up to about 1.4. However even for  $\Lambda = 0.3$  this falls short of the collider energies ( $E_{\text{cm}} = 540 \text{ GeV}$ ) and in any case no such parameterisation has been performed for the corresponding spin-dependent distributions.

In order to integrate eqns. (2.2.9) it is convenient to rewrite them in terms of  $\bar{s}$  by noting that

$$\begin{aligned}
\frac{d}{dt} &= -\frac{\beta_0}{4\pi} \alpha_s^2(t) \frac{d}{d\alpha_s(t)} \\
&= \frac{\beta_0}{4\pi} \alpha_s(t) \frac{d}{d\bar{s}}.
\end{aligned}
\tag{A4.10}$$

The + regularisation of the singular kernels is best handled by integration by parts which gives



$$\int_x^1 dy \frac{f(y)}{(1-y)_+} = \ln(1-x) f(x) + \int_x^1 \frac{dy}{y} \frac{x}{y} \left[ \frac{\frac{x}{y} f(y) - f(x)}{1 - \frac{x}{y}} \right]. \quad (\text{A4.11})$$

The Altarelli-Parisi equations in the non-singlet sector can thus be written as

$$\begin{aligned} \frac{d}{d\bar{s}} [x q_i^{\text{val}}(x, \bar{s})] &= \frac{2}{\beta_0} \left\{ 2 [x q_i^{\text{val}}(x, \bar{s})] + \frac{4}{3} \int_x^1 \frac{dy}{y} \frac{x}{y} \left(1 - \frac{x}{y}\right) [y q_i^{\text{val}}(y, \bar{s})] \right. \\ &\quad \left. + \frac{8}{3} Z_p [x q_i^{\text{val}}(x, \bar{s})] \right\}, \end{aligned} \quad (\text{A4.12})$$

with an identical equation for  $x \Delta q_i^{\text{val}}(x, \bar{s})$  and where  $Z_p$  is defined by

$$Z_p [f(x)] = \int_x^1 dy \frac{f(y)}{(1-y)_+}. \quad (\text{A4.13})$$

The equations for the other densities can be found in ref. [13], with the substitutions  $6/27 \rightarrow 2/\beta_0$ ,  $6/27$  is the value for three quark flavours while for four it becomes  $6/25$ .

Using the above method and a numerical technique similar to that described in [13] the distribution were evolved up to  $\bar{s} = 1.5$ . For  $\Lambda = 0.2(0.5)$  GeV and  $Q_0^2 = 1.8$  GeV<sup>2</sup> this corresponds to  $Q \approx 10^3(42)$  GeV. The distributions are shown in Figs. A4.1 and .2 (note the differing scales). Since the shapes change very little one sees that the effects of  $Q^2$  evolution on asymmetries will in general be only slight. Moreover from Fig. A4.2 one sees that inclusion of spin-dependent sea distributions is of very marginal importance; in general, processes are not particularly sensitive to these.

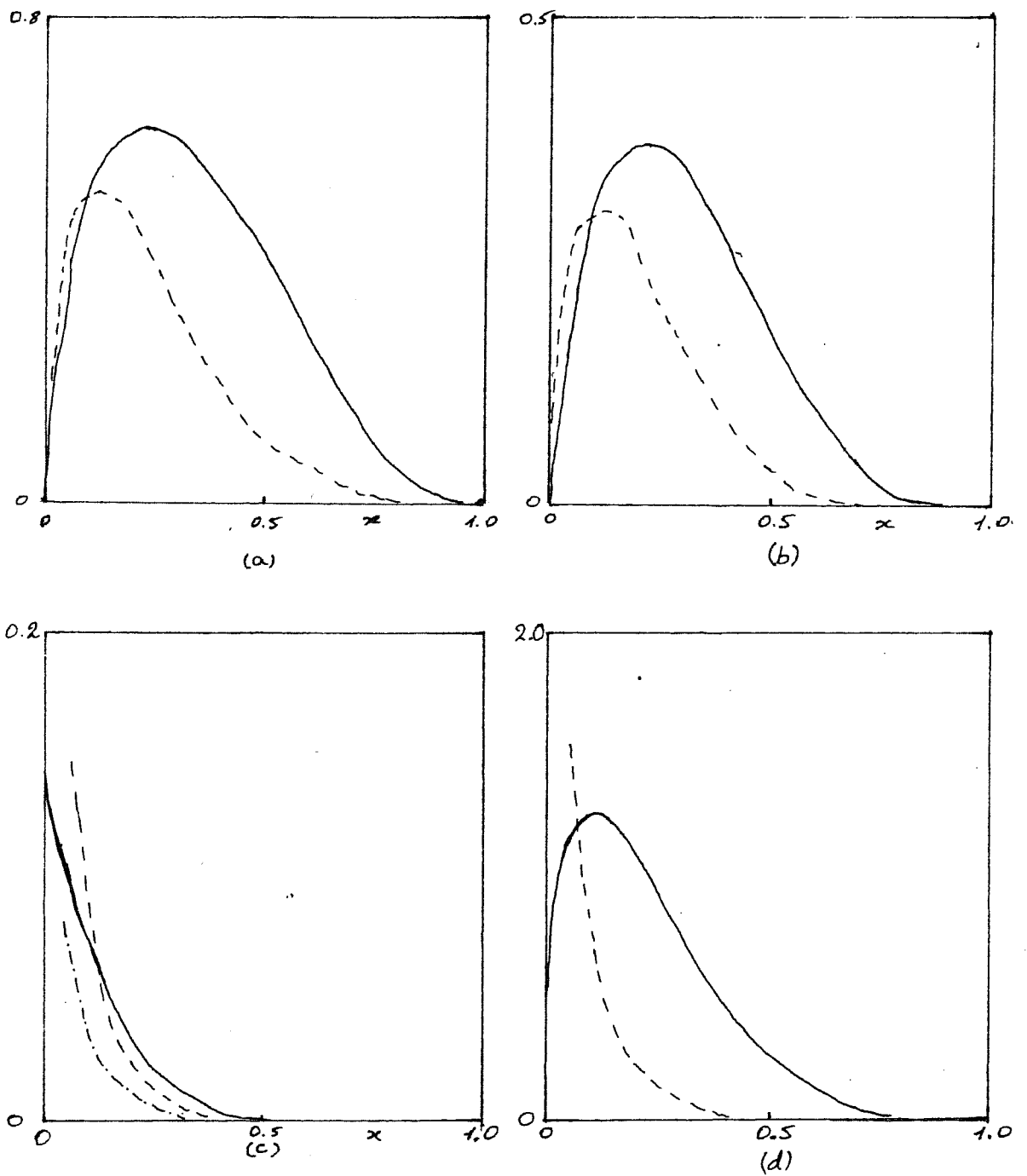


Fig. A4.1 - Spin-averaged parton distributions for (a) up-quark, (b) down quark, (c) non-charmed and charmed (chain-dashed curve) sea, (d) gluons, for  $Q_0^2 = 1.8 \text{ GeV}^2$  (solid curves) and  $\bar{s} = 1.5$  (dashed curves).

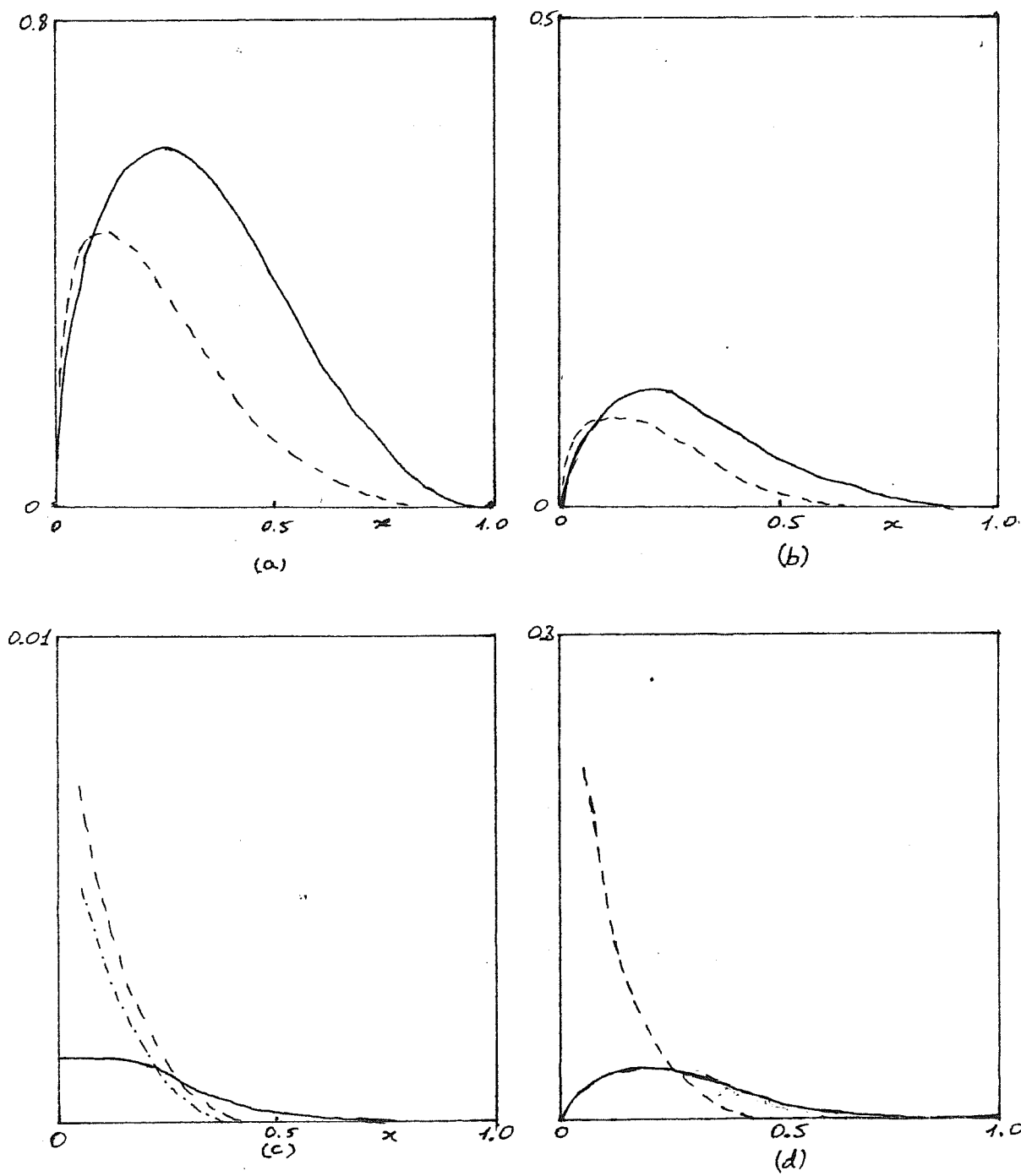


Fig. A4.2 + Helicity-dependent parton distribution for (a) up-quark, (b) down-quark, (c) non-charmed and charmed (chain-dashed curve) sea, (d) gluons for  $Q_0^2 = 1.8 \text{ GeV}^2$  (solid curves) and  $\bar{s} = 1.5$  (dashed curves).

References to Appendices A1 - 4

- [1] R. Cutler and D. Sivers, Phys. Rev. D17, 196 (1978).
- [2] P. De Causmaecker, R. Gastmans, W. Troost and T.T. Wu, Nucl. Phys. B206, 53 (1982); Phys. Lett. 105B, 215 (1981).
- [3] J.S.R. Chisholm, Nuovo Cimento 30, 426 (1963); Comp. Phys. Comm. 4, 205 (1972).
- [4] See for example S. Brodsky and G.R. Farrar, Phys. Rev. D11, 1309 (1975).  
G.P. Lepage and S. Brodsky, ref. [1] chapter 6.  
A. Mueller, Phys. Rep. 73, 237 (1981).
- [5] G. R. Farrar and F. Neri, Rutgers preprint RU-83-20 (1983).
- [6] G. 't Hooft and T. Veltman, Nucl. Phys.
- [7] See for example ref. [14] chapter 7.
- [8] See ref. [21] chapter 1.
- [9] W. Konetschny, Vienna preprint (Nov 1982).
- [10] See for example 't Hooft and Veltman ref [19] chapter 1.
- [11] D. Akyeamong and R. Delborgo, Nuova Cimento 19A, 219 (1974).
- [12] M. Chanowitz, M. Furman and I. Hinchliffe, Nucl. Phys. B159, 225 (1979).
- [13] See appendix of ref. [1] chapter 3.
- [14] A.J. Buras and K.J.F. Gaemers, Nucl. Phys. B132, 249 (1978).  
J.F. Owens and E. Reya, Phys. Rev. D17, 3003 (1978).
- [15] E.M. Riordan et al., SLAC-PUB-1634 (1975).  
R.E. Taylor, Proc. 1975 Int. Symp. on lepton and photon interactions at high energies, Stanford (ed. W.T. Kirk).  
H. Anderson et al., Measurement of the proton structure function, Conf. Proc. Tbilisi (1976).